Appendix B Probabilistic Assessment Cases for Reactor Pressure Vessel Head Penetration Nozzles (RPVHPNs)

B.1 Scope of assessment

There is currently a subpopulation of 24 reactor vessel top heads with Alloy 600 penetration nozzles operating in the U.S. that are potential candidates for peening mitigation. The reactor vessel heads in 45 U.S. PWRs have been replaced (or are scheduled for replacement by the end of 2014) with heads having PWSCC-resistant Alloy 690 nozzles. Of the 24 heads that are potential candidates for peening, 19 operate at cold-leg temperature (i.e., cold heads) and five operate at a temperature significantly above cold-leg temperature (i.e., non-cold heads).

The probabilistic calculations presented in this section are designed to bound the conditions for all 24 of these heads, such that the conclusions of the probabilistic model are applicable to all U.S. PWRs that may perform peening mitigation of RPVHPNs. As described below, probabilistic calculations are performed for a non-cold head case (i.e., hot head) with an assumed head temperature (600°F) bounding that for the five candidate non-cold heads and for a cold head case with an assumed head temperature (554°F) bounding that for the 19 candidate cold heads.

B.1.1 CRDM and CEDM Nozzles

The design information tabulated in MRP-48 [11] shows that the large majority of RPVHPNs in the 24 candidate heads (1822 of 1890) are CRDM or CEDM nozzles. The basic geometry of CRDM/CEDM nozzles is illustrated in Figure B-1. All CRDM nozzles have the same basic nozzle tube dimensions (OD = 4.00 inches, ID = 2.75 inches, and wall thickness = 0.625 inch), while CEDM nozzles have roughly similar dimensions that vary among different plants designed by Combustion Engineering. The base case calculations presented in this section are based on the standard CRDM nozzle dimensions, while sensitivity cases are used to investigate the specific CEDM nozzle dimensions for the two CE-designed heads that are candidates for peening.

B.1.2 Other RPVHPNs

A relatively small number of the RPVHPNs that are candidates for peening are nozzle types other than CRDM or CEDM nozzles (68 of 1890):

- 16 in-core instrumentation (ICI) nozzles in two CE-designed heads
- 22 J-groove head vent nozzles in 22 heads
- 8 J-groove auxiliary head adapter (AHA) nozzles in two Westinghouse-designed cold heads
- 2 "butt-weld" type head vents in two Westinghouse-designed heads
- 20 "butt-weld" type auxiliary head adapter (AHA) nozzles in five Westinghouse-designed cold heads

MRP-44 Part 2 [18] includes sketches illustrating each of these nozzles types. Because of their relatively small number, these other nozzles types were not explicitly included in the probabilistic calculations. The conclusions of the probabilistic calculations are considered to extend to the full set of RPVHPNs attached using J-groove (i.e., partial penetration) welds for the following reasons:

- The greater diameter of the ICI nozzles results in a larger crack growth distance required for nozzle ejection compared to the case for a CEDM nozzle. Furthermore, there has not been any reported cases of PWSCC detected in ICI nozzles [10]. This, the ICI nozzles are conservatively represented with CEDM nozzle dimensions in the probabilistic calculations.
- For the same reasons as for the case of ICI nozzles, the J-groove type AHA nozzles are represented by CRDM nozzle dimensions in the probabilistic calculations.
- As was the case for the MRP-105 [8] probabilistic calculations forming a key part of the basis for inspection requirements for unmitigated RPVHPNs, the J-groove type head vent nozzles are not included in the probabilistic modeling. There is no more than one such nozzle in each head, it represents a much smaller potential break size than CRDM nozzles (about 1-inch diameter break compared to 2.75-inch ID typical for CRDM nozzles), and an ejection of a head vent nozzle would not result in an ejected control rod. It is considered that the head vent nozzle has a negligible effect on the probabilistic assessment of the set of RPVHPNs in a particular head.

Finally, the small number of "butt-weld" type nozzles noted above were not assessed as part of this study. These nozzles explicitly fall outside of the scope of ASME Code Case N-729-1 [9]. Thus, the technical basis of this report for inspection requirements for use with peening is not applicable to such nozzles not attached to the head with J-groove (i.e., partial penetration) welds.

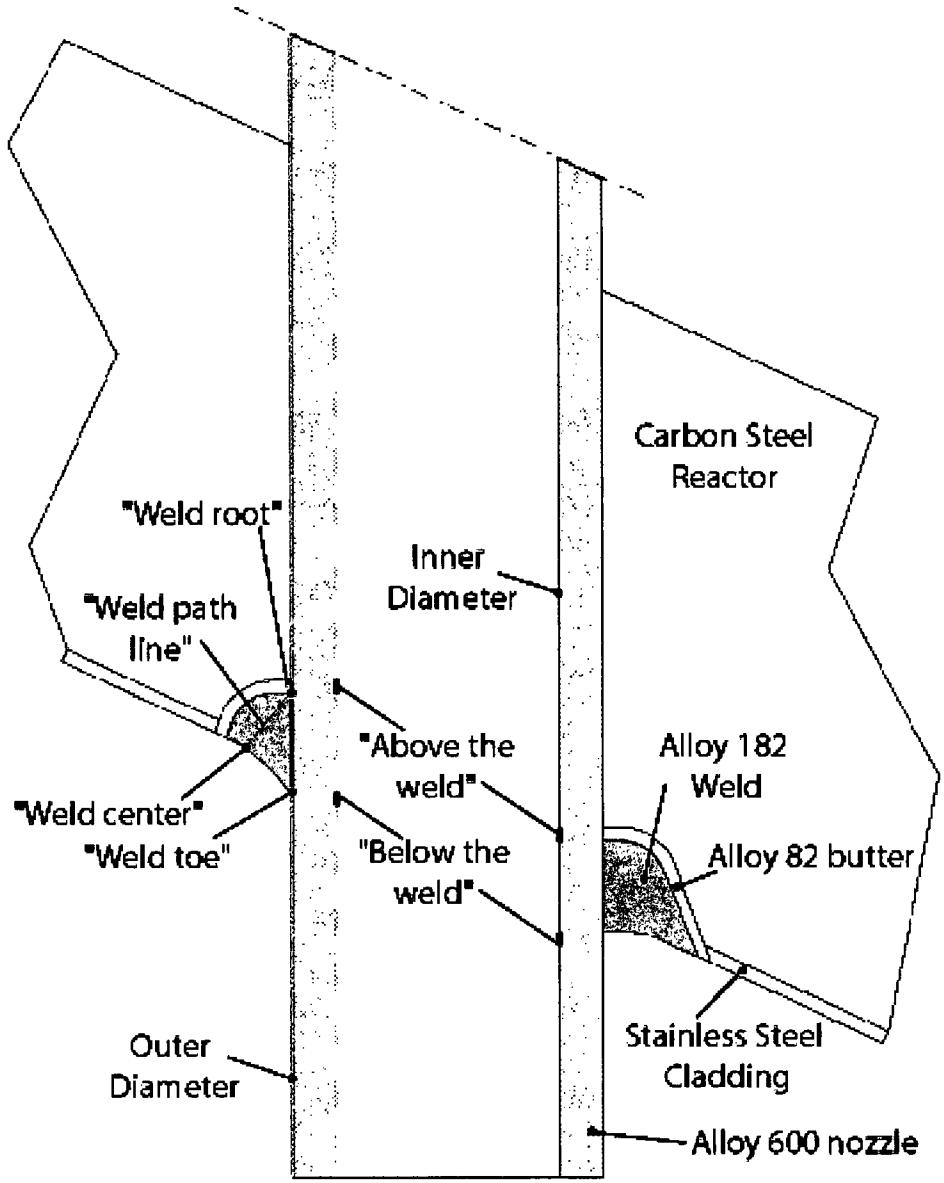

Figure B-1
Summary of General RPVHPN Geometry

B.2 Overall modeling methodology

The probabilistic model that was developed to study PWSCC in RPVHPNs was derived from the DM weld probabilistic model that is fully detailed in Appendix A. While the two models share a similar simulation framework, and several sub-models, there are many significant differences that will be discussed in this appendix. For conciseness, this appendix will reference portions of Appendix A where large overlap exists between the two models. To facilitate comprehension, this appendix has been organized analogously to Appendix A, in as much as possible.

A full description of the RPVHPN probabilistic modeling framework is given in the Section B.2.1. This is followed by Section B.2.2, which introduces the specific cracking mechanisms (e.g., type, location, orientation, etc.) for which PWSCC initiation and growth are modeled; these mechanisms will be referenced frequently throughout this appendix.

B.2.1 Probabilistic modeling methodology

The integrated probabilistic modeling framework that is used to study the effect of peening on RPVHPN PWSCC combines the individual models discussed in Sections B.3 through B.6. Namely, the probabilistic modeling framework is used to predict ejection criterion statistics, as discussed in Section B.7. Results generated with this model, using the inputs and uncertainties discussed in Section B.8, are given in Section B.9.

The RPVHPN probabilistic model applies a framework similar to the DM weld probabilistic model. In summary:

- Uncertainty propagation is handled by sampling input and parameter values from appropriately selected probability distributions (with appropriately selected bounds) in the main model loop, prior to the time looping structure. Important correlations are included.
- Event scheduling for a given weld, including operating, mitigation, inspection, and PWSCC initiation times, is developed in the main loop prior to entering the time looping structure.
- If one or more of the predicted PWSCC initiation times, adjusted for differences in temperature, are less than the final operating time and the time of peening (if applied), the time looping structure is entered. Each active flaw is allowed to grow until it reaches the end of the operation, its penetration is repaired, or its penetration nozzle is ejected.
- Initiations, ejections, repairs, among other events, are tracked as a function of operating cycle for each Monte Carlo realization and summary statistics are compiled at the end of each Monte Carlo run.

The central differences between the DM weld and RPVHPN models include:

- The RPVHPN model accounts for flaw initiation and growth on multiple penetrations (often between 70 and 100 in a reactor head), while the DM weld model only accounts for a single component, per Monte Carlo realization. Accordingly, a penetration loop sits inside the main loop and contains the time looping structure.
- The RPVHPN model accounts for several diverse mechanisms of PWSCC initiation and growth (as detailed in Section B.2.2) as opposed to just axial and circumferential ID cracks. In fact, the majority of the model augmentation required for the RPVHPN model was to address new crack types and locations.
- In the case of DM welds, through-wall growth (i.e., leakage) is considered the end criteria (at which point simulation ends and summary statistics are

compiled). For RPVHPNs, the end criteria is nozzle ejection; when leakage occurs due to a flaw at any location, it is assumed that this flaw immediately transitions to through-wall circumferential crack that grows along the top of the J-groove weld contour until it is repaired or it becomes large enough to fulfill the ejection criterion.

- Visual examination for leakage is modeled.
- There are other technical augmentations or logical revisions to be disclosed fully in the following sections.

A high level presentation of the main loop of the probabilistic model for a given weld is presented in Figure B-2 and a more detailed presentation of the time looping structure is given in Figure B-3. The remainder of this section provides an end-to-end description of a single RPVHPN Monte Carlo run. Contrary to the rest of this appendix, this description will spare no detail and may have substantial overlap with Appendix B.

The initial conditions for the run are defined prior to entering the main loop. These initial conditions include all input parameters that remain constant throughout the run, such as the number and length of operating cycles, the frequency of inspections, certain weld geometry attributes, and the times of mitigation.

Following the definition of the initial conditions, the main loop is entered. The main loop is cycled for each Monte Carlo realization and is exited once all of the user-specified Monte Carlo realizations have been completed. After exiting the main loop, the program evaluates the results of the run, outputs certain information relevant to the study, and terminates the run.

At the beginning of each Monte Carlo realization, the values of reactor-head specific distributed inputs are determined by random sampling. The distributions for each of the distributed inputs are user-defined. Then, the first flaw initiation model (detailed in Section B.4) is called to predict the reference initiation time for the reactor head; the average time of the first PWSCC initiation in the head.

Following the definition of the reactor head-specific values, the penetration loop is entered. This loop is cycled until PWSCC initiation and growth has been simulated for each penetration in the reactor head. Upon exiting the penetration loop, the penetration results are cumulated to form penetration-specific and reactor head-specific results.

At the beginning of each penetration cycle, penetration-specific distributed inputs are determined by random sampling. Then, the program invokes the multiple flaw initiation model (detailed in Section B.4) to predict the initiation times at all potential flaw sites. The flaw initiation times are compared to the "initiation end time": the final operating time, or, if peening is scheduled, the peening application time. The current penetration cycle is terminated if all of the predicted initiation times exceed the "initiation end time". If not, the initiation model assigns initiation conditions to each flaw with an initiation time occurring before the "initiation end time".

After determining that there are flaws that will initiate during the initiation time window in the current penetration, the program calls the load models (detailed in Section B.3) to determine the relevant loads at the various crack sites (including peening loads if peening is scheduled before the end of plant operation). This is different from, and more computationally efficient than, the DM weld model, which calculates load prior to initiation. The DM weld initiation model utilizes load information to incorporate a functional dependence of initiation time versus surface stress; the RPVHPN model does not; i.e., it is assumed that all locations are equally likely to initiate PWSCC.

After attaining the stresses at locations of interest, the program enters the time looping structure for the current penetration.

The time looping structure is composed of an outer cycle-by-cycle loop with a nested within-cycle loop. The cycle-by-cycle loop may be terminated if the penetration is repaired or ejected. If this occurs, the program stores relevant information and cycles to the next penetration.

The within-cycle loop is entered if there is an active flaw on the current penetration whose initiation time is less than the time of the end of the current operating cycle. Immediately prior to entering the within-cycle loop, any peening application that is scheduled for the current cycle is invoked resulting in new stress profiles utilized to predict crack growth.

If no flaw initiations occur prior to the end of the current sub-step in the within-cycle loop, the sub-step is skipped. Otherwise, at the beginning of the sub-step, the stress intensity factor for each active flaw is calculated based on the location of the flaw, the geometry of the flaw and its respective stress profile at the beginning of the sub-step. During each sub-step, all active flaws are grown using the flaw propagation model (detailed in Section B.5) that determines the flaw propagation rate and increases the depth and length of the flaw at a constant rate for the duration of the sub-step.

Before completing a given sub-step, the program checks if any flaw has reached through-wall (or through-weld in the case of the weld location), and if so, the cycle number is stored for a statistical summary generated at the end of Monte Carlo run. Flaws that grow through-wall may or may not cause a leak (e.g., flaws that grow through-wall below the weld do not produce a leak). If a flaw does cause a leak, it is assumed to transition immediately to a circumferential through-wall crack that grows along the top of the J-groove weld contour. Flaws that are below the weld must grow in length to the nozzle OD annulus (i.e., the weld toe) before they are considered to leak.

At the end of each sub-step, any through-wall circumferential flaws are evaluated to predict if, cumulatively, they occupy enough of the nozzle circumference to cause ejection (detailed in B.7). If ejection is predicted to occur (and the ejection time does not contradict the results of an assumed user-defined past inspection), the penetration is removed from service, the cycle number is stored for a statistical summary generated at the end of the Monte Carlo simulation, the current penetration simulation is terminated, and the program moves on to the

next penetration. If the ejection result does contradict the results of the assumed past inspection, the code exits the penetration loop without saving any results and restarts the current Monte Carlo realization from the beginning of the main loop.

When all sub-steps of a given cycle have been completed, the program determines if an examination is to be performed at the end of the current cycle, and if the examination is to be ultrasonic (UT), eddy current (ET), bare-metal visual (BMV) or some combination of the three. If so, the inspection models (discussed in Section B.6) are called appropriately. If any flaw is detected (and its detection time does not contradict the results of an assumed user-defined past inspection) it is repaired, the cycle number is stored for a statistical summary generated at the end of the Monte Carlo simulation, the current penetration simulation is terminated, and the program moves on to the next penetration. In a similar fashion to an ejection occurrence, if the detection result contradicts the results of the assumed past inspection, the code exits the penetration loop without saving any results and restarts the current Monte Carlo realization from the beginning of the main loop. If a flaw is not detected, it remains active. After all scheduled inspections, the code returns to the cycle-by-cycle loop and continues to the next cycle or returns to the penetration loop if the cycle-by-cycle loop is complete.

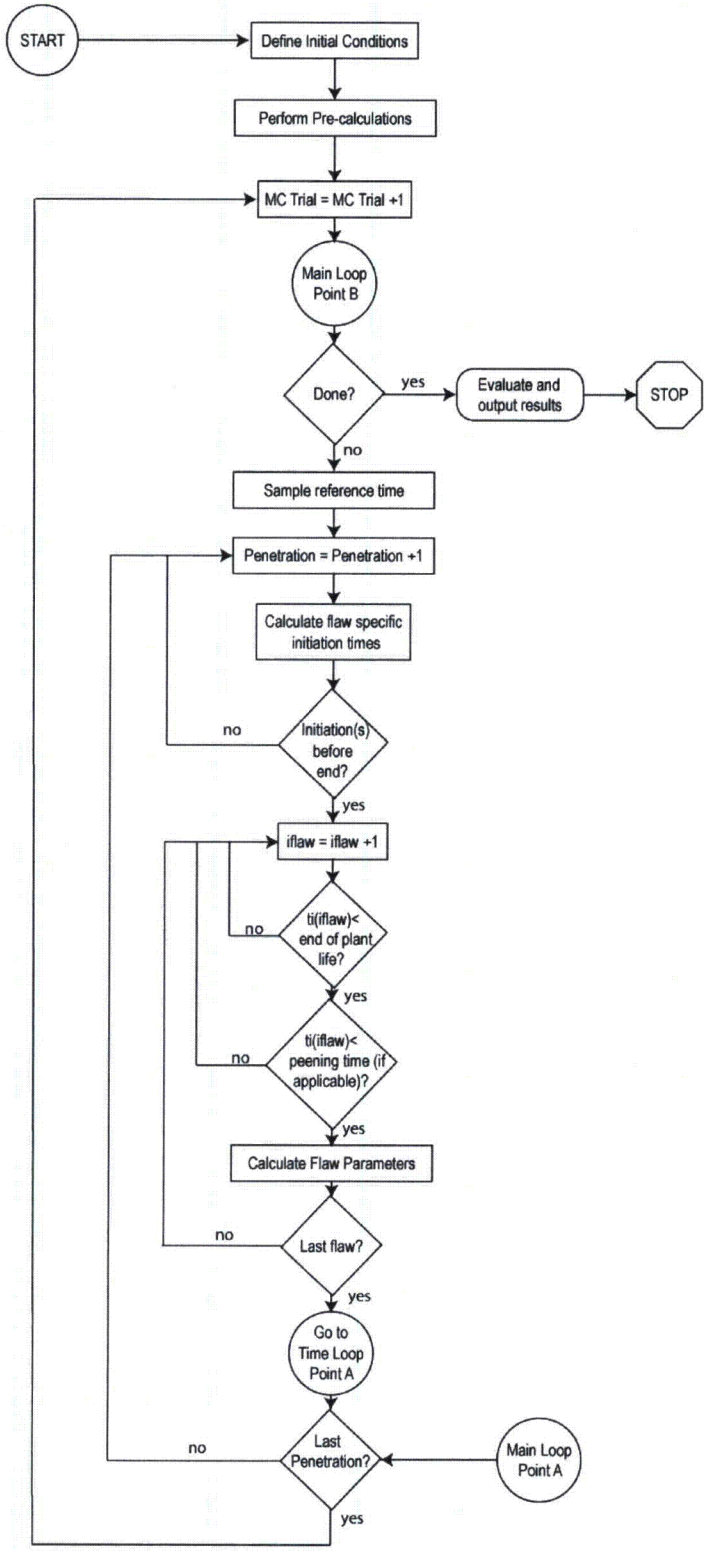

Figure B-2
RPVHPN Probabilistic Model Flow Chart: Main Loop

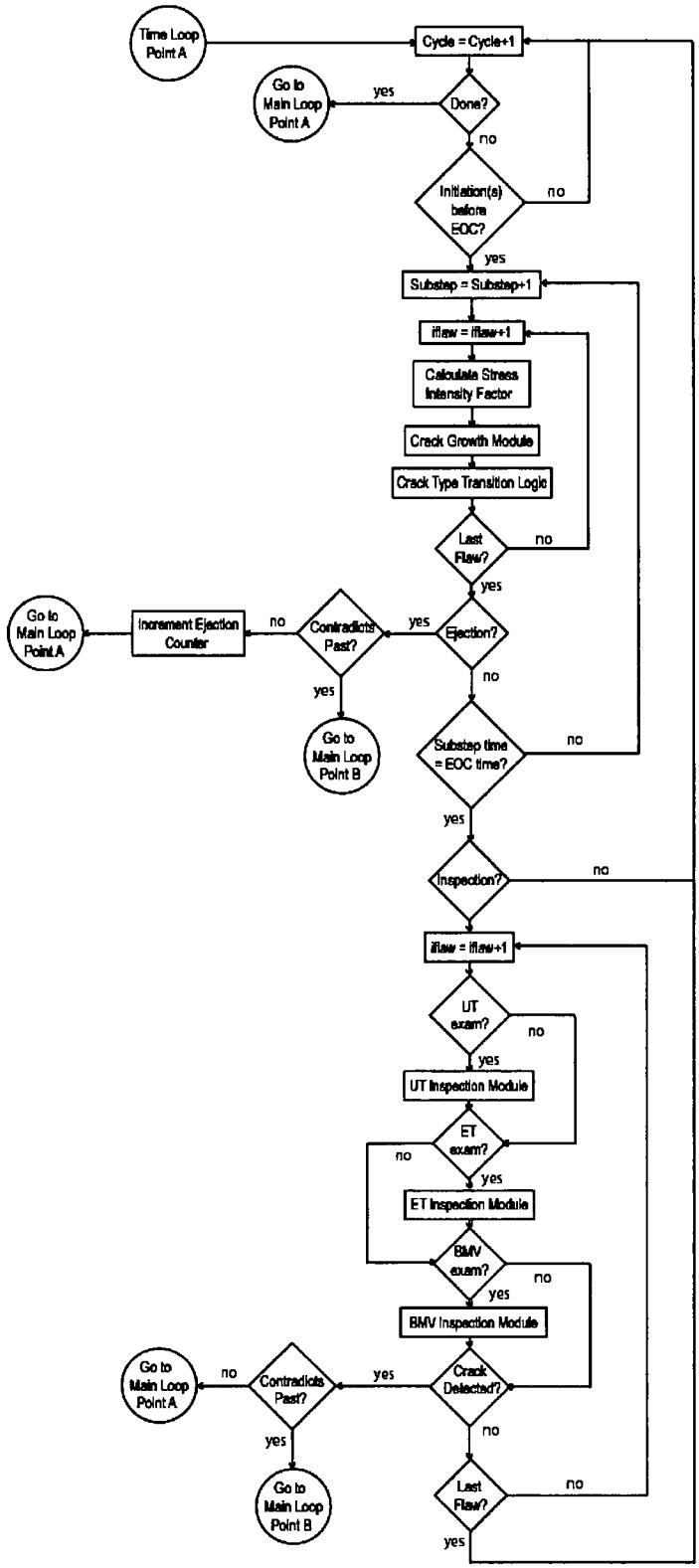

Figure B-3
RPVHPN Probabilistic Model Flow Chart: Detail of Time Loop

B.2.2 Definition of RPVHPN Cracking Mechanisms

This section introduces the spatial discretization used to model PWSCC in RPVHPNs and, subsequently, the different cracking mechanisms modeled at the various locations. Each cracking mechanism reflects a cracking type observed on reactor heads in industry. Due to varying geometry, accessibility, material condition, etc., each mechanism is modeled with a unique set of initiation, load, growth, and examination techniques. It is important to distinguish each mechanism, as they will be referenced frequently throughout this appendix. Table B-1 summarizes each mechanism. Figure B-4 provides a schematic of a general RPVHPN and indicates the primary growth direction (i.e., the direction that leads to leakage) of each modeled PWSCC mechanism.

For the purpose of this study, each RPVHPN is divided into an uphill and downhill side. Each cracking mechanism may form on either the uphill or downhill sides, both of which have their own unique loading conditions. The downhill and uphill sides are selected as the only circumferential locations for crack initiation. This convention is based on the fact that the downhill and uphill locations are the locations of highest tensile weld residual stresses (due to nozzle ovalization), as well as plant experience that shows that most detected PWSCC flaws are located clustered around the downhill and uphill azimuths.

The key characteristics of the cracking mechanisms modeled in this study are given below:

- **ID axial cracks** – partial through-wall cracks located on the penetration nozzle ID. These cracks are conservatively assumed to initiate in the region above the weld such that they immediately result in leakage if they penetrate through-wall into the OD nozzle annulus. These cracks are opened by hoop stresses in the penetration nozzle.
- **OD axial cracks** –partial through-wall cracks located on the penetration nozzle OD located below the weld. These cracks cause leakage if they grow in length to reach the nozzle OD annulus; they may transition to through-wall axial cracks if they go through-wall before reaching the annulus. These cracks are opened by hoop stresses in the penetration nozzle.
- **Through-wall axial cracks** - through-wall cracks located below the weld. These cracks may only form if an OD axial crack reaches through-wall before reaching the nozzle OD annulus. These cracks cause leakage if they grow long enough to reach the nozzle OD annulus. These cracks are opened by hoop stresses in the penetration nozzle.
- **Radially-oriented weld cracks** – cracks located on the J-groove weld that grow toward the weld toe. These cracks cause leakage if they reach the weld toe. These cracks are opened by hoop stresses in the J-groove weld.
- **Circumferential through-wall cracks** – through-wall cracks located on the weld contour above the weld. These cracks are assumed to occur immediately following leakage caused by any of the preceding crack mechanisms, either by branching of the flaw causing the leakage or by initiation of a new flaw on

the OD surface of the nozzle. These cracks are opened by a complex stress field acting orthogonally to the weld contour.

Table B-1
Summary of PWSCC Mechanisms Modeled on RPVHPNs

Crack Mechanism ID	Orientation	Shape	Material Characteristics	Location	Transitions to…
1	Axial	Semi-elliptical, partially through-wall	Alloy 600	Top of weld, inner diameter	Crack mechanism 5 upon growing through-wall
2	Axial	Semi-elliptical, partially through-wall	Alloy 600	Bottom of weld, outer diameter	Crack mechanism 5 upon growing to weld root, or crack mechanism 4 upon growing through-wall
3	Radially-oriented	Semi-elliptical, partially through-weld	Alloy 182/82	On weld	Crack mechanism 5 upon growing to weld root
4	Axial	Rectangular, through-wall	Alloy 600	Bottom of weld	Crack mechanism 5 upon growing to weld root
5	Circumferential	Through-wall	Alloy 600	Along upper weld contour	Ejection upon growing past stability threshold

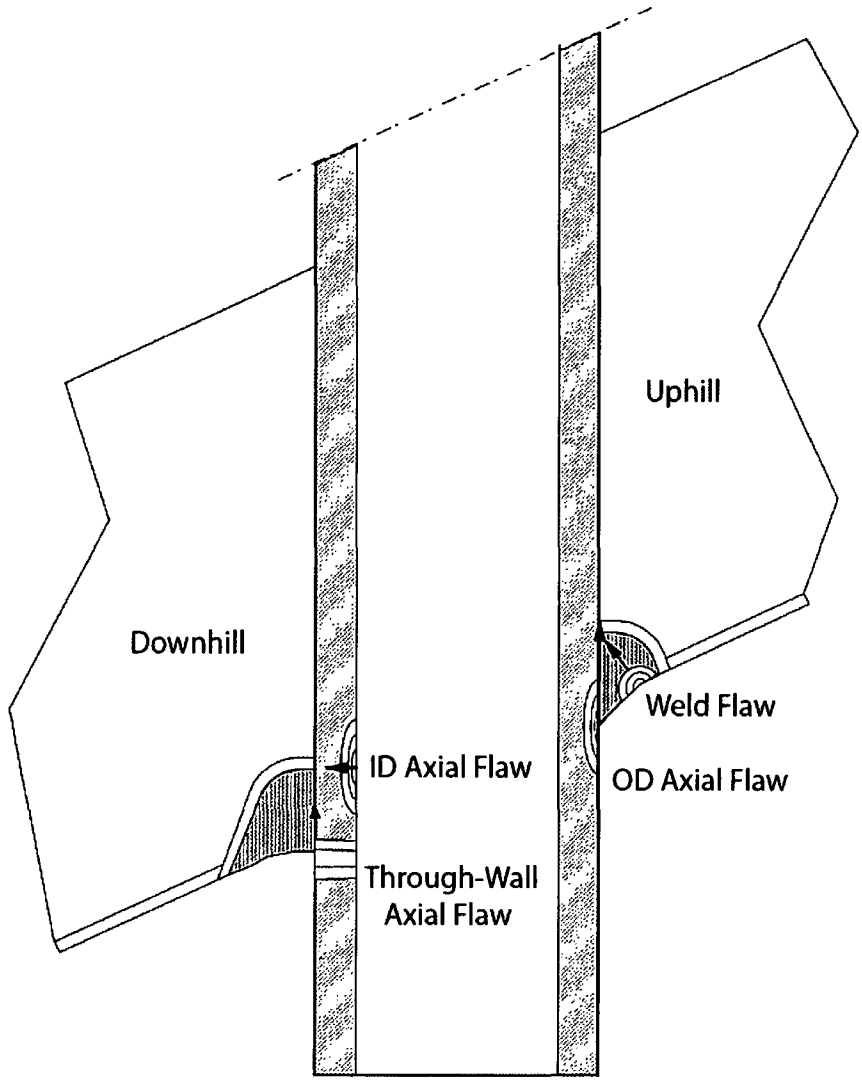

Figure B-4
Schematic of Modeled Cracking Mechanisms for RPVHPN Probabilistic Assessment (Arrows Indicate Direction of Growth Toward Leakage)

B.3 Load and stress model

Load models are used to calculate stresses at the different locations of interest for PWSCC on RPVHPNs. The crack growth model uses this stress information; it is noted, however, that the RPVHPN crack initiation model does not explicitly account for stress dependence.

The load models account for welding residual stresses as well as operational loads. In addition, a peening residual stress model is introduced for modeling crack growth during cycles after a peening application, if applicable.

The methodologies for calculating stresses due to operational loads, penetration welding, and peening are discussed in Sections B.3.1, B.3.2, and B.3.3, respectively. Considerations for the effects of temperature and load cycling are discussed in Section B.3.4. The loads used for growth at the various locations are summarized in Section B.3.5.

B.3.1 Internal pressure and piping loads

The operational stresses, which are due predominantly to internal pressure, are separated from the residual stresses in this analysis (as they were for the DM weld load models). This separation serves a practical purpose in modeling peening because it allows for peening effects to be applied to existing residual stresses, without altering operational stresses. The operational stresses can be superimposed with post-peening residual stresses to provide the total stresses used to estimate crack growth.

Unlike DM welds, the complex geometry of a reactor head penetration precludes the accurate estimation of operational stresses at the various locations of interest by way of analytical, or textbook, approaches. Accordingly, operational stresses at each location have been ascertained from the results of various J-groove weld finite element analyses (the general methodology of such RPVHPN FEA studies is outlined in [1]). Specifically, operational stresses are attained by subtracting stress states predicted by FEA during operation from those predicted during shutdown (i.e., operational = total – residual).

Operational stress at each location of interest is treated as being constant through-wall (or through-weld), with a magnitude equal to the *surface* operational stress predicted by FEA results. This convention accurately accounts for the separation of residual and operational stresses near the peened surface. Careful separation of the residual and operational stresses away from the peened surface is not necessary; the total stress profile after peening is largely insensitive to the way residual and operational stresses are separated away from the surface (as becomes apparent after reviewing the peening modeling methodology in Section A.3.3).

The FEA results reveal that operational stresses are negligible at the OD and weld surfaces (in comparison to the welding residual stresses at these surfaces). As with DM welds, pressure acting to open a crack face is included after crack formation such that the operational stresses become:

$$\sigma_{oper,OD} = P$$
$$\sigma_{oper,weld} = P \qquad \text{[B-1]}$$

Hoop operational stresses at the ID surface are modeled using a stress concentration that is applied to the nominal hoop stress estimated with thin-walled cylinder theory:

$$\sigma_{oper,ID} = F_{oper,ID}\frac{PD_i}{2t} + P \qquad \text{[B-2]}$$

where $F_{oper,ID}$ is the ID hoop stress concentration factor, P is the normal operating pressure, D_i is the penetration nozzle inner diameter, and t is the penetration nozzle thickness. The ID stress concentration factor has been derived from FEA results as is detailed in Section B.8.1. Note that this equation too includes the pressure acting to open the crack face after crack formation.

B.3.2 Welding residual stress before peening

The J-groove welding residual stress profiles at six locations/directions (vectors) of interest are derived from the same set of FEA results used for operational stresses in the previous section. Specifically, six vectors are relevant for predicting the crack growth mechanisms discussed in Section B.2.2: hoop stress from the penetration nozzle ID to the OD above the weld (uphill/downhill), hoop stresses from the penetration nozzle OD to the ID below the weld (uphill/downhill), and hoop stresses from the weld surface to the weld toe (uphill/downhill). These vectors are depicted in Figure B-5.

For all six vectors, a second-order polynomial function of through-wall (or through-weld) fraction is used to model the total stress profile. These polynomials are fit to FEA results during operational loading (and the residual stresses are attained by subtracting the operational stresses discussed in the previous section). This is different from the third- and fourth-order curves used for welding residual stresses in DM welds, but is considered accurate for capturing the essential gradient and curvature characteristics observed in RPVHPN FEA results [1]. The resulting general equation form is:

$$\sigma_{tot,loc}\left(\frac{x}{D}\right) = \sigma_{0,tot,loc} + \sigma_{1,tot,loc}\left(\frac{x}{D}\right) + \sigma_{2,tot,loc}\left(\frac{x}{D}\right)^2 \qquad \text{[B-3]}$$

where the *loc* subscript is a placeholder for the various locations of interest, D is a general dimension equal to the penetration nozzle thickness for ID and OD locations and equal to the weld path length for weld locations, and $\sigma_{0,WRS,loc}$, $\sigma_{1,WRS,loc}$, and $\sigma_{2,WRS,loc}$ are curve-fit parameters. Note that the crack face pressure is not included in the equation above because cracks are not included in the FEA models used to derive the curve-fit parameters.

The fit parameters are calculated such that they give the second-order polynomial stress profile that interpolates the following three points:

1. The stress at the initiation surface:

$$\sigma_{tot,loc}(0) = \sigma_{0,tot,loc} \qquad \text{[B-4]}$$

2. The stress at the opposite surface (or the weld root for weld locations):

$$\sigma_{tot,loc}(1) = R_{1,loc}\sigma_{0,tot,loc} \qquad \text{[B-5]}$$

3. The stress at the mid-radius (or the mid-point between the weld center and the weld root for weld locations):

$$\sigma_{tot,loc}(0.5) = R_{0.5,loc}\left(\frac{\sigma_{0,tot,loc} + R_{1,loc}\sigma_{0,tot,loc}}{2}\right) \qquad \text{[B-6]}$$

The $R_{1,loc}$ and $R_{0.5,loc}$ terms are indicative of the average gradient and curvature of the resulting stress profile. Together with the surface stress at the location/direction of interest ($\sigma_{0,WRS,loc}$), these terms have been fit to FEA results, as detailed in Section B.8.1.

For completeness, the general welding residual stress equation is given below:

$$\sigma_{WRS,loc}\left(\frac{x}{D}\right) = \sigma_{0,tot,loc} + \sigma_{1,tot,loc}\left(\frac{x}{D}\right) + \sigma_{2,tot,loc}\left(\frac{x}{D}\right)^2 + P - \sigma_{oper,loc} \qquad \text{[B-7]}$$

B.3.3 Residual stress after peening

As discussed previously, peening has the effect of adding a thin region of compressive stress in all three principal directions near the surface of its application. This compressive region both prevents crack initiation and slows the growth of cracks (especially short cracks), and hence peening is required to be captured in this modeling effort.

At all locations of interest for each penetration, the peening effect is modeled in the same manner as in the DM weld program (see Section A.3.3); i.e., using a four-region piecewise equation that combines a compressive region near the surface with the pre-existing residual stresses while maintaining the same equivalent force through-wall (or through-weld) before and after peening. For that reason, the details of peening modeling will not be repeated here. Any differences in the way peening is applied in the DM weld program and the RPVHPN program are noted below:

- For RPVHPNs, the initial compressive surface stress and the penetration depth are sampled independently at each location. This is different from the DM weld program, which assumes that the peening is applied uniformly to all ID locations.
- For RPVHPNs, the compressive residual stress depths are sampled from separate distributions for the ID locations, as compared to the OD and weld locations. A peening compressive residual stress to a depth of at least 3 mm is assumed for the wetted nozzle OD and weld surfaces of the RPVHPN. This greater compressive stress depth ensures that pre-existing flaws on the nozzle OD that are deeper than the compressive stress layer are reliably detectably by UT exams performed from the nozzle ID.
- For weld locations, the through-element dimension is the weld path length instead of the penetration nozzle thickness (i.e., in Eqs. [A-18] through [A-21]).
- The effect of peening on growth is conservatively neglected for several scenarios described below:
- ID peening stresses above the weld are assumed to have no effect on the growth of circumferential through-wall cracks. The growth of circumferential through-wall cracks is based on stress intensity factors that were calculated with finite element software and these models did not include stresses representative of a peened nozzle.
- OD peening stresses below the weld are assumed to have no effect on the growth of partial through-wall axial OD cracks that have grown under the weld far enough that the upper crack surface tip is outside of the peening compressive layer (as demonstrated in Figure B-6).
- ID peening stresses do not affect nearly through-wall axial OD cracks (as demonstrated in Figure B-6), i.e., the thin compressive region near the ID is not given credit for abating the growth of mostly (90-100%) through-wall cracks.

B.3.4 Effect of operating temperature and load cycling

Residual stress relaxation due to temperature and load cycling can occur at penetration locations, as it can in DM weld components. As discussed for DM welds, residual stress relaxation may be especially important in this study because, if it is unaccounted for, the beneficial impact of peening residual compressive stresses may be overestimated for later cycles in a plant's operating life.

As in the DM weld program, the RPVHPN program eschews a time-dependent relaxation model for a more simple and conservative approach to relaxation. In this approach, a reduction is applied to the initial peening residual stress magnitude to account for relaxation over the life of the component. The derivation of relaxation factor from experimental data is discussed in Section B.8.5.3.

B.3.5 Summary of load model

The RPVHPN load model is used to attain through-wall (or through-weld) stress profiles on the different vectors that are attributed to the growth of the various cracking mechanisms.

Total stresses and operational stresses (i.e., those stresses due to loads present during operation) are derived from FEA results and welding residual stresses are attained from the difference between the total and operational stresses. The total stress profile at each location is modeled with second-order polynomial function of the through-wall fraction. The operational stress profile at each location is modeled with a constant stress.

Prior to peening, the total stress profiles used to predict crack growth are those derived from FEA results (plus the crack face pressure contribution).

The peening load model modifies the welding residual stress profiles to predict post-peening residual stresses. After peening is applied, the post-peening residual stress profile is superimposed with the operational stresses to attain the total stress profiles used to predict crack growth.

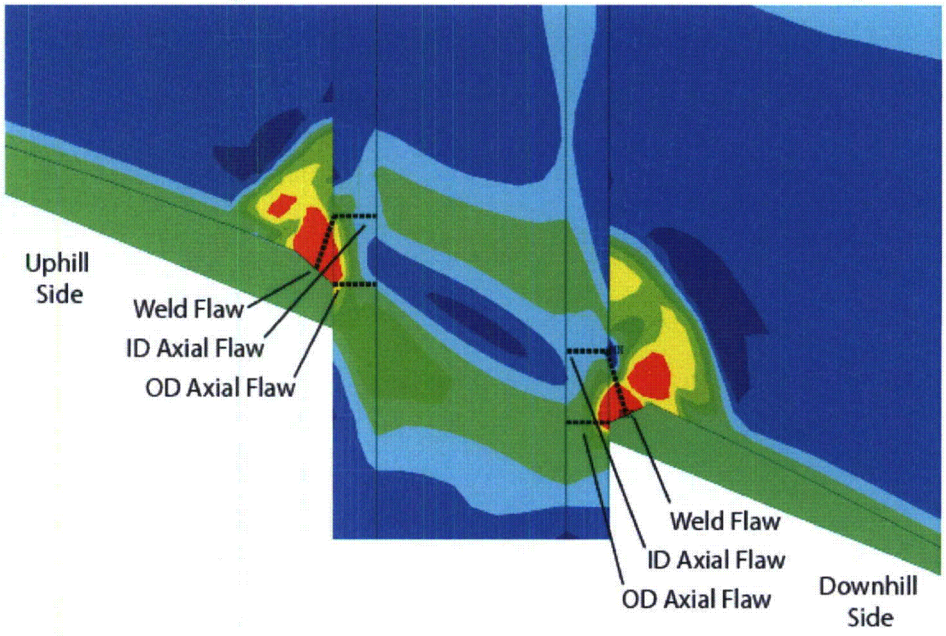

Figure B-5
Depiction of Stress Profile Vectors for Each Crack Mechanism Location (six bold dotted lines) and Welding Residual Hoop Stress Contour Plot

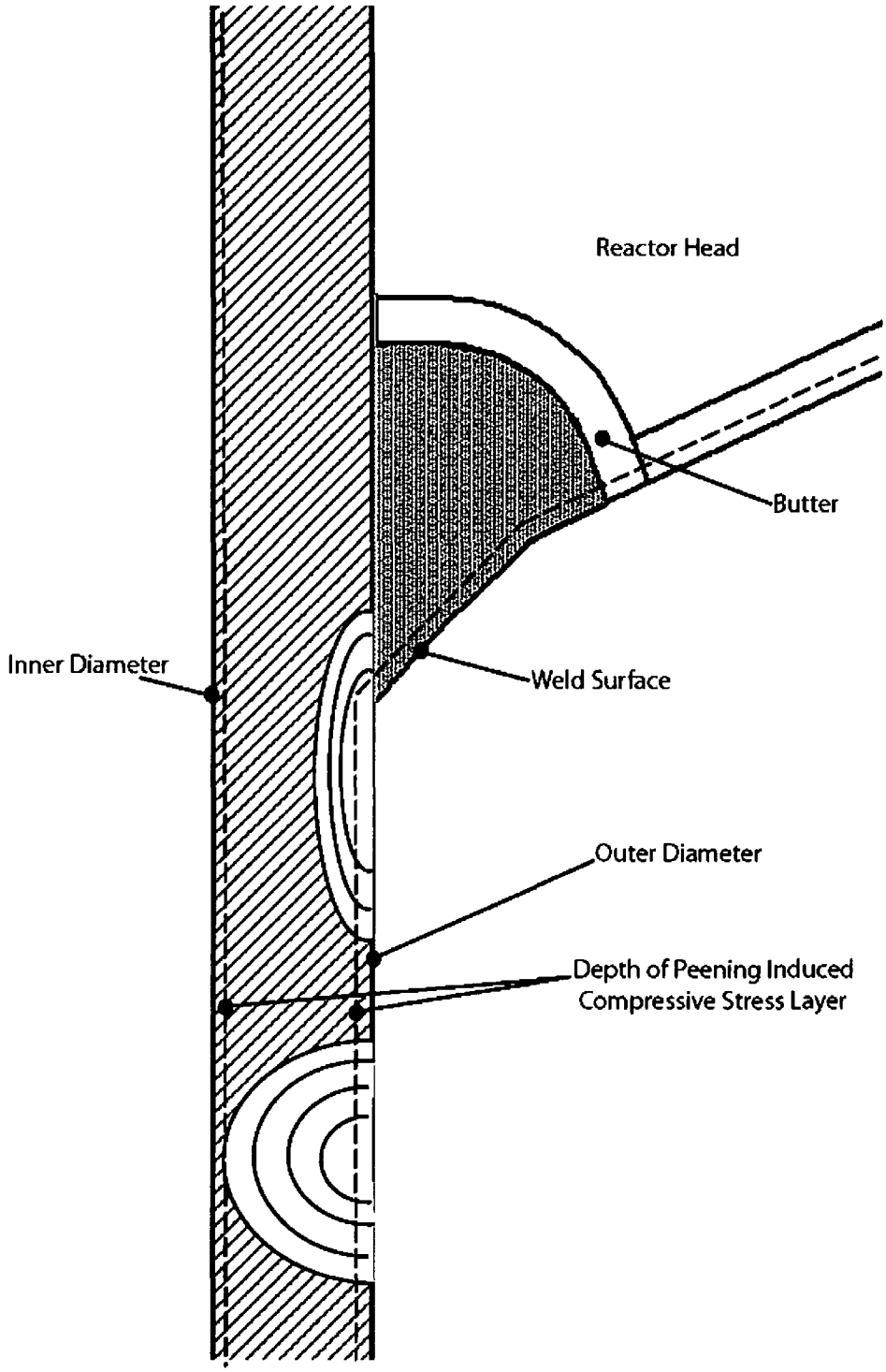

Figure B-6
Scenarios for Neglected Peening Effects in RPVHPNs: a) Crack Extends Below Weld, Past Compressive Stress Layer; b) OD Crack Depth Reaches ID Compressive Stress Layer

B.4 Crack initiation model

This study employs a statistical Weibull approach for predicting crack initiation that is similar to the approach used by the DM weld program (discussed in Section A.4). As such, much of the information presented for DM welds will not be repeated in this section, which will instead focus on detailing the differences between the initiation models.

The key difference in the initiation models is that the RPVHPN initiation model does not include a surface stress adjustment. This adjustment was considered unfounded for RPVHPNs based on the following information:

- The surface stresses at all RPVHPN locations of interest are randomly sampled and are similar in tensile magnitude while surface stresses at DM weld locations vary systematically as a function of distance from the point of maximum tensile bending stress. Accounting for this systematic stress variation on the DM weld circumference is important for modeling coalescence.
- No clear stress-dependent location preference emerges from industry experience of PWSCC initiation on RPVHPNs.
- There is no known precedent for applying a stress-adjustment when modeling initiation of PWSCC on RPVHPNs.

A second notable difference is that the RPVHPN initiation model predicts PWSCC initiation across all of the penetrations in a single reactor head, as opposed to a single component.

B.4.1 Spatial Discretization of Crack Sites

The spatial discretization of the crack locations is described in Section B.2.2. To summarize, six mechanisms are considered for crack initiation in this study: axial cracks on the nozzle ID at the top of the weld (uphill/downhill), axial cracks on the nozzle OD at the bottom of the weld (uphill/downhill), and radially-directed cracks at center of the weld surface (uphill/downhill).

These six *locations* are considered for the number of penetrations in the reactor head, N_{pen}, resulting in $6N_{pen}$ total initiation *sites*.

In this section, the subscript *loc* is used to denote the different locations and the subscript *i* is used to denote the different penetrations on the reactor head.

B.4.2 Initiation Time of First Crack

As was done to predict time of first initiation on DM welds, a Weibull model has been selected for predicting the time of first initiation of PWSCC in RPVHPNs. The use of this statistical model reflects systematic and statistical variations in material properties and environmental conditions from reactor head to reactor head, across the industry. The advantages of the Weibull model, and a general description, can be found in Section A.4.2.

The Weibull slope, β, an arbitrary failure fraction, F_1, (e.g., 0.1%, 1%, 10%, etc.), and the time at which this arbitrary failure fraction is reached, t_1, are provided as inputs to the probabilistic model. The value of the Weibull characteristic time parameter, θ, is then determined during runtime using Eq. [A-30]. The process by which β, F_1, and t_1 are fit to existing data for first crack initiation in RPVHPNs is discussed in Section B.8.2.

Once β and θ are known for the current Monte Carlo realization, they can be used to sample a reference initiation time in EDY (t_{ref}). The sampled initiation time is adjusted for temperature (to convert to EFPY) using the Arrhenius relationship:

$$t_f = t_{ref} \times e^{\left(\frac{Q}{R}\right)\left(\frac{1}{T}-\frac{1}{T_{ref}}\right)} \qquad \text{[B-8]}$$

The result of the above equation is considered to be the *average* time of the first PWSCC initiation for the reactor head. Unlike the DM weld initiation model, this time is not applied to any specific initiation site. Similar to the DM weld initiation model, this time is used by the multiple crack initiation model, which is discussed next.

B.4.3 Initiation Times of Multiple Cracks

A Weibull model has been selected for use in predicting times of initiation of multiple PWSCC cracks on a reactor head. The use of this statistical model reflects systematic and statistical variations in material properties and environmental conditions from location to location, and from penetration to penetration, on a single reactor head.

The multiple crack initiation Weibull model uses a new Weibull slope, $\beta_{mult,i}$, to reflect a new rate at which PWSCC degradation spreads to multiple sites on a reactor head after the first crack initiation. This Weibull slope is sampled for each penetration to reflect the premise that each penetration has unique conditions relevant to multiple flaw initiation[13]. The distribution selected for $\beta_{mult,i}$ is discussed in Section B.8.2.

Since the time provided by Eq. [B-8] is indicative of the average time of the first PWSCC initiation across all $6N_{pen}$ crack sites, it is therefore associated with the cumulative probability (F_{1st}) given in Eq. [B-9] below:

[13] It is noted that sampling the multiple flaw Weibull slope for each penetration results in the clustering of flaws on affected penetrations. This clustering effect may have a strong impact on leakage and ejection probabilities due to the detection, repair, and stability logic. In a sensitivity study, the Weibull slope will only be sampled for each reactor head to demonstrate the relative effect of the sampling strategy.

$$F_{1st} = \frac{1 - 0.3}{6N_{pen} + 0.4} \qquad [B\text{-}9]$$

For each penetration, the characteristic time parameter for the multiple flaw Weibull model, $\theta_{mult,i}$, is calculated from $\beta_{mult,i}$, t_{ref}, and F_{1st} above using Eq. [A-30]. Then, an initiation time for each crack site, $t_{ref,i,loc}$, is sampled from the resulting Weibull distribution. Sampled initiation times are not truncated at t_{ref} as they were for DM welds.

The above approach allows for the initiation of multiple cracks and it can be shown that, on average, a single initiation across all initiation sites is expected prior to t_{ref}, the average time of first initiation based on industry experience.

B.4.4 Crack Initialization

Crack initialization refers here to assigning initial conditions to each crack at its initiation time. These initial conditions include size, location and capacity for growth. The crack mechanisms are fixed by the initiation site, as discussed in Section B.4.1.

Initial crack depth is sampled from a distribution of positive, non-zero, crack depths. This reflects both that the Weibull initiation models discussed above were fit to industry data recording first detection of crack indications and that crack detection is only possible for finite crack sizes. Initial crack lengths are attained by scaling the initial depth by a sampled aspect ratio.

Initiation location is not tracked for ID cracks. ID cracks are assumed to initiate at an arbitrary axial location near the weld top. Similarly, weld cracks are assumed to initiate at the weld center.

Initiation location is tracked for OD cracks. The variability in OD crack axial location affects the crack's susceptibility to leakage; i.e., the OD crack location together with the OD crack length provides a means to predict if the crack has grown long enough to reach the nozzle OD annulus. For OD cracks, the initial axial location is attained by taking a uniform sample between the weld toe and the axial location where the weld residual surface stress falls below 80% of yield stress. For a typical Alloy 600 penetration nozzle, this results in an initiation location threshold of approximately 30-40 ksi. This threshold is larger than the 20 ksi presumed to be required for PWSCC initiation [2], but conservatively results in initiation locations nearer to the OD nozzle annulus. Furthermore, crack initiation locations are likely to be biased toward the higher stress region. The location of 80% of yield was derived from results of J-groove welding residual stress FEA results [1].

In a similar fashion to the DM weld initialization, the capacity for growth of each crack is dependent on sampled crack growth variation terms: f_{weld} and $f_{ww,i}$ for Alloy 182/82 cracks or f_{heat} and $f_{wh,i}$ for Alloy 600 cracks. The accepted

tendency of components that are more susceptible to PWSCC initiation to have higher flaw propagation rates can be included by correlating the sampled f_{weld} and f_{heat} terms with the average time of first initiation, t_{ref}.

B.5 Crack growth model

The RPVHPN crack growth model is similar to the DM weld model in many regards. Namely, both models allow the prediction of PWSCC growth rate as a function of crack geometry, component loading, and other conditions. However, the RPVHPN includes more conditionality due to the various different PWSCC locations and mechanisms (e.g., Alloy 600 vs. Alloy 182/82, ID vs. OD, etc.) and the fact that cracking is modeled beyond through-wall crack growth such that ejection can be predicted.

This section details the model augmentation required to make growth predictions of the RPVHPN cracking mechanisms. The new methods for the calculation of stress intensity factors, which are the result of new crack and component geometries, are presented in Sections B.5.1 through B.5.4. The rate equations for crack growth in Alloy 600 are presented in Section B.5.5. Section B.5.6 discusses other special considerations made for predicting growth given the geometry characteristics specific to a RPVHPN component. Section B.5.7 discusses the special considerations made for predicting growth given a stress profile characteristic of a peened component (i.e., with a compressive stress region near the surface).

B.5.1 Stress intensity factor calculation using influence coefficient method

The influence coefficient method for the calculation of stress intensity factor is presented in detail in Section A.5.1. This method assumes that the stress profile acting orthogonally to the crack face (i.e., hoop stresses for the cracking mechanisms of interest in this study) is defined by a polynomial function in the direction of crack depth and is uniform along the crack length. The first of these two conditions is upheld prior to peening provided the second-order polynomial stress profiles described in Equation [B-7]. The second condition, stress profile uniformity along the crack length, is not upheld in reality due to the rapidly changing residual stress distributions near the J-groove weld. For modeling purposes, the stress results extracted from FEA on the approximate vectors shown in Figure B-5 are assumed uniform over the crack face; as can be observed from the hoop stress contour plot, these vectors tend to lie over more severe stress magnitudes, for the respective crack type.

The general form of the stress intensity factor calculation, for a second-order stress profile, by way of the influence coefficient method is:

$$K = \left[\sigma_0 G_0 + \sigma_1 G_1 \left(\frac{a}{D} \right) + \sigma_2 G_2 \left(\frac{a}{D} \right)^2 \right] \sqrt{a\pi} \qquad \text{[B-10]}$$

where the G terms are the influence coefficients specific to the crack and component geometries and the location on the crack. Once again, D is a general dimension equal to the penetration nozzle thickness for ID and OD locations and equal to the weld path length for weld locations.

The influence coefficients are interpolated from tables built by way of finite element parametric analyses. In the DM weld study, lookup tables were used for ID, semi-elliptical, surface cracking (Tables 15 and 39 of Reference [2]). Tables 16 and 44 of the same Reference [2] provides lookup tables for OD, semi-elliptical, surface cracks. Interpolation and extrapolation of these tables use the criteria presented in Table A-1.

The calculation of stress intensity factors for weld cracks is not as clear as for the ID or OD crack locations. This is because there are no pre-determined influence coefficient lookup tables for cracks with the unique boundary conditions of the J-groove weld. As an approximation, cracks at the weld locations are treated as being on a flat plate with a thickness equal to the reactor head thickness, t_{head}. Under this assumption, the influence coefficients may be interpolated from either the ID or OD lookup tables, using an R_i/t lookup value of 1000 and a through-wall fraction lookup value of a/t_{head}. For an R_i/t ratio value of 1000, both the ID and OD solutions have asymptotically converged to the solution for a flat plate.

B.5.2 Stress intensity factor calculation using weight function method

After peening, the stress profile cannot be defined accurately by a polynomial function in the through-wall direction so the more versatile weight function method is used to calculate stress intensity factors.

The weight function method is fully detailed for calculating stress intensity factors of DM weld cracks in Section A.5.2. Since the methodology outlined in that section adequately covers stress intensity factor calculation at RPVHPN locations, no new information is given here.

B.5.3 Stress intensity factor calculation for through-wall axial cracks

If an axial OD crack goes through-wall prior to reaching the nozzle OD annulus, growth continues in the length direction. In this case, the semi-elliptical crack shape assumed in Sections B.5.1 and B.5.2 breaks down and a through-wall model is required to accurately predict stress intensity factor at the crack tips.

Reference [2] provides an influence coefficient method for the prediction of stress intensity factor of a rectangular through-wall crack. The influence coefficient equation is:

$$K = \sigma_m F_m \sqrt{c\pi} \qquad \text{[B-11]}$$

where c is the half-length of the through-wall crack, σ_m is the membrane elastic stress, and F_m is the lone influence coefficient.

In this study, the membrane elastic stress is approximated as the through-wall average of the total stress profile, attained by taking the analytical integral of the total stress polynomial. It is noted that this value does not change after peening because of the peening force balancing term; as a corollary, peening does not act to slow the growth of through-wall axial cracks in this study.

The influence coefficient is interpolated from a lookup table using the following dimensionless parameter:

$$\lambda = \frac{c}{\sqrt{R_m t}} \qquad \text{[B-12]}$$

where R_m is the mid-radius of the penetration nozzle.

Table 35 of Reference [2] provides an FEA-based lookup table spanning values of λ from 0.2 to 5.0. Conservatively, for the rare case that a crack occurs with a value of λ less than 0.2, the stress intensity factor for λ=0.2 is used. Values of λ greater than 5.0 do not occur for typical RPVHPN geometries because at this size these hypothetical cracks will have reached the nozzle OD annulus resulting in a leak and a transition to the circumferential through-wall crack.

B.5.4 Stress intensity factor calculation for through-wall cracks on the weld contour

In the RPVHPN probabilistic analysis, any crack predicted to leak is assumed to transition immediately to a through-wall crack along the J-groove weld contour. The growth of such cracks is required to be modeled until the nozzle ejection criterion is reached.

Because of the spiral geometry of these cracks, and the complex stress profile along the length of the crack, there exists no parameterized method for predicting stress intensity factors at the crack tips as a function of the stress distribution characteristics (as has been done for all previous K calculations). Instead, stress intensity factors are predicted as a function of crack length exclusively, using FEA results.

References [4] and [5] describe finite element analyses performed to predict stress intensity factors at the tips of through-wall cracks growing along the contour of RPVHPN J-groove welds, from both the uphill and downhill sides of the nozzle, at various elevations. These analyses include effects of welding residual stress and operational loads. Both analyses use the geometry of the outermost nozzle at the subject plant, resulting in a generally bounding welding residual stress profile along the crack face.

Across these studies, the most bounding average K versus crack length curves have been selected for use in this probabilistic analysis (those from Reference [5]). Figure B-7 shows these K curves, for the uphill and downhill sides of the nozzle. Linear interpolation is used between FEA evaluated points. (Extrapolation is never necessary because these cracks initiate at 30°, by convention, and ejection of the nozzle occurs at or less than 330°, as will be discussed in forthcoming sections.)

Conservatively, the K curves presented in Figure B-7 are used for all through-wall cracks along the J-groove weld contour, regardless of the penetration angle of the nozzle being simulated.

Finally, although the analyses in References [4] and [5] are state-of-the-art, and are expected to give relatively accurate results in comparison to similar analyses performed in the nuclear industry, there still exists large uncertainty given welding process variation and plant-to-plant geometry variation. To include this uncertainty, a distributed variable, $K_{circ,mult}$, may be used to scale the circumferential through-wall crack K curves. The distribution selected for this variable is discussed in Section B.8.3.2.

B.5.5 MRP-263 crack growth rate model for Alloy 182/82 (weld) and MRP-55 crack growth rate model for Alloy 600 (tube)

The model selected in this study to estimate PWSCC crack growth in the Alloy 182/82 weld metal is the same model presented in MRP-263 [6]. This model is fully described in Section A.5.3 for DM welds and accordingly is not represented here.

The model selected in this study to estimate PWSCC crack growth in the Alloy 600 base metal based on CGR data presented in MRP-55 [7]. This model uses the same equation form as the Alloy 182/82 crack growth rate model:

$$\frac{\delta}{\delta t}(d) = e^{-\frac{Q_g}{R}\left(\frac{1}{T}-\frac{1}{T_{ref}}\right)} \alpha f_{heat} f_{wh} \left(K_I - K_{Ith}\right)^b \qquad \text{[B-13]}$$

where d is a general crack dimension (e.g., depth or length). The time-stepping procedure used to solve for RPVHPN crack growth is identical to the one presented for DM welds.

Some of the empirical parameters for Alloy 600 growth differ from those applied to Alloy 182/82 growth; specifically, these are the power-law coefficient α, the crack-tip stress intensity factor threshold K_{Ith}, and the stress intensity factor exponent b. Section B.8.3 presents the derivation of these parameters based on Alloy 600 data.

The additional factors, f_{heat} and f_{wh}, are used to describe the aleatoric uncertainty in the Alloy 600 crack growth rate model. The within-heat variation, f_{wh}, is a

value sampled for each flaw site from a distribution reflective of the growth rate variation observed in laboratory studies of cracks in a controlled Alloy 600 specimen. Similarly, the heat-to-heat growth rate variation, f_{heat}, is a value sampled for each reactor head from a distribution reflective of the growth rate variation observed in laboratory studies of cracks in identically controlled Alloy 600 specimens, after accounting for the within-heat variation. Section B.8.3 describes derivation of these distributions.

The sampled heat-to-heat variation terms may be correlated with the average time of first initiation to simulate the premise that reactor heads that are more susceptible to PWSCC initiation tend to have higher flaw propagation rates.

Finally, for circumferential through-wall cracks growing along the weld contour, a distributed variable, $c_{mult,circ}$, is used to scale the growth rate predicted using Equation [B-13]. This distributed variable is intended to capture the possibility of the growth rate being accelerated by the concentrated chemical environment that may develop in the annulus on the nozzle OD above the weld. The potential for chemical concentration in the annulus is discussed in MRP-55 [7]. The distribution selected for this variable is discussed in Section B.8.3.2.

B.5.6 Special considerations for crack growth on RPVHPNs

This section discusses the special constraints and interactions applied to the various cracking mechanisms modeled for RPVHPNs. Similar to DM welds, these constraints and interactions are imposed by a set of modeling "rules" used to approximate known physical behaviors. While these physical behaviors are complex in nature, the simple set of rules is applied in the probabilistic model in order to capture the most essential growth characteristics.

Axial ID cracks are not given any particularly special modeling considerations. As discussed, these cracks are assumed to initiate at the top of the weld, grow until through-wall, and subsequently transition to the weld contour through-wall growth model.

Axial OD cracks are assumed to initiate below the weld, somewhere between the weld toe and the point where surface stress falls below 80% of yield. If the upper crack tip of an axial OD crack reaches the weld root, i.e., the nozzle OD annulus, the crack transitions to the weld contour through-wall growth model. If the crack depth penetrates through-wall prior to reaching the nozzle OD annulus, the crack transitions to the through-wall axial crack model.

Weld cracks are assumed to initiate at the center of the J-groove weld and grow under the influence of hoop stresses in the weld until reaching the weld root; at this point, the crack transitions to the weld contour through-wall growth model. Weld crack lengths are prevented from growing past the half-width of the weld – the width of the weld half-way along the weld path line as demonstrated in Figure B-8. This is done to approximate the premise that weld cracks would arrest in length growth upon reaching either the penetration nozzle or Alloy 82 weld butter material interface.

As mentioned several times previously, leakage of any crack is immediately followed by the formation of a through-wall crack growing along the J-groove weld contour. The crack is assumed to initiate with a length equivalent to 30° around the weld contour. This assumption has a precedent in MRP-105 [8] and, together with the immediate transition to through-wall growth on the weld contour after leakage, is expected to result in conservative estimates for the time to ejection following leakage.

The program considers the rare case where through-wall crack growth along the weld contour initiates on both the uphill and downhill sides of the penetration nozzle. In this case, the lengths of the uphill and downhill cracks are combined to assess for nozzle ejection (as detailed in Section B.7).

B.5.7 Special considerations for crack growth on a peened surface

The special considerations made for predicting growth in a component with a stress profile characteristic of a peened component (i.e., with a compressive stress region near the surface) are the same as those expressed for a DM weld component in Section A.5.5: accounting for crack closure and "balloon" growth. The strategies used to account for these effects on RPVHPN cracks are identical to those used on DM weld cracks.

Separate sensitivity studies are presented later to demonstrate the relative effect of the crack closure and "balloon" growth on ejection probability of RPVHPNs.

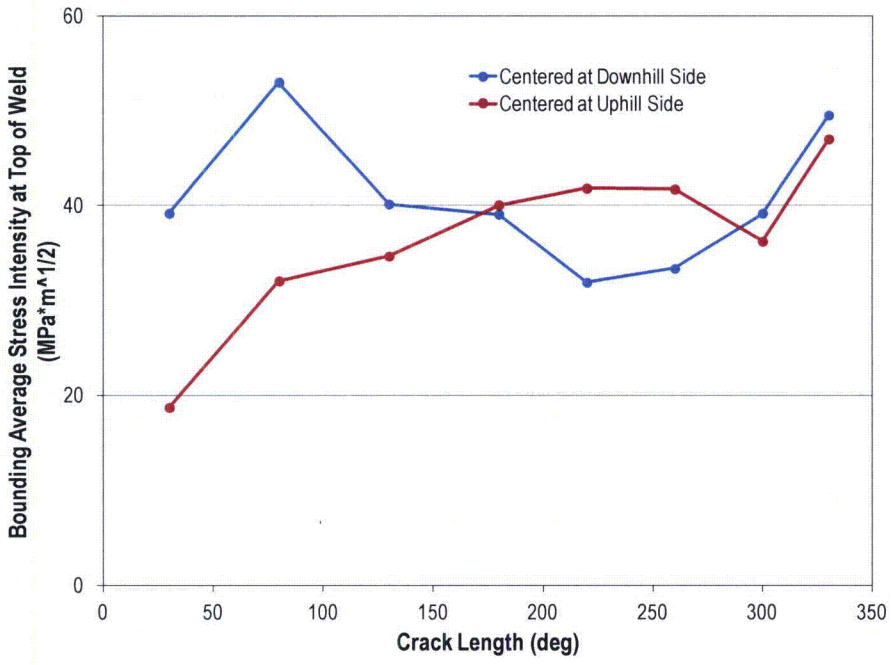

Figure B-7
Modeled Average Stress Intensity Factor vs. Crack Length for a Through-Wall Crack along the J-Groove Weld of a RPVHPN [5]

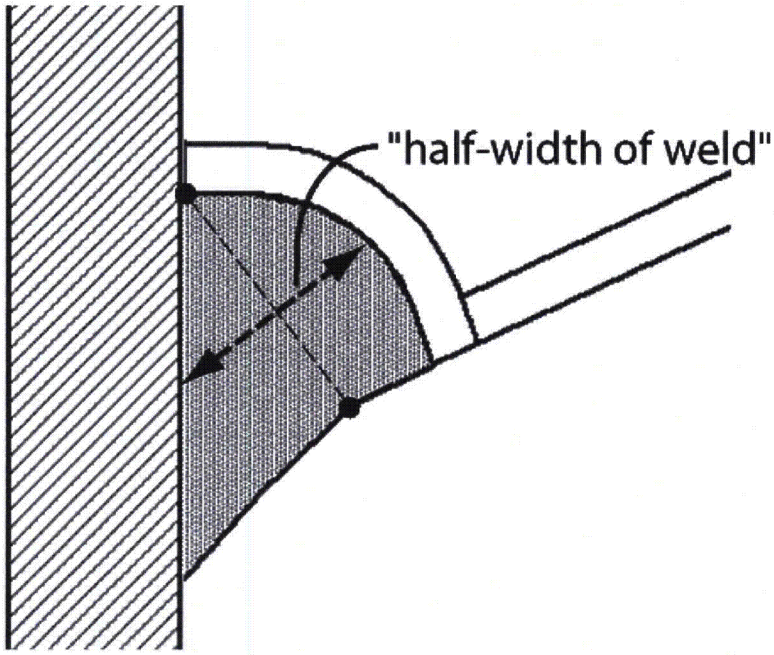

Figure B-8
Description of Weld Half-Width

B.6 Flaw detection model

This section describes the models applied to simulate ultrasonic, eddy current, and visual examinations of RPVHPNs.

Section B.6.1 discusses how examinations are scheduled, before and after peening, Section B.6.2 describes the inspection models, i.e., how POD is modeled factoring for the geometry of the crack. Finally, Section B.6.3 describes the detection and repair modeling rules.

B.6.1 Examination scheduling

UT inspection intervals for unmitigated RPVHPNs (e.g., prior to peening) is based on N-729-1 [9], which gives the maximum number of operating cycles that are permitted between non-visual non-destructive examinations (NDEs) as a function of operating head temperature, cycle length, and capacity factor. The time of the first modeled UT inspection is set by the user.

Bare metal visual (BMV) inspection intervals for RPVHPNs are also based on N-729-1, which gives the scheduling interval as a function of the plant's effective degradation years (EDY). The first modeled BMV inspection is scheduled at the same outage of the first modeled UT inspection.

When peening is applied, different examination scheduling requirements and options are included in the model. First, during the peening application outage, immediately prior to peening, a UT and/or an ET inspection can be conducted to simulate a pre-peening inspection.

A follow-up UT examination is included before entering the relieved in-service inspection (ISI) schedule. In this study, the follow-up inspection is varied from 1 to 3 cycles after the peening application.

After the follow-up examination, a new ISI schedule is used. The central goal of this probabilistic modeling effort is to demonstrate that the ISI inspection interval after peening can be elongated, compared to N-729-1 requirements, without increasing the cumulative probability of leakage and ejection over the entire plant life. Accordingly, several different ISI intervals will be trialed after peening and compared to operation without peening.

For the base case, no inspection relief due to peening is given to the BMV intervals prescribed by N-729-1. However, several sensitivity cases explore relived BMV inspection schedules after peening.

B.6.2 Inspection modeling

This section describes the inspection models (i.e., the determination of POD) for UT, ET and BMV inspections. It also defines the coverage of each examination technique.

For DM welds, the POD curve used for UT examinations was the result of a rigorous experimental study. Given the drastically different radius and thickness of a typical penetration nozzle, the UT curve from the DM weld study is not considered applicable here. Instead, the more general POD model described for ET inspections in Section A.6.2 is used for UT inspection modeling of RPVHPNs. Instead of using absolute dimension as the POD argument, through-wall fraction is used to incorporate the dependence of UT performance on both the depth of the crack and the thickness of the component, resulting in the following POD equation:

$$POD_{UT}\left(\frac{a}{t}\right)=\frac{e^{\beta_{1,UT}+\beta_{2,UT}\ln\left(\frac{a}{t}\right)}}{1+e^{\beta_{1,UT}+\beta_{2,UT}\ln\left(\frac{a}{t}\right)}} \qquad \text{[B-14]}$$

Section B.8.4.2 gives the through-wall fraction/POD pairings used to define the probabilistic UT inspection curves for penetration nozzles (i.e., to calculate $\beta_{1,UT}$ and $\beta_{2,UT}$).

It is noted that UT detection of both axial and circumferential through-wall cracks is modeled using an effective crack depth equal to the penetration nozzle thickness, i.e., a through-wall fraction of 1.

It is assumed for the purpose of the probabilistic model that any flaws located exclusively in the J-groove attachment weld are not detectable by UT inspection performed from the ID of the nozzle. In reality, it is possible that flaws in the weld metal that extend close to the fusion line with the base metal might be detectable by the UT examination.

The ET inspection model for penetration nozzles uses the same approach as used for ET modeling in DM welds. Section B.8.4.3 gives the depth size/POD pairings used to define the probabilistic ET inspection curves for penetration nozzles (i.e., to calculate $\beta_{1,ET}$ and $\beta_{2,ET}$).

ET inspection is only modeled for detection of ID axial cracks, given the irregular surfaces of outer RPVHPN locations.

BMV inspections are given a constant POD of p_{BMV} for leaking penetrations (i.e., RPVHPN with through-wall cracking to the nozzle annulus).

B.6.3 Detection and repair modeling

After probabilities of detection for the various examination methods have been calculated, detection is modeled in the same probabilistic manner as described for DM welds in Section A.6.3, including the capability to correlate back-to-back crack inspections.

Leaking nozzles are inspected with the BMV probability a single time, regardless of the number of leaking cracks present on the nozzle.

If a crack is identified on a penetration, before or after the crack leads to leaking, the entire penetration is considered to be repaired or removed from service. The reactor head is assumed to stay in operation after this repair/removal.

Credit can be taken for the condition that the unit(s) of interest have had no flaw detections prior to some user-defined past inspection time. If the detection occurs before this user-defined past inspection time, the Monte Carlo realization for the reactor head is rejected and repeated with newly sampled inputs.

B.7 Nozzle ejection criterion

At the end of each Monte Carlo realization, the probabilistic model discussed in this report stores a limited number of metrics related to the extent of flaw growth and the repair status of individual penetrations and the reactor head as a whole, including the timing and mechanism type of related events. Most importantly, during each realization, the code tracks if any penetration nozzle suffers ejection and, if so, the number of the cycle of the ejection.

Credit can be taken for the condition that the unit(s) of interest have had no nozzle ejections prior to some user-defined past inspection time. If a nozzle is predicted to eject before this user-defined past inspection time, the Monte Carlo realization is rejected and repeated with newly sampled inputs, and the ejection is not counted toward the metric discussed above.

B.7.1 Ejection Criterion

The critical size for a through-wall crack on the circumference of a penetration nozzle is a user-defined constant, in degrees. The choice of critical size for penetration nozzle ejection is discussed in Section B.8.6.

It is noted that credit is taken for penetration nozzle incidence angle when converting crack length to degrees. Specifically, crack angle, Θ, is calculated by the following equation:

$$\Theta = \frac{2c}{2\pi R_m}\cos(\phi) \qquad \text{[B-15]}$$

where ϕ is the penetration nozzle incidence angle. It is noted that this results in a greater effective length for ejection for all non-central nozzles.

B.7.2 Ejection Statistics

One metric of interest in the qualification of peening mitigation for RPVHPNs is the probability of ejection cumulated over all cycles after the time of peening. This probability is compared to the probability of ejection cumulated over the same period for an unmitigated reactor head with no inspection relief. This comparison quantifies the relative difference in ejection risk for unmitigated and peened reactor heads.

A second metric of interest is the incremental probability of ejection during a given cycle. This metric has precedent in MRP-105 [8] and is included in this study. It is defined as the quotient of the number of realizations during which ejection occurred during a given cycle and the total number of trials. This is adjusted to a probability per year by dividing by the number calendar years per cycle.

A third metric of interest is the average ejection frequency (AEF). It is defined as the average number of predicted ejections per reactor head, per year. In this study, a key metric will be AEF calculated from the time of peening to the end of plant life. As discussed in MRP-117 [16] and MRP-105 [8], the effect of nozzle ejection on nuclear safety can be assessed through multiplication of the frequency of nozzle ejection (i.e., the initiating event frequency, IEF) with an appropriate conditional core damage probability (CCDP) value. The resulting core damage frequency (CDF) is typically averaged over long-term operation and compared to the acceptance criteria of Regulatory Guide 1.174. Regulatory Guide 1.174 [17] specifies an acceptable change in core damage frequency of 1×10^{-6} per reactor year for permanent changes in plant design parameters, technical specifications, etc.

For each Monte Carlo realization, a 60 year plant life value has been evaluated. This corresponds to the duration of an original license (40 years) plus an initial renewal (an additional 20 years). The cumulated probability and average frequency of ejection are determined from the time of peening to this plant life value.

B.8 Probabilistic model inputs

The RPVHPN probabilistic modeling framework takes both deterministic and distributed inputs. The values of the deterministic inputs are constant for every Monte Carlo realization. The values of the distributed inputs are determined by sampling probability distributions during each Monte Carlo realization.

The inputs selected for use in the probabilistic model are discussed in Section B.8.1 through B.8.5.

B.8.1 Reactor head geometry, operating time, temperature, and loads

The choice of inputs for geometry, operating time, temperature, and loading are discussed in this section. These inputs are given for the two cases for which results will be presented: a characteristic hot and a cold reactor head. Table B-2 tabulates the hot head case inputs and Table B-3 tabulates the cold head inputs.

There is currently a subpopulation of 24 reactor vessel top heads with Alloy 600 penetration nozzles operating in the U.S. (excluding heads that are scheduled to be replaced by the end of 2014 with nozzles fabricated using PWSCC-resistant Alloy 690 material). Of these 24 heads, 19 operate at cold-leg temperature (i.e., cold heads) and five operate at a temperature significantly above cold-leg temperature (i.e., non-cold heads). The penetration nozzles of these heads are potential candidates for peening mitigation. The characteristics of these plants were incorporated to generate results in this report, inasmuch as possible. Namely, the hottest hot head and hottest cold head temperatures from this subpopulation are used.

B.8.1.1 Reactor Geometry

The penetration nozzle wall thickness and outer diameter used for the hot and cold head are taken as deterministic inputs, assumed constant across penetration nozzles.

The nozzle thickness and OD that are applied for all hot head penetration nozzles are based on information provided in MRP-48 [11] for CEDM nozzles in CE reactor heads. ICI nozzles are modeled with the same geometries, despite the fact that, in reality, ICI nozzles have larger ODs and smaller thicknesses. This simplification is not considered to be non-conservative because reviews of plant experience and inspection history have not uncovered any reports of PWSCC on ICI components [12].

The nozzle thickness and OD that are applied for all cold head penetration nozzles are based on information provided in MRP-48 for CRDM nozzles in Westinghouse and B&W reactor heads.

The reactor vessel thickness for the hot and cold head is taken as 6.0in, a length that is representative of industry reactor heads.

The number of penetrations and the apportionment of penetration nozzle incidence angles are based on specific plants, for the hot and cold heads. For the hot head, the number of penetrations includes CEDM and ICI nozzles. For the cold head, the number of penetrations includes all CRDM nozzles. A heat vent penetration is not included in this modeling effort.

As discussed in the modeling sections, crack initiation and growth are modeled through the J-groove weld region of the RPVHPNs. For various modeling aspects, some key J-groove weld geometries are required including: the distance from the weld toe to the weld root ("weld toe-to-root distance", the distance from the weld surface to the weld root ("weld path length"), and the weld width halfway along the weld path length ("weld half-width") as depicted in Figure B-8. The variation of these geometries across penetrations was incorporated by fitting normal distributions to inputs for various J-groove weld FEA studies [1] (which span different reactor heads and penetration locations), at the uphill and downhill locations separately[14]. An example of such a fit (i.e., for the uphill weld path length) is given in Figure B-9. Lower and upper truncation limits were set based on engineering judgment and the extreme values from the FEA studies. The distribution parameters for all distributed geometries are given in Table B-4.

The ratio of the weld path length and the weld half-width was found to be approximately constant across penetration nozzles and accordingly was treated as a deterministic input.

B.8.1.2 Operating Time

The hot and cold reactor heads are simulated from plant startup until shutdown. Shutdown is considered to occur approximately 60 years after startup (i.e., a 40-yr original license and a 20-yr license renewal). Cumulative statistics are provided at the end of plant life.

Both reactor heads are assumed to have a capacity factor of 0.92. This value is representative of US PWRs.

Both reactor heads are simulated with 24-month operating cycles. Given the temperatures described in the next section, this results in equal or larger times between inspections, as compared to 18-month operating cycle, using the N-729-1 inspection guidelines.

As discussed in the modeling sections, credit can be taken for the fact that the simulated unit has not experienced ejections or repairs before present day. Monte Carlo realizations that predict ejections or repairs before some user-defined outage are rejected and rerun with new samples. This option is not invoked for the baseline results presented in this report. Accordingly the cumulative probabilities and ejection frequencies that are presented are not conditioned on any assumption of no ejection or repair before some date, and can be thought of

[14] Trends in the geometry characteristics as a function of penetration incidence angle were analyzed. The trends were not strong enough to justify their implementation in this study.

as applying to the general population of reactor heads with characteristics similar to those defined in Table B-2 and Table B-3.

In two sensitivity cases, a user-defined outage, before which it is assumed that no ejections or repairs have occurred, will be set for each of the hot and the cold reactor heads. The statistics presented in these two cases apply conditionally to reactor heads that have experienced no ejections or repairs to date, but otherwise have characteristics similar to those defined in Table B-2 and Table B-3, respectively

B.8.1.3 Temperature

The mean hot and cold head temperatures are based on the highest temperatures of active reactor heads with Alloy 600 RPVHPNs being considered for peening application [10].

Variation in reactor head temperature and measurement error is incorporated into the model by using a normal distribution with a standard deviation of 5°F.

B.8.1.4 Operational Loads

As discussed in the modeling section, operational stresses (i.e., those stresses due to operational pressures and thermal gradients) are required to be separated from welding residual stresses. Results of finite element analyses of J-groove welding residual stresses [1] were used to estimate these operating stresses by subtracting the FEA-predicted stress state present during operation from the welding residual stress state.

The results of these analyses revealed that the penetration nozzle OD and weld surface stresses had negligible contribution from operational loads.

At the penetration nozzle ID, the results of these analyses revealed a distribution on the hoop stress concentration factor, $F_{oper,ID}$, defined in Equation [B-2]. A normal distribution provides an adequate fit to describe the variation in this concentration factor across penetration locations, as demonstrated in Figure B-10.

B.8.1.5 Welding Residual Stresses

Welding residual stress profiles on six vectors of interest (shown in Figure B-5) on RPVHPNs were synthesized from the results of J-groove weld FEA analyses [1]. More accurately, curves were fit to the total stress profiles (operational + residual) predicted by FEA analyses and the residual stresses are calculated during runtime by subtracting operational stresses from the total stress profiles.

Equation [B-3] describes the second-order polynomial form of the stochastic family of curves fit to the FEA results. The coefficients of each polynomial stress profile are solved each Monte Carlo realization based on the constraint that the total stress curve must pass through sampled stresses at three locations: x/D=0, x/D=1, and x/D=0.5, where:

- x/D=0 is defined as the location where cracks are expected to initiate: the ID above the weld for ID axial cracks, the OD below the weld for OD axial cracks, or the weld surface center for weld cracks.
- x/D=1 is defined as the location toward which cracks are expected to grow: the OD above the weld for ID axial cracks, the ID below the weld for OD axial cracks, or the weld root for weld cracks.
- x/D=0.5 is defined as being halfway between the previous two locations.

Equations [B-4] through [B-6] give parameterized equations for the stresses at x/D=0, x/D=1, and x/D=0.5. Uncertainty inherent in data, as well as the uncertainty due to unknown variation of missing data, is introduced by allowing distributed inputs for the parameters in these equations: the surface stress, $\sigma_{0,tot}$, the gradient quantifier, $R_{1,tot}$, and the curvature quantifier, $R_{0.5,tot}$.

For each location of interest, a semi-analytical, iterative procedure was used to derive parameter distributions that resulted in a family of stress profile curves that bound the data and provide an adequate excess of uncertainty. Fifty instances from each of these families of curves, overlaid on the FEA data, are shown for each location of interest in Figure B-11 through Figure B-16 (the median stress profile is shown with a dotted black line). The parameter distributions used to make these families of curves are summarized in Table B-5. Conservatively, a minimum of zero is used for all parameters to ensure tensile hoop stresses at the three interpolated depths.

Table B-2
Summary of Inputs Specific to Hot Reactor Vessel Closure Head

Symbol	Description	Source	Units	Distrib. Parameter	Value for Base Case
	Number of operating cycles	Selected to yield desired cumulative operating time	Nondim		30
	Nominal cycle length	Upper end for cycle length of US PWRs	yr		2.0
CF	Operating capacity factor	Representative capacity factor for US PWR	Nondim		0.92
	EOC of first UT inspection	Selected based on history of unit serving as characteristic hot head	Nondim		12
	EOC of assumed past inspection	Not used for base case study.	Nondim		N/A
	UT inspection frequency	N-729-1	$(\#\ cycles)^{-1}$		1
	BMV inspection frequency	N-729-1	$(\#\ cycles)^{-1}$		1
N_{pen}	Number of modeled penetrations	Selected based on properties of unit serving as characteristic hot head	Nondim		89
	Incidence angles for penetrations	Selected based on properties of unit serving as characteristic hot head	degrees	type	discrete list
				average	34.0
				min	0.0
				max	56.1
t	Nozzle thickness	Representative of CEDM nozzle thickness of unit serving as characteristic hot head	m		0.0158
D_o	Nozzle outer diameter	Representative of CEDM nozzle OD of unit serving as characteristic hot head	m		0.1016
t_{head}	Reactor head thickness	Representative of industry PWRs	m		0.152
T	Operating temperature	Selected based on properties of unit serving as characteristic hot head	°F	type	Normal
				mean	600.0
				stdev	5.0
				min	570.0
				max	630.0
P_{op}	Normal operating pressure	Representative normal operating pressure	MPa		15.5

Table B-3
Summary of Inputs Specific to Cold Reactor Vessel Closure Head

Symbol	Description	Source	Units	Distrib. Parameter	Value for Base Case
	Number of operating cycles	Selected to yield desired cumulative operating time	Nondim		30
	Nominal cycle length	Upper end for cycle length of US PWRs	yr		2.0
CF	Operating capacity factor	Representative capacity factor for US PWR	Nondim		0.92
	EOC of first UT inspection	Selected based on history of unit serving as characteristic cold head	Nondim		6
	EOC of assumed past inspection	Not used for base case study.	Nondim		N/A
	UT inspection frequency	N-729-1	$(\#\ cycles)^{-1}$		3
	BMV inspection frequency	N-729-1	$(\#\ cycles)^{-1}$		3 prior to 8.0 EDY 1 after 8.0 EDY
N_{pen}	Number of modeled penetrations	Selected based on properties of unit serving as characteristic cold head	Nondim		78
	Incidence angles for penetrations	Selected based on properties of unit serving as characteristic cold head	degrees	type	discrete list
				average	31.8
				min	0.0
				max	48.8
t	Nozzle thickness	Representative of CRDM nozzle thickness of unit serving as characteristic cold head	m		0.0158
D_o	Nozzle outer diameter	Representative of CRDM nozzle OD of unit serving as characteristic cold head	m		0.1016
t_{head}	Reactor head thickness	Representative of industry PWRs	m		0.152
T	Operating temperature	Selected based on properties of unit serving as characteristic cold head	°F	type	Normal
				mean	561.0
				stdev	5.0
				min	531.0
				max	591.0
P_{op}	Normal operating pressure	Representative normal operating pressure	MPa		15.5

Table B-4
Summary of Weld Geometry Inputs

Symbol	Description	Source	Units	Distrib. Parameter	Value for Base Case
	Representative length from weld surface to weld root, uphill	Finite element analyses of J-groove weld residual stresses; across various penetration geometries	in	type	Normal
				mean	1.05
				stdev	0.18
				min	0.5
				max	1.7
	Representative length from weld surface to weld root, downhill	Finite element analyses of J-groove weld residual stresses; across various penetration geometries	in	type	Normal
				mean	0.97
				stdev	0.23
				min	0.5
				max	1.7
	Representative length from weld toe to weld root, uphill	Finite element analyses of J-groove weld residual stresses; across various penetration geometries	in	type	Normal
				mean	1.38
				stdev	0.30
				min	0.8
				max	2.9
	Representative length from weld toe to weld root, downhill	Finite element analyses of J-groove weld residual stresses; across various penetration geometries	in	type	Normal
				mean	1.36
				stdev	0.37
				min	0.8
				max	2.9
	Ratio of weld path length to weld half-width, uphill	Finite element analyses of J-groove weld residual stresses; across various penetration geometries	Nondim		1.62
	Ratio of weld path length to weld half-width, downhill	Finite element analyses of J-groove weld residual stresses; across various penetration geometries	Nondim		1.24

Table B-5
Summary of Loading Inputs for RPVHPN Weld Model

Symbol	Description	Source	Units	Distrib. Parameter	Value for Base Case
$f_{oper,ID}$	Penetration ID hoop stress concentration factor	Finite element analyses of operational stresses on CRDM nozzle; across various penetration angles	Nondim	type	Normal
				mean	3.48
				stdev	0.73
				min	0
				max	7.85
$\sigma_{0,tot,1}$	Total hoop stress at penetration ID above weld, uphill	Finite element analyses of J-groove weld residual stresses (14 independent analyses)	MPa	type	Normal
				mean	282.6
				stdev	50.6
				min	0.0
				max	586.2
$\sigma_{0,tot,2}$	Total hoop stress at penetration OD below weld, uphill	Finite element analyses of J-groove weld residual stresses (14 independent analyses)	MPa	type	Normal
				mean	370.8
				stdev	68.4
				min	0.0
				max	781.2
$\sigma_{0,tot,3}$	Total hoop stress at weld surface center, uphill	Finite element analyses of J-groove weld residual stresses (14 independent analyses)	MPa	type	Normal
				mean	413.5
				stdev	39.5
				min	176.5
				max	650.5
$\sigma_{0,tot,-1}$	Total hoop stress at penetration ID above weld, downhill	Finite element analyses of J-groove weld residual stresses (14 independent analyses)	MPa	type	Normal
				mean	297.7
				stdev	57.2
				min	0.0
				max	640.9
$\sigma_{0,tot,-2}$	Total hoop stress at penetration OD below weld, downhill	Finite element analyses of J-groove weld residual stresses (14 independent analyses)	MPa	type	Normal
				mean	462.5
				stdev	73.1
				min	23.9
				max	901.1
$\sigma_{0,tot,-3}$	Total hoop stress at weld surface center, downhill	Finite element analyses of J-groove weld residual stresses (14 independent analyses)	MPa	type	Normal
				mean	426.0
				stdev	39.8
				min	187.2
				max	664.8

Table B-5
Summary of Loading Inputs for RPVHPN Weld Model (continued)

Symbol	Description	Source	Units	Distrib. Parameter	Value for Base Case
$R_{1,tot,1}$	Gradient quantifier at penetration ID above weld, uphill	Finite element analyses of J-groove weld residual stresses (14 independent analyses)	Nondim	$type_l$	Normal
				$mean_l$	1.11
				$stdev_l$	0.24
				min_l	0.00
				max_l	2.55
$R_{1,tot,2}$	Gradient quantifier at penetration OD below weld, uphill	Finite element analyses of J-groove weld residual stresses (14 independent analyses)	Nondim	$type_l$	Normal
				$mean_l$	0.84
				$stdev_l$	0.14
				min_l	0.00
				max_l	1.68
$R_{1,tot,3}$	Gradient quantifier at weld surface center, uphill	Finite element analyses of J-groove weld residual stresses (14 independent analyses)	Nondim	$type_l$	Normal
				$mean_l$	0.89
				$stdev_l$	0.32
				min_l	0.00
				max_l	2.81
$R_{1,tot,-1}$	Gradient quantifier at penetration ID above weld, downhill	Finite element analyses of J-groove weld residual stresses (14 independent analyses)	Nondim	$type_l$	Normal
				$mean_l$	0.60
				$stdev_l$	0.41
				min_l	0.00
				max_l	3.06
$R_{1,tot,-2}$	Gradient quantifier at penetration OD below weld, downhill	Finite element analyses of J-groove weld residual stresses (14 independent analyses)	Nondim	$type_l$	Normal
				$mean_l$	0.51
				$stdev_l$	0.13
				min_l	0.00
				max_l	1.29
$R_{1,tot,-3}$	Curvature quantifier at weld surface center, downhill	Finite element analyses of J-groove weld residual stresses (14 independent analyses)	Nondim	$type_l$	Normal
				$mean_l$	0.36
				$stdev_l$	0.17
				min_l	0.00
				max_l	1.38

Table B-5
Summary of Loading Inputs for RPVHPN Weld Model (continued)

Symbol	Description	Source	Units	Distrib. Parameter	Value for Base Case
$R_{0.5,tot,1}$	Curvature quantifier at penetration ID above weld, uphill	Finite element analyses of J-groove weld residual stresses (14 independent analyses)	Nondim	$type_l$	Normal
				$mean_l$	1.08
				$stdev_l$	0.09
				min_l	0.54
				max_l	1.62
$R_{0.5,tot,2}$	Curvature quantifier at penetration OD below weld, uphill	Finite element analyses of J-groove weld residual stresses (14 independent analyses)	Nondim	$type_l$	Normal
				$mean_l$	0.87
				$stdev_l$	0.13
				min_l	0.09
				max_l	1.65
$R_{0.5,tot,3}$	Curvature quantifier at weld surface center, uphill	Finite element analyses of J-groove weld residual stresses (14 independent analyses)	Nondim	$type_l$	Normal
				$mean_l$	1.21
				$stdev_l$	0.12
				min_l	0.49
				max_l	1.93
$R_{0.5,tot,-1}$	Curvature quantifier at penetration ID above weld, downhill	Finite element analyses of J-groove weld residual stresses (14 independent analyses)	Nondim	$type_l$	Normal
				$mean_l$	1.46
				$stdev_l$	0.13
				min_l	0.68
				max_l	2.24
$R_{0.5,tot,-2}$	Curvature quantifier at penetration OD below weld, downhill	Finite element analyses of J-groove weld residual stresses (14 independent analyses)	Nondim	$type_l$	Normal
				$mean_l$	0.78
				$stdev_l$	0.09
				min_l	0.24
				max_l	1.32
$R_{0.5,tot,-3}$	Curvature quantifier at weld surface center, downhill	Finite element analyses of J-groove weld residual stresses (14 independent analyses)	Nondim	$type_l$	Normal
				$mean_l$	1.47
				$stdev_l$	0.19
				min_l	0.33
				max_l	2.61

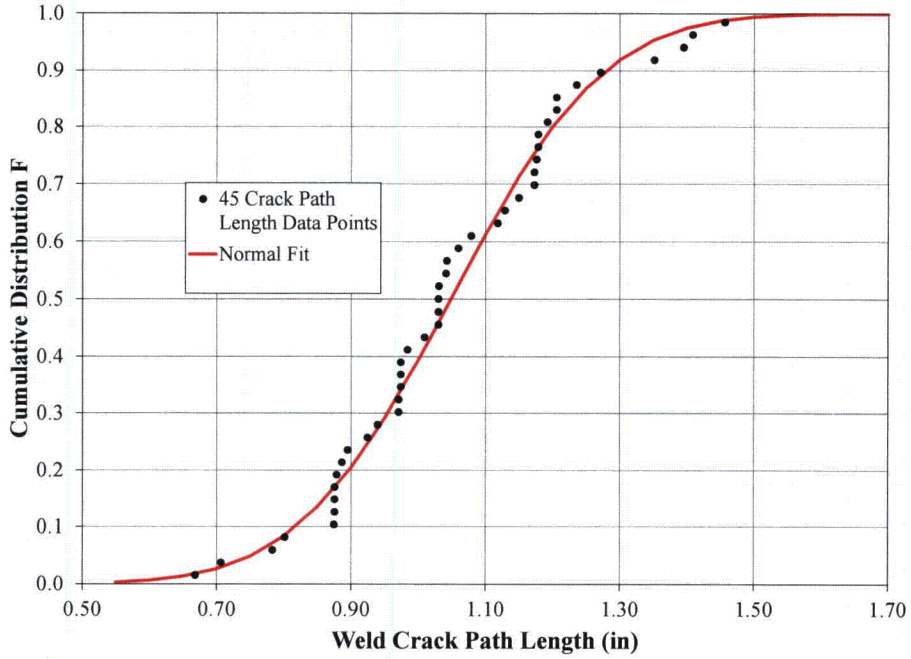

Figure B-9
Example of Normal Distribution Fit to Geometry Data Varying Across Penetration Nozzle Incidence Angles: Uphill Weld Path Length

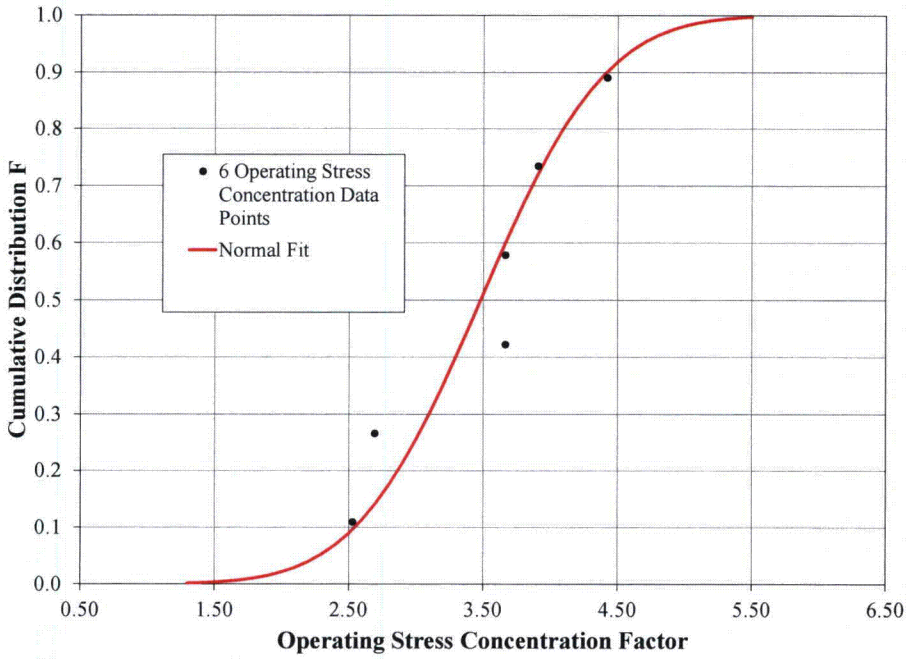

Figure B-10
Normal Distribution Fit to Penetration Nozzle ID Hoop Stress Concentration Factors Predicted by FEA Study

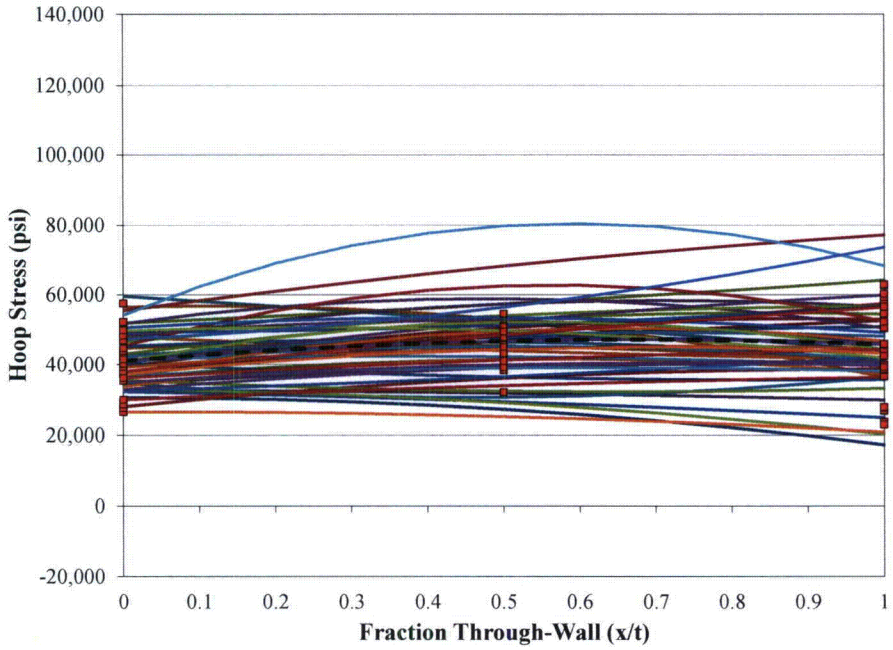

Figure B-11
Stochastic Family (50 instances) of Curves and FEA Results for the Total Stress Profile between the Penetration Nozzle ID Above the Weld and the Penetration Nozzle OD Above the Weld, Uphill Side

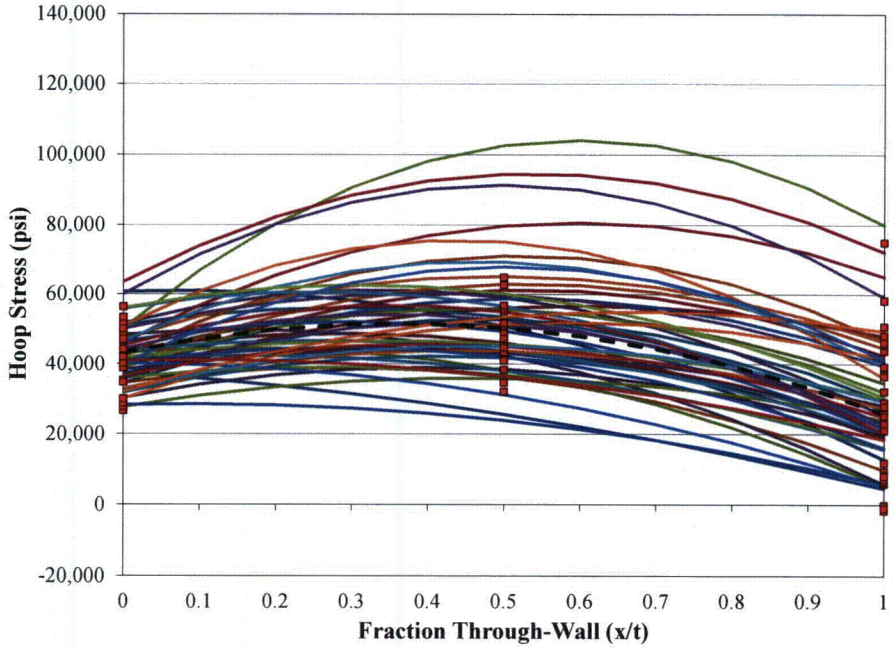

Figure B-12
Stochastic Family (50 instances) of Curves and FEA Results for the Total Stress Profile between the Penetration Nozzle ID Above the Weld and the Penetration Nozzle OD Above the Weld, Downhill Side

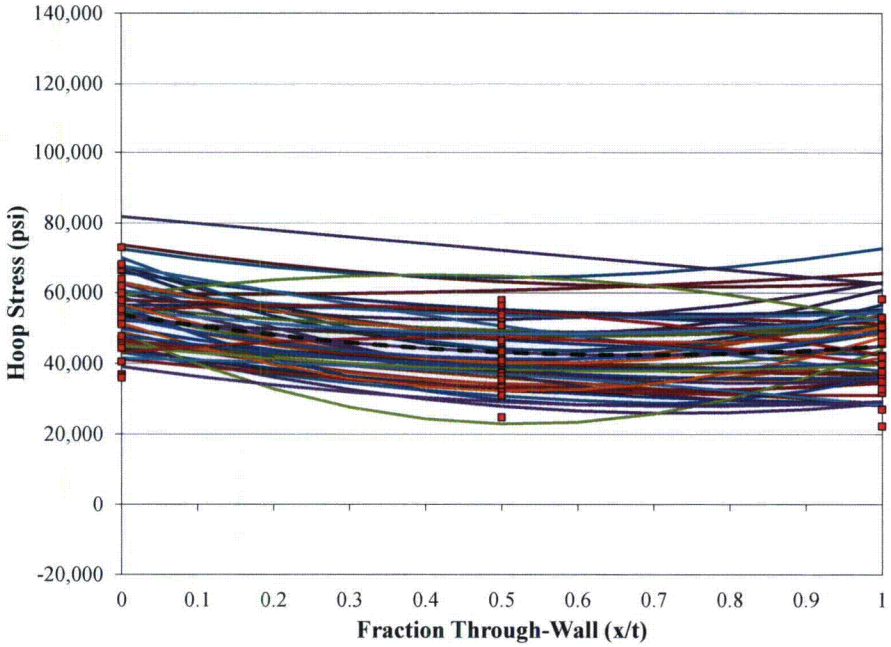

Figure B-13
Stochastic Family (50 instances) of Curves and FEA Results for the Total Stress Profile between the Penetration Nozzle OD Below the Weld and the Penetration Nozzle ID Below the Weld, Uphill Side

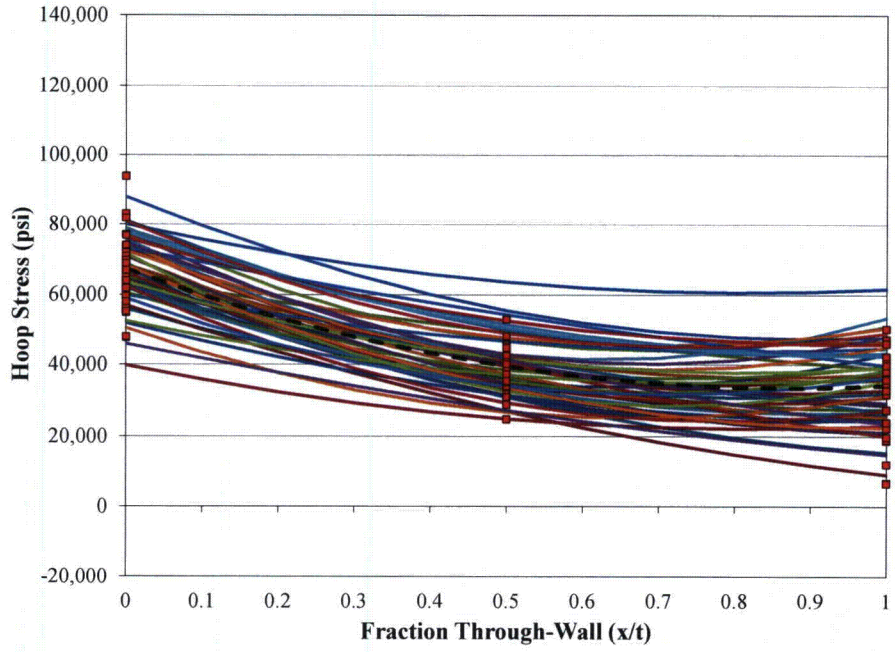

Figure B-14
Stochastic Family (50 instances) of Curves and FEA Results for the Total Stress Profile between the Penetration Nozzle OD Below the Weld and the Penetration Nozzle ID Below the Weld, Downhill Side

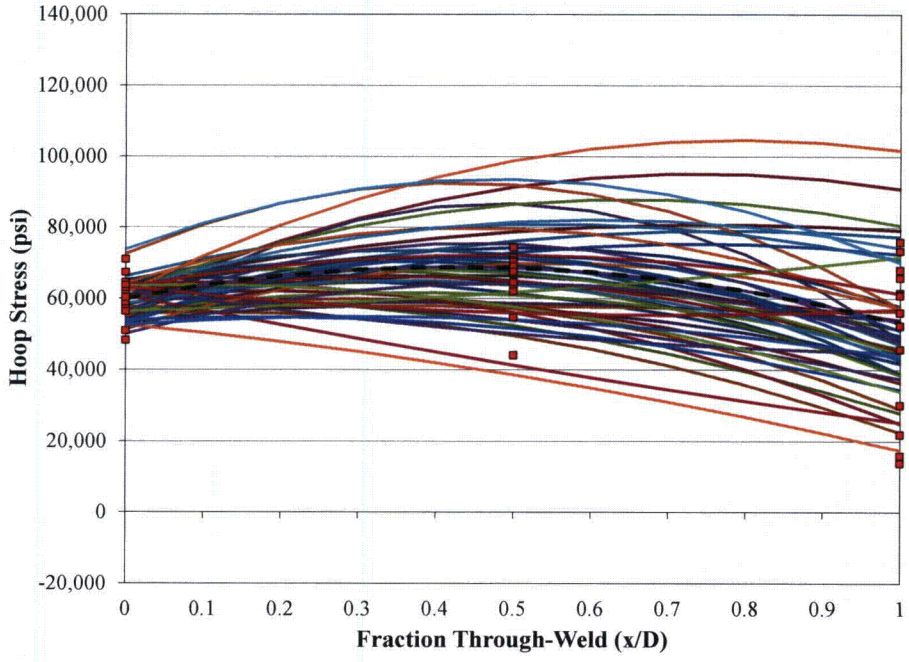

Figure B-15
Stochastic Family (50 instances) of Curves and FEA Results for the Total Stress Profile between the Weld Center and the Weld Root, Uphill Side

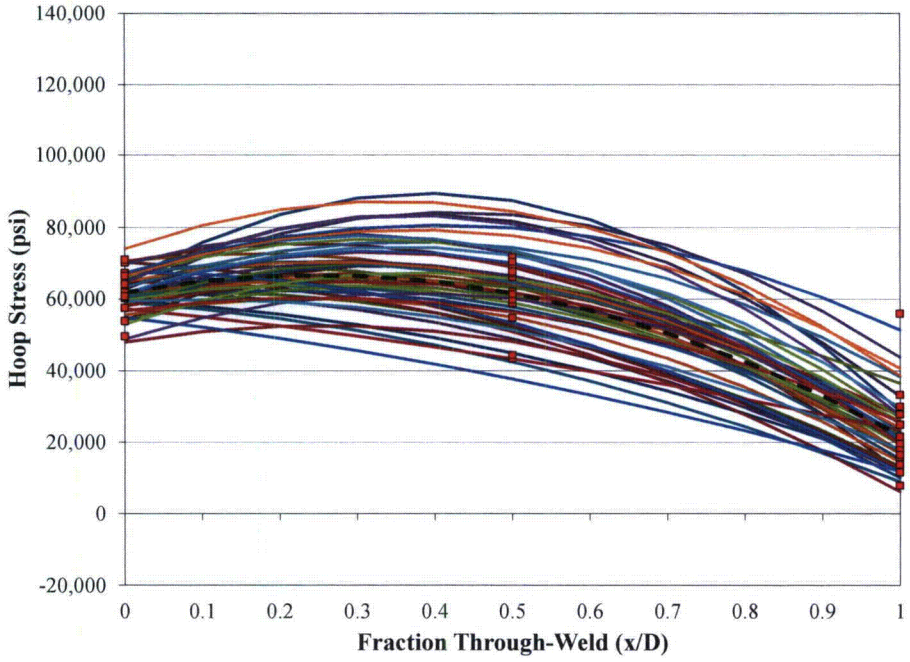

Figure B-16
Stochastic Family (50 instances) of Curves and FEA Results for the Total Stress Profile between the Weld Center and the Weld Root, Downhill Side

B.8.2 Crack initiation model

The set of inputs for the RPVHPN PWSCC initiation model is described in Table B-6 at the end of this section. Various inputs are detailed in the following subsections.

B.8.2.1 Industry Inspection Data used to Develop Initiation Model

Plant inspection data for RPVHPNs fabricated from Alloy 600 with J-groove welds fabricated from Alloys 82 and 182 were evaluated by DEI in MRP 2011-034 [10]. Table B-7 lists the RPVHPNs in which cracking indications were detected that were used in this report.

B.8.2.2 Weibull Fitting Procedure for Average Time of First Initiation

The procedure used to fit a Weibull model to the time of first PWSCC initiation on a reactor head differed from the like procedure for a DM weld, as presented in Section A.8.2. This is principally due to the fact that, generally, more than one cracking indication was discovered on reactor heads during inspection, whereas inspection data for DM welds demonstrate only single cracking indications. In order to estimate the time of the first crack initiation on a particular head, a multiple flaw Weibull slope needed to be assumed; a value of 3.0 was chosen [10]. After the time of first PWSCC initiation on each head was estimated, the Weibull model was determined using a least squares fitting procedure.

B.8.2.3 Analysis Results for Average Time of First Initiation

Figure B-17 shows an example MLE Weibull distribution fit to the industry experience with RPVHPNs fabricated from Alloy 600 with welds from Alloys 82 and 182 given in Table B-8. The failure and suspension times were adjusted to a common reference temperature of 315°C (600°F) using a thermal activation energy of 184 kJ/mole (the mean value given in B.8.2.10).Table B-9 summarizes the MLE fit parameters of the Weibull analysis. Also included in Table B-9 are the standard errors in the Weibull fit parameter, β, and the vertical intercept of the linearized Weibull curve (which is used to determine the value of θ).

It is noted that the standard error in the vertical intercept of the linearized Weibull fit (referred to here as σ_c) is presented because it is used during runtime to account for the uncertainty in the value of the anchor point time, t_1.

B.8.2.4 Uncertainty in First Initiation Time Weibull Slope

The uncertainty in the Weibull slope, β, is modeled with a normal distribution having the mean and standard deviation given in Table B-9. These are the least-squares fit estimators for the slope and the standard error of the slope [13].

B.8.2.5 Uncertainty in Anchor Point Time (t_1)

The anchor point time for the RPVHPN initiation model is calculated for each Monte Carlo realization in the same manner as described for DM welds in Section A.8.2.5.

B.8.2.6 Uncertainty in the Multiple Flaw Weibull Slope

As discussed in the modeling section, a second Weibull model is used to predict the initiation of multiple flaws on a single reactor head. The key input to this model is the Weibull slope.

The slope of the multiple flaw Weibull model, β_{flaw}, quantifies the rate at which flaws occur after the initiation of the first flaw. An analytical data fitting procedure, as done for the first initiation time model, was not considered appropriate to fit β_{flaw} given the modeling complexities involved in sampling multiple flaw initiation times. Instead, a mean value of 2.0 was selected for the β_{flaw}. This value has a precedent in probabilistic modeling of SCC in steam generators [14]. A normal distribution with a mean of 2.0 and a standard deviation of 0.5 is employed to incorporate uncertainties due to material and manufacturing disparities. A lower truncation bound of 1.0 was selected t0 prevent a multiple flaw Weibull model in which the PWSCC initiation rate decreases over time.

A numerical experiment was run with a value of 2.0 for β_{flaw} in order to demonstrate the resulting number of cracks per reactor head, given the parameter distributions discussed throughout this Section B.8. Figure B-18 depicts the resulting distribution of number of flaws in reactor heads with at least a single flaw, at 21.5 EFPY, given an operating temperature of 600°F. The average

number of flaws at 21.5 EFPY, given that at least a single flaw exists, is 12.5. This average number of flaws approximately matches industry data (depicted in Figure B-19) for which the average number of cracking indications per hot reactor head with at least one cracking indication was 14.6.

To account for undetected flaws in industry, namely those located on the J-groove welds, a sensitivity study will be included in which the multiple flaw Weibull model is increased resulting in a higher average number of flaws per head with at least one flaw.

B.8.2.7 Uncertainty in Initial Flaw Location

As discussed in the modeling section, an initial flaw location is required for OD axial flaws. This initial flaw location, together with the sampled weld toe to weld root distance, defines the OD axial crack half-length that would result in the opening of the OD nozzle annulus (i.e., leakage).

For each initiated OD axial flaw, the flaw center location is uniformly sampled between the weld toe and the location where the residual stresses in the penetration nozzle fall below 80% of yield stress. The distance from the weld toe to the 80% yield location (the "80% yield stress length") is taken as a distributed input and is fit to results of finite analysis of J-groove welding residual stresses [1]. The variation in the 80% yield stress length is due to process variation and geometrical variation across different penetration nozzle incidence angles[15].

A unique normal distribution was used for the uphill and downhill sides of the penetration. The resulting fits are shown in Figure B-20 and Figure B-21. The distribution parameters are given in Table B-6.

B.8.2.8 Uncertainty in Initial Flaw Depth

The initial through-wall fraction for each flaw location is sampled at the time of flaw initiation. To remain consistent with the initial through-wall fractions used in the DM weld program (which are based on experimental data for UT inspection of cracking in DM welds), a log-normal distribution with a median of 5% through-wall and an upper 95% confidence bound of 10% through-wall is used. For the penetration nozzle thickness presented earlier (15.8 mm) this results in a median absolute initiation depth of 0.8 mm.

The lower truncation limit was defined to prevent the initiation of very small flaws for which the stress intensity factor (based on the input distributions of the surface welding residual stress) would be significantly less than the range of stress intensity factors (about 15-20 MPa $m^{1/2}$ or 14 to 18 ksi $in^{1/2}$) evaluated in the laboratory studies used to define the flaw propagation models given in MRP-55.

A sensitivity case is used to explore an initial depth distribution that results in cracks that initiate approximately 5 times smaller. This is included to assess the

[15] Trends in the 80% yield stress length as a function of penetration incidence angle were analyzed. The trends were not strong enough to justify their implementation in this study.

potential effect on leakage probability of smaller cracks not being identified during inspections prior to peening.

A second sensitivity study is presented in which cracks initiate with the same *absolute* depths (as opposed to through-wall percentages) used for the DM weld program.

B.8.2.9 Uncertainty in Flaw Aspect Ratio

There was not enough data available for initial RPVHPN crack sizes to allow a distribution to be fit for aspect ratio, as was done for DM weld cracks. Instead, a log-normal distribution was fit to give a modal aspect ratio of 4.0 and a 99% confidence interval aspect ratio of 10.0.

B.8.2.10 Uncertainty in Temperature Effect

The uncertainty in temperature and its effect on initiation is handled in same manner as described for DM welds in Section A.8.2.10.

Table B-6
Summary of Inputs for RPVHPN Initiation Model

Symbol	Description	Source	Units	Distrib. Parameter	Value for Base Case
Q_I	Thermal activation energy for PWSCC flaw initiation	Q distribution based on laboratory data and judgment from experience with Weibull analysis	kJ/mole	type	Normal
				mean	184.23
				stdev	12.82
				min	107.32
				max	261.13
β	Weibull slope for PWSCC flaw initiation on RVCHPs	Flaw initiation data assessed in this report	Nondim	type	Normal
				mean	1.603
				stdev	0.071
				min	1.177
				max	2.029
F_I	Arbitrary failure fraction selected to define Weibull PWSCC initiation function	Selected to reflect failure fractions observed for plant data	Nondim		0.01
t_I	Time at which failure fraction F_I is reached on RVCHPs	Flaw initiation data assessed in this report	EDY	type	Normal
				mean	1.32
				stdev	see σ_c
				min	0.73
				max	2.38
σ_c	Standard error in intercept of linearized Weibull fit	Linearized Weibull fit to flaw initiation data assessed in this report	ln(EDY)		0.159
N_{flaw}	Maximum number of flaws modeled per penetration	Selected to capture PWSCC locations and mechanisms observed in industry RVCHPs	Nondim		6
β_{flaw}	Weibull slope for PWSCC multple flaw initiation on RVCHPs	Based on representative value for formation of PWSCC at multiple locations in industry SGs	Nondim	type	Normal
				mean	2.0
				stdev	0.5
				min	1.0
				max	5.0
T	Component operating temperature	See component-specific tables in this report	°F		
$T_{ref,i}$	Reference temperature to normalize PWSCC flaw initiation data	Temperature used to adjust flaw initiation data assessed in this report	°F		600.0

Table B-7
Summary of Inputs for RPVHPN Initiation Model

Symbol	Description	Source	Units	Distrib. Parameter	Value for Base Case
a_0	Initial depth assigned to newly initiated flaw	Consistency with initial through-wall fractions of DM weld model	m	type	Log-Normal
				linear μ	8.00E-04
				log-norm μ_l	-7.14
				log-norm σ	0.35
				min	5.00E-04
				max	0.0158
AR	General initial aspect ratio assigned to newly initiated flaw	Engineering judgment and aspect ratios for cracks at other locations	Nondim	type	Log-Normal
				linear μ	4.77E+00
				log-norm μ_l	1.50
				log-norm σ	0.34
				min	5.75E-01
				max	35.2336
	Distance from weld toe to location where welding residual stress is equal to 80% of yield stress, uphill side	Finite element analyses of J-groove weld residual stresses; across various units and penetration geometries	in	type	Normal
				mean	0.25
				stdev	0.13
				min	0.00
				max	1.03
	Distance from weld toe to location where welding residual stress is equal to 80% of yield stress, uphill side	Finite element analyses of J-groove weld residual stresses; across various units and penetration geometries	in	type	Normal
				mean	0.24
				stdev	0.06
				min	0.00
				max	0.61

Table B-8
Summary of Flaw Detection Experience in Alloy 600 RPVHPNs with Alloy 182/82 J-groove Welds [10]

Plant	Head Temp	Inspection EDY	Number of Nozzles Inspected	Number of Cracks
AW	551.0	1.57	78	4
G	550.4	2.25	78	1
BS	613.0	3.49	69	12
T	600.1	4.15	65	45
BO	593.9	4.43	69	14
L	595.0	8.55	65	4
BP	595.6	8.63	91	5
AF	586.4	8.93	45	2
AK	597.8	8.94	16	6
AX	601.0	9.74	12	8
AH	602.0	10.35	69	19
AT	600.7	10.71	78	2
J	595.0	11.01	65	2
AG	602.0	11.05	69	14
BI	602.0	13.75	69	8
BL	613.0	13.91	69	5
BC	591.6	15.50	49	1
BB	602.0	16.37	23	5
O	600.1	19.89	30	1
BK	601.0	22.31	9	1

Table B-9
Summary of Weibull Probability Distribution Parameter Fitting for RPVHPN Analysis

Fitting Method	β	θ (EDY)	Standard Error in Weibull Slope	Standard Error in Vertical Intercept (ln(EDY))
Linearized Least Squares	1.603	23.2	0.071	0.159

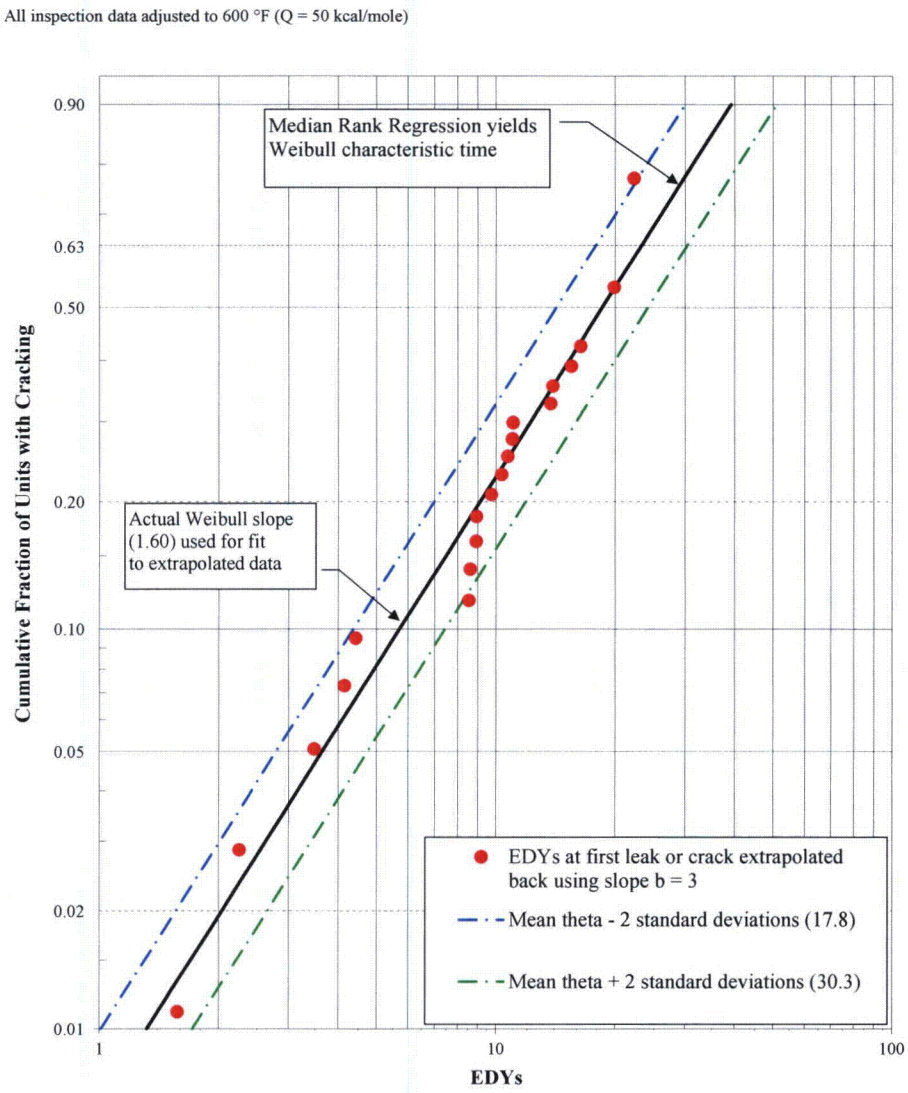

Figure B-17
Example MLE Weibull Probability Distribution for Alloy 600 RPVHPNs with Alloy 182/82 J-groove Welds

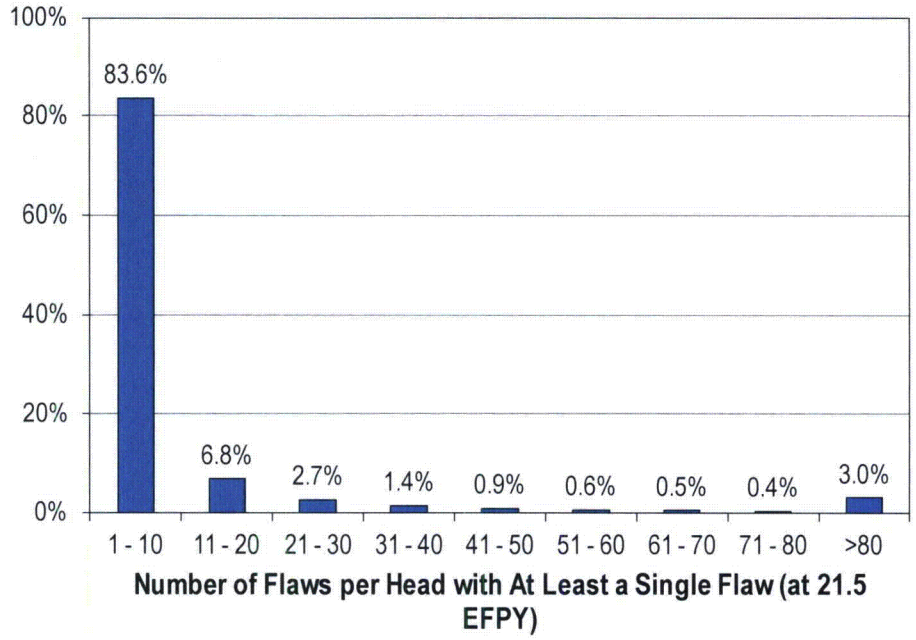

Figure B-18
Result of RPVHPN Numerical Initiation Study: Distribution of Number of Flaws per Hot Head with at Least a Single Flaw

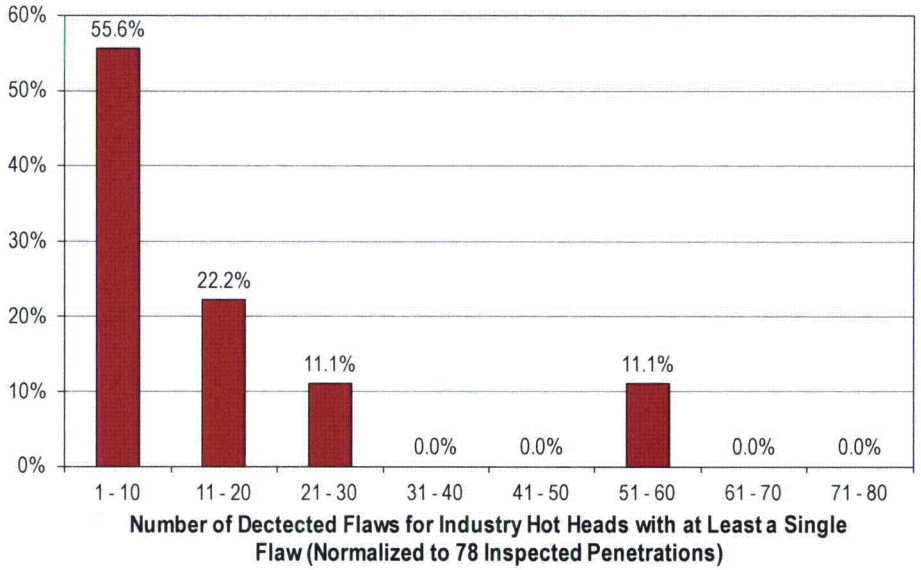

Figure B-19
Industry RPVHPN Flaw Initiation Data: Distribution of Number of Crack Indications per Head with at Least a Single Indication (18 plants)

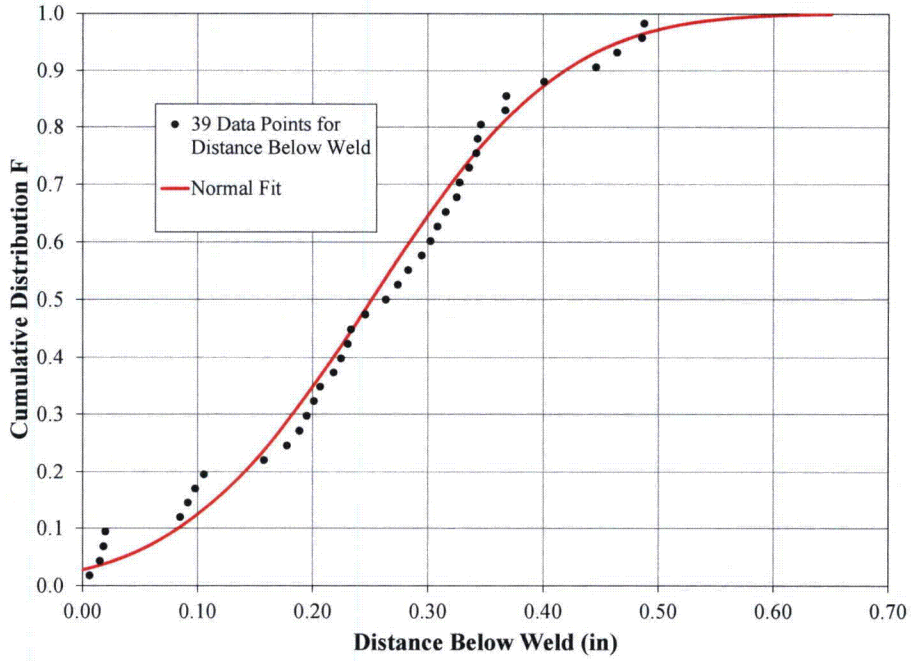

Figure B-20
Normal Distribution Fit to 80% Yield Stress Length on Uphill Side of Penetration Predicted by Different FEA Studies

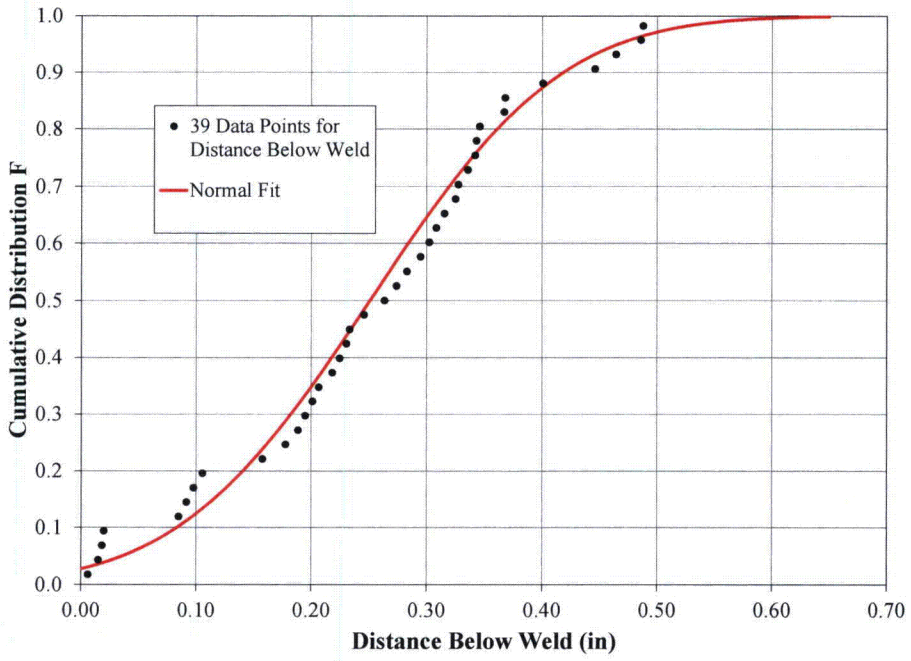

Figure B-21
Normal Distribution Fit to 80% Yield Stress Length on Downhill Side of Penetration Predicted by Different FEA Studies

B.8.3 Crack growth model

The set of inputs for the PWSCC propagation model is described in Table B-10 at the end of this section, including deterministic and distributed inputs. Various inputs are detailed in the following subsections.

B.8.3.1 Empirical Growth Parameters

The empirical growth parameters for Alloy 182/82 weld cracks are identical to those used for the DM weld program (see Section A.8.3.1).

The empirical growth parameters for Alloy 600 are based on the crack growth data compiled and presented in MRP-55 [7]. Instead of using a crack growth curve with a stress intensity factor threshold of 9 (as suggested in MRP-55), a more bounding curve with a stress intensity factor threshold of 0.0 is fit to the data. Both curves are shown with the Alloy 600 CGR data in Figure B-22. The parameters for Alloy 600 curve that will be used in this study are given Table B-10.

B.8.3.2 Growth Variation Factors

The growth variation factor for Alloy 182/82 weld cracks are identical to those used for the DM weld program (see Section A.8.3.2).

Similar to the way growth uncertainty is accounted for in the weld material, the uncertainty of flaw propagation in Alloy 600 is characterized by f_{heat} and f_{wh} parameters.

The f_{heat} parameter is a common factor applied to all specimens fabricated from the same raw material to account for the effects of manufacturing variation. For this study, a log-normal distribution is fit to the heat factors for 26 laboratory heat specimens assessed in MRP-55 (see Figure B-23).

A "within-heat factor" (f_{wh}) describes the variability in flaw propagation rate for different Alloy 600 specimens from the same raw material (heat). A log-normal distribution was developed to describe the variability in f_{wh} for the data generated in MRP-55. The f_{wh} distribution describes the scatter in the flaw propagation rate model that remain after all effects addressed by the model are considered including the particular f_{heat} parameter calculated for the test heat. For this study, a log-normal distribution is fit to the heat factors for 140 laboratory crack specimens assessed in MRP-55 (see Figure B-24).

The lower and upper bounds for the growth variability distributions are set in the same manner as described for DM weld growth variation factors.

In addition to the heat-to-heat and within-heat variation terms, other forms of uncertainty are incorporated for the growth of circumferential through-wall cracks, as discussed in the modeling section. First, for the random multiplicative factor used to scale the FEA-derived K curves, a triangular distribution with a minimum and mode of 1.0 and a maximum of 2.0 is used. This results in a

modestly increased *K* curve to account for any non-conservative bias in the FEA results.

Second, for the environmental factor that scales the length growth rate predicted by the Alloy 600 CGR curve, a triangular distribution with a minimum and mode of 1.0 and a maximum of 2.0 is used. Based on the consensus of the international PWSCC expert panel convened by EPRI in 2001-2002, the crack growth rate for flaws connected to the OD annulus environment is most likely not significantly accelerated due to chemical concentration effects. However, as documented in MRP-55 [7], the expert panel conservatively recommended an environmental factor of 2 for deterministic calculations of growth of circumferential flaws in contact with the annulus environment. The triangular distribution described above was selected based on this work.

B.8.3.3 Uncertainty in Temperature Effect

The uncertainty in temperature and its effect on propagation is handled in same manner as described for DM welds in Section A.8.3.3.

B.8.3.4 Correlation in Relating Flaw Initiation and Propagation

As done for DM welds, the correlation in relating flaw initiation and propagation is neglected for base case analysis.

Table B-10
Summary of Inputs for RPVHPN Flaw Propagation Model

Symbol	Description	Source	Units	Distrib. Parameter	Value for Base Case
Q_g	Thermal activation energy for PWSCC flaw propagation	Q values from MRP-263; stdev based on judgment; see Note 1	kJ/mole	type	Normal
				mean	130
				stdev	5
				min	100
				max	160
				deterministic	130
T	Component operating temperature	See component-specific tables in this report			
f_{weld}	Weld factor: common factor applied to all specimens fabricated from the same weld to account for weld wire/stick heat processing and for weld fabrication	By definition, the median within weld factor is one; Distributions from fits shown in figures of this document	Nondim	type	Log-Normal
				linear μ	1.13
				log-norm μ	0.00
				log-norm σ	0.4895
				min	0.440
				max	2.24
f_{ww}	Within Weld factor: factor accounting for the variability in crack growth rate for different specimens fabricated from the same weld	By definition, the median within weld factor is one; Distributions from fits shown in figures of this document	Nondim	type	Log-Normal
				linear μ	1.07
				log-norm μ	0.00
				log-norm σ	0.3742
				min	0.355
				max	2.04
f_{heat}	Heat factor: common factor applied to all specimens fabricated from the same material to account for manufacturing variations	Fit to heat factors from MRP-55	Nondim	type	Log-Normal
				linear μ	1.68
				log-norm μ	0.00
				log-norm σ	1.016
				min	0.143
				max	5.32
f_{wh}	Within Heat factor: factor accounting for the variability in crack growth rate for different specimens fabricated from the same raw material	Fit to within-heat factors from MRP-55 after normalizing for heat factors	Nondim	type	Log-Normal
				linear μ	1.18
				log-norm μ	0.00
				log-norm σ	0.5695
				min	0.208
				max	3.68

Table B-10
Summary of Inputs for RPVHPN Flaw Propagation Model (continued)

Symbol	Description	Source	Units	Distrib. Parameter	Value for Base Case
ρ_{weld}	Correlation coefficient for PWSCC initiation and propagation of all cracks in Alloy 182/82 weld	No basis for selection of non-zero base case value	Nondim		0.00
ρ_{heat}	Correlation coefficient for PWSCC initiation and propagation of all cracks in Alloy 600	No basis for selection of non-zero base case value	Nondim		0.00
α_{weld}	Flaw propagation rate equation power law constant for Alloy 182/82 weld	Table F-2 of MRP-263	$(m/s)/(MPa\text{-}m^{0.5})^{1.6}$		2.01E-12
b_{weld}	Flaw propagation rate equation power law exponent for Alloy 182/82 weld	Best fit per MRP-263	Nondim		1.6
$K_{ith,weld}$	Flaw propagation rate equation power law constant for Alloy 182/82 weld	MRP-263	$MPa\text{-}m^{0.5}$		0
α_{heat}	Flaw propagation rate equation power law constant for Alloy 600	Derived from MRP-55 data with power law constant of 1.6 and stress intensity factor threshold of 0	$(m/s)/(MPa\text{-}m^{0.5})^{1.6}$		1.97E-13
b_{heat}	Flaw propagation rate equation power law exponent for Alloy 600	Derived to MRP-55 data with stress intensity factor threshold of 0	Nondim		1.6
$K_{ith,heat}$	K_I Stress intensity factor threshold for Alloy 600	Assumed threshold such that all cracks in tensile field have positive growth	$MPa\text{-}m^{0.5}$		0
$T_{ref,g}$	Absolute reference temperature to normalize PWSCC flaw propagation data	MRP-263	°F		617
Δt	Time step size for crack increment	1 month assumed	yr		1/12
$K_{circ,mult}$	Circumferential through-wall crack K curve multiplier	Assumed to assure conservative application of FEA-predicted K curves	Nondim	type mode min max	Triangular 1.0 1.0 2.0
$c_{circ,mult}$	Circumferential through-wall crack environmental factor	Based on anecdotal information about environment effects on circumferential through-wall cracks	Nondim	type mode min max	Triangular 1.0 1.0 2.0
K_{90}	Stress intensity factor at deepest point on crack front	SIF model	$MPa\text{-}m^{0.5}$		calculated by SIF models
K_0	Stress intensity factor at surface point on crack front	SIF model	$MPa\text{-}m^{0.5}$		calculated by SIF models

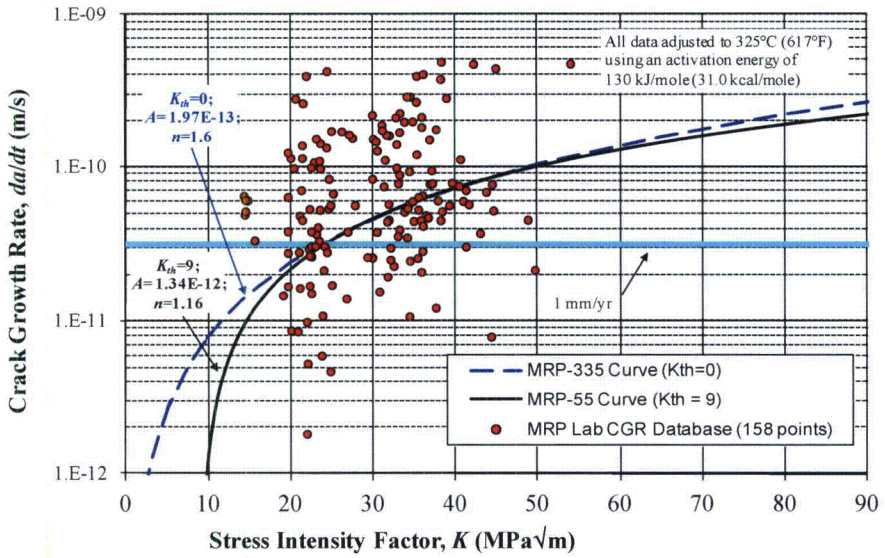

Figure B-22
Alloy 600 Crack Growth Rate Curves: MRP-55 (K_{th}=9) Curve and MRP-335 (K_{th}=0) Curve

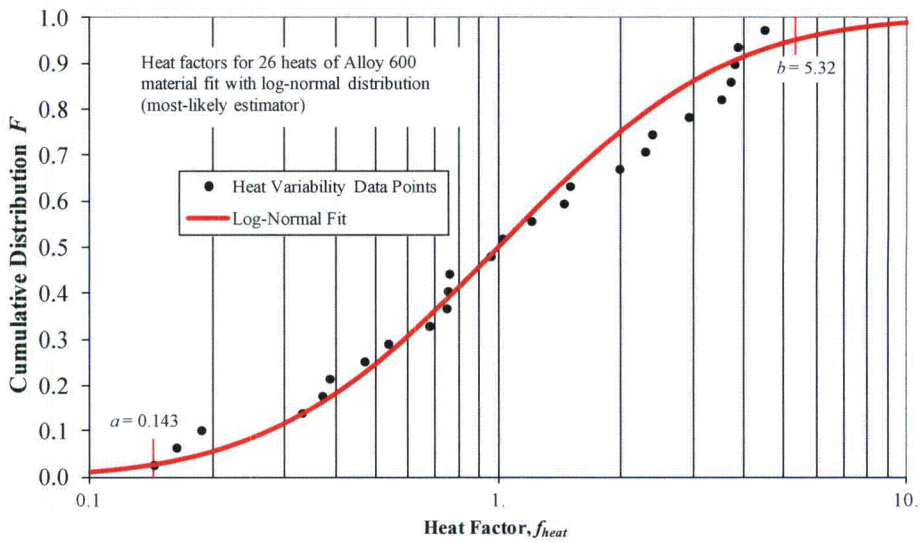

Figure B-23
Heat Factor f_{heat} Distribution with Log-Normal Fit for MRP-55 Alloy 600 Data

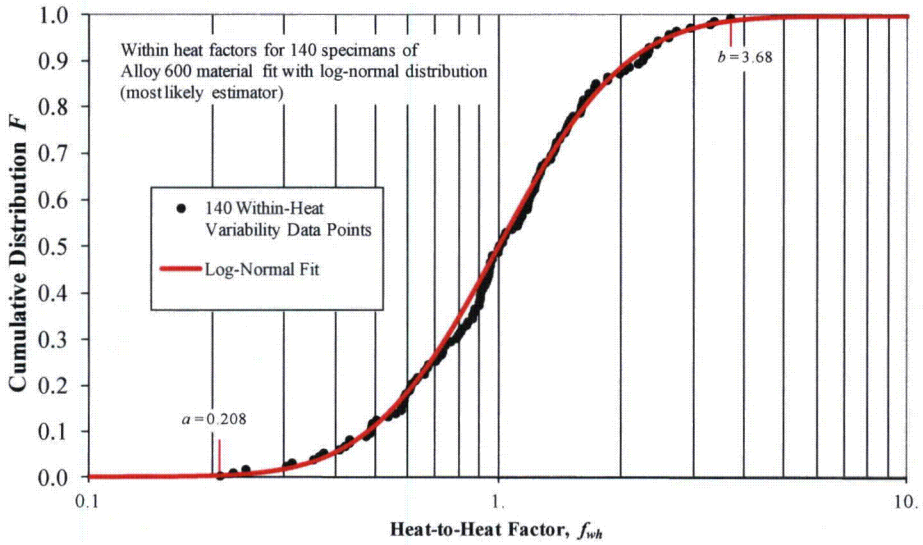

Figure B-24
Within-Heat Factor f_{wh} Distribution with Log-Normal Fit for MRP-55 Alloy 600 Data

B.8.4 Flaw inspection and detection model

The set of inputs for the flaw examination models is described in Table B-11 at the end of this section, including deterministic and distributed inputs. Various inputs are detailed in the following subsections.

B.8.4.1 Examination Scheduling

As mentioned in the modeling section, UT inspection scheduling prior to peening for RPVHPNs is based on N-729-1 [9]. In accordance with this standard, a UT inspection is simulated once every cycle for the hot reactor head (600.0°F operating temperature, 0.92 capacity factor, 24-month operating cycle) and once every two cycles for the cold reactor head (561.1°F operating temperature, 0.92 capacity factor, 24-month operating cycle). The first UT inspection is modeled as occurring at the end of the 12th cycle for the hot reactor head and at the end of the 6th cycle for the cold reactor head. These cycles correspond with the specific units that were used to develop the operating timeline, temperature, geometry inputs discussed in Section B.8.1.

In accordance with N-729-1, BMV inspections for leakage are conducted once every three cycles while a reactor head has less than 8.0 EDY of operation and once every cycle afterward. This BMV schedule is not considered to be relieved by peening by the base case analysis.

In cases where peening is scheduled, the follow-up and in-service inspection intervals are varied to generate comparative results. The follow-up interval is varied between 1, 2, or 3 cycles for both reactor heads. The in-service inspection interval is varied from 3 cycles to the plant lifetime for the hot and cold reactor heads.

For the baseline set of results, ET inspections are not simulated during the pre-peening inspection. This scenario is included as a sensitivity.

B.8.4.2 UT Probability of Detection

The probabilistic UT POD model is described by Equations [A-45] and [A-46]. The model is generated from upper and lower POD curves which each represent a two standard deviation offset from the mean POD curve. The upper bound (favorable) curve was chosen such that there is an 80% POD for cracks 20% through-wall and a 95% POD for cracks 40% through-wall. The lower bound (unfavorable) curve was chosen such that there is a 65% POD for cracks 40% through-wall and a 90% POD for cracks 70% through-wall. Finally, a maximum POD of 95% is used to account for human/equipment error or other factors. The lower, upper, and mean POD curves are shown in Figure B-25.

This curve is based in part on 10 CFR 50.55a(g)(6)(ii)(D), which requires an 80% flaw detection rate for qualification testing of UT procedures and personnel used to inspect RPVHPNs for mockup test blocks. Under the assumption that the test crack sizes are uniformly distributed between 10% and 90%, the mean curve given in Figure B-25 would give a 78% success rate, slightly below a worst-case qualified UT detection instrument.

A correlation coefficient relating the results of successive inspections can be included to take into account the increasing likelihood of non-detection if a crack has already been missed in a previous inspection. Because this value has not been experimentally determined, a modest correlation coefficient of 0.5 is used for the base case input.

B.8.4.3 ET Probability of Detection

The ET inspection model used for crack detection on the penetration nozzle ID is identical to the one presented for crack detection on the DM weld component ID in Section A.8.4.3.

B.8.4.4 BMV Probability of Detection

The BMV inspection model employs a constant POD, irrespective of leak rate, duration of leak, etc. A value of 90% is used based on engineering judgment, and is considered conservatively low based on plant experience that through-wall cracking of CRDM and CEDM nozzles is accompanied by boric acid deposits that are reliably detected during direct visual examinations of the intersection of the nozzle with the upper surface of the reactor vessel head [12].

A strong correlation coefficient, 0.95, is used to correlate successive inspections of the same leaking penetration. It can be shown numerically that this results in approximately a 21%, 17%, and 14% POD for a leaking nozzle at the first, second, and third inspections following an original inspection in which a leaking nozzle was not detected.

Table B-11
Summary of Inputs for RPVHPN Examination Model

Symbol	Description	Source	Units	Distrib. Parameter	Value for Base Case
$(a/t_{U,1,UT}, p_{U,1,UT})$	First defined coordinate for favorable UT POD curve	Engineering judgment, NDE experts, literature	Nondim		(0.2,0.8)
$(a/t_{U,2,UT}, p_{U,2,UT})$	Second defined coordinate for favorable UT POD curve	Engineering judgment, NDE experts, literature	Nondim		(0.4,0.95)
$(a/t_{L,1,UT}, p_{L,1,UT})$	First defined coordinate for unfavorable UT POD curve	Engineering judgment, NDE experts, literature	Nondim		(0.4,0.65)
$(a/t_{L,2,UT}, p_{L,2,UT})$	Second defined coordinate for unfavorable UT POD curve	Engineering judgment, NDE experts, literature	Nondim		(0.7,0.90)
$p_{max,UT}$	Maximum probability of detection for UT inspection	Engineering judgmet	Nondim		0.95
$\rho_{insp,UT}$	Correlation coefficient for successive UT inspections	Engineering judgment	Nondim		0.50
$(a_{U,1,ET}, p_{U,1,ET})$	First defined coordinate for favorable ET POD curve	Engineering judgment, NDE experts, literature	(mm,Nondim)		(0.5,0.5)
$(a_{U,2,ET}, p_{U,2,ET})$	Second defined coordinate for favorable ET POD curve	Engineering judgment, NDE experts, literature	(mm,Nondim)		(0.7,0.75)
$(a_{L,1,ET}, p_{L,1,ET})$	First defined coordinate for unfavorable ET POD curve	Engineering judgment, NDE experts, literature	(mm,Nondim)		(1.0,0.5)
$(a_{L,2,ET}, p_{L,2,ET})$	Second defined coordinate for unfavorable ET POD curve	Engineering judgment, NDE experts, literature	(mm,Nondim)		(1.2,0.75)
$p_{max,ET}$	Maximum probability of detection for ET inspection	Engineering judgmet	Nondim		0.95
$c_{min,ET}$	Minimum detectable crack length	Engineering judgment, NDE experts, literature	mm		2.00
p_{BMV}	Probability of detection for visual inspection of leaking nozzle	Engineering judgment, NDE experts, literature	Nondim		0.90
$\rho_{insp,BMV}$	Correlation coefficient for successive BMV inspections	Engineering judgment	Nondim		0.95

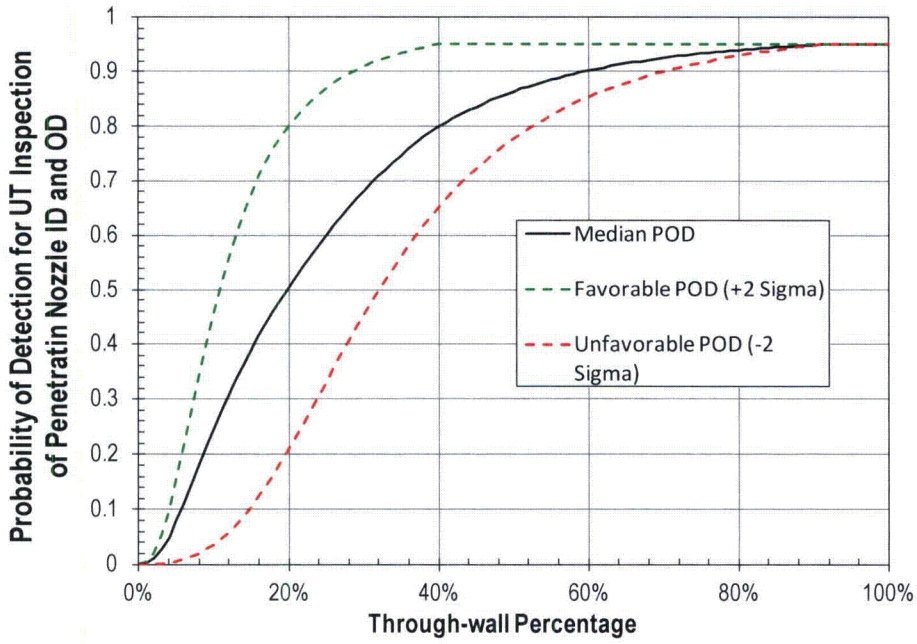

Figure B-25
Assumed POD Curve for UT Inspection of Cracks on the ID or OD of Penetration Nozzle

B.8.5 Effect of peening on residual stress

The set of inputs related to peening considerations is described in Table B-12 at the end of this section, including deterministic and distributed inputs. Various inputs are detailed in the following subsections.

B.8.5.1 Peening Application Scheduling

The peening applications for the hot and cold head are scheduled based on the operating and inspection experience of the subpopulation of reactor vessel heads with Alloy 600 penetration nozzles that are still in service in U.S. PWRs. Peening application is considered to occur during the next cycle that coincides with a scheduled UT inspection.

The hot reactor head has peening scheduled at EOC 17 resulting in 5 UT inspections prior to peening (not including the pre-inspection).

The cold reactor head has peening scheduled at EOC 12 resulting in 2 UT inspections prior to peening (not including the pre-inspection).

B.8.5.2 Post-Peening Residual Stresses

Uncertainty in the peening stresses is incorporated by using distributions for the magnitude of the compressive surface stress and the penetration depth. These distributions were determined based on data and qualitative information provided

by the peening vendors (e.g., Hitachi-GE, Toshiba, MHI, MIC). A full overview of the vendor-supplied data is given in Section A.8.5.2.

Two distinct stresses profiles are required for the modeling of peening on RPVHPNs: peening of the penetration nozzle ID locations and the peening of the penetration nozzle OD and weld locations.

The peening of the penetration nozzle ID is expected to be performed with WJP or ULP. For the bottom mounted nozzle (BMN) geometry, which has a much smaller ID than that for CRDM/CEDM nozzles, the stress measurement data reported in MRP-267 Revision 1 [15] indicate a compressive residual stress depth as small as about 0.5 mm for the WJP method due to the inability to direct the peening jet normal to the ID surface. Even though the ID of CRDM and CEDM nozzles is much greater than that for BMNs, the compressive stress depth for peening of the ID surfaces of RPVHPNs was conservatively based on the residual stress data for BMN mockups treated by WJP. A normal distribution with a mean of 0.5 mm and a standard deviation of 0.125 mm is used to account for process variation and spatial variation. The non-realistic case of negative penetration depth is prevented by using a lower truncation bound of 0 mm. The initial surface stress magnitude distribution is based on WJP and ULP data, as detailed in Section A.8.5.2.

The peening of the penetration nozzle OD and weld locations is expected to be performed with ALP. The ALP vendor indicates that the ALP process is capable of imparting compressive layers as deep as 8 mm depending on the treated material and the chosen ALP process parameters. A normal distribution with a mean of 3.0 mm and a standard deviation of 0.5 mm is assumed. The non-realistic case of negative penetration depth is prevented by using a lower truncation bound of 0 mm. The initial surface stress magnitude distribution is based on WJP and ULP data, as detailed in Section A.8.5.2.

It is noted that application of ALP without a sacrificial ablative layer results in a very thin tensile region near the surface before the compressive region is realized. The thin tensile region lasts approximately 10-30 μm before the 2-5 mm compressive region. The very thin tensile region is not included in the probabilistic model in this study.

Although the very thin tensile region may allow the initiation of very shallow cracks, these cracks would arrest at very small depths (on the order of tenths of millimeters) and are not considered significant. As a result, initiations after ALP are not treated in this study (similar to the treatment of initiation for a general peened surface).

With respect to crack growth (and the calculation of stress intensity factors), the effect of this very thin tensile region is considered negligible due to the relative thinness of the region, compared to 0.8 mm median crack initiation depth, the 2-5 mm compressive stress region and the 15-100 mm component thicknesses that cracks grow through. In reality, the tensile region may result in the growth of very shallow cracks that are not relevant to the study of leakage and ejection.

Finally, the same transition length ratios defined in Section A.8.5.2 are applied for peening stress profiles on RPVHPNs.

B.8.5.3 Effect of Thermal and Load Cycling

The stress relaxation factor for peening applied to DM welds is discussed in Section A.8.5.3.

An analogous stress relaxation study was done by Hitachi-GE [15] using Alloy 600 samples. Analysis of the data from this study yields a slightly lower relaxation factor for Alloy 600 than for Alloy 182/82. This relaxation value is conservatively applied to all locations including welds in the study of RPVHPNs.

B.8.5.4 Effect of Peening on Growth

For base case results, growth of cracks is simulated without consideration for crack closure. This effect is considered as a sensitivity case.

Also for the baseline results, full credit is given to growth of the length of a crack under the peening surface. As discussed in the modeling section, this is done by using the "balloon" growth approximation – neglecting peening stresses for the calculation of length growth. The "balloon" growth approximation is lifted for a sensitivity study.

Table B-12
Summary of Peening-Specific Inputs for RPVHPN Weld Model

Symbol	Description	Source	Units	Distrib. Parameter	Value for Base Case
	Outage of peening application for hot reactor head	Scheduled at next outage coinciding with a UT inspection	EOC		17
	Outage of peening application for cold reactor head	Scheduled at next outage coinciding with a UT inspection	EOC		12
	Number of cycles between peening application and follow-up	MRP-336	# cycles		varied from 1,2,3
	Inspection frequency after peening for hot reactor head	MRP-336	$(\#\ cycles)^{-1}$		varied from 3,5,10,∞
$\sigma_{0,PPRS}(t=0)$	Initial peening stress on applied surface	Vendor-supplied data for fiber laser- and water jet-peened surfaces	MPa	type	Normal
				mean	-544
				stdev	181
				min	-1000
				max	0
$x_{1,PPRS,ID}$	Depth from penetration ID surface where peening stress crosses zero	Information for vendors and vendor-supplied data for fiber laser- and water jet- peened surfaces	mm	type	Normal
				mean	0.50
				stdev	0.125
				min	0.00
				max	1.25
$x_{1,PPRS,ext}$	Depth from penetration OD and weld surface where peening stress crosses zero	Information for vendors and vendor-supplied data for laser shock-peened surfaces	mm	type	Normal
				mean	3.00
				stdev	0.50
				min	0.00
				max	6.00
$f_{1,PPRS}$	Ratio of minimally-affected depth to penetration depth	Engineering judgment	Nondim		2.00
$f_{2,PPRS}$	Fraction of depth between penetration depth and minimally-affected depth where peening results in no effect	Engineering judgment	Nondim		0.70
f_{relax}	Estimated reduction factor of peening residual stresses after approximately 60 years at operational temperatures	Hitatchi experimental data for relaxation of Alloy 600 specimans after WJP	Nondim		0.693
	Flag indicating if crack growth will be predicted considering the effect of crack closure	Crack closure effects are neglected for base case	Logical		False
	Flag indicating if cracks may growth in length without the effect of peening stresses	Cracks are allowed to grow in length without effect of peening to approximate sub-surface balloon growth of crack	Logical		True

B.8.6 Flaw stability model

The two key inputs to the flaw stability model presented in this report are the initial size of a circumferential through-wall crack and the critical crack length at which ejection is predicted to occur. Both are deterministic inputs and are presented in Table B-13.

Via the precedent set in MRP-105 [8], circumferential through-wall cracks along the weld contour are assumed to initiate with a length equivalent to 30° around the weld contour. Together with the immediate transition to through-wall growth on the weld contour after leakage, this is expected to result in conservative estimates for the time to ejection following leakage

The critical crack length for ejection, or net section collapse, is based on calculations presented in MRP-110 (Appendix D of Reference [12]). A length equivalent to 300° around the weld contour is used for all base case analyses in this report in order to bound the critical flaw angles projected for CRDM and CEDM nozzles under standard design pressure in MRP-110. (For a sensitivity case presented later, the critical flaw length is used based on MRP-110 calculations in which a safety factor of 2.7 was applied to the standard design pressure.)

Table B-13
Summary of Inputs for RPVHPN Stability Model

Symbol	Description	Source	Units	Distrib. Parameter	Value for Base Case
$\theta_{circ,init}$	Initial angle for circumfernetial through-wall cracks immediately following leaks	MRP-105	degrees		30
$\theta_{circ,crit}$	Critical flaw angle for nozzle ejection	MRP-110	degrees		300

B.9 Results of probabilistic cases

This section presents results generated using the integrated probabilistic model described in Sections B.2 through B.6, with particular focus on the prediction of the ejection criterion described in Section B.7. Using the inputs described in Section B.8, this section presents predictions for PWSSC on RPVHPNs on a hot and cold reactor head, without peening mitigation (Section B.9.1) and with peening mitigation (Section B.9.2).

Section B.9.3 presents the results of sensitivity studies wherein one or more inputs or modeling methodologies are varied from those described in Sections B.2 through B.8. The aim of these sensitivity studies is to demonstrate the relative change in the predicted ejection risk for a reactor head when an input or modeling assumption is varied.

Because various assumptions and simplifications were involved in the development of the integrated probabilistic model, the magnitudes of the predicted risks for any given case may include a substantial bias error. Accordingly, the more vital conclusions are drawn from the relative differences between risks predicted for different cases (e.g., between the risks predicted for one peening schedule vs. those predicted with a different peening schedule).

B.9.1 Results for the unmitigated case

Using the inputs specified in Section A.8, predictions were made for unmitigated RPVHPNs. Leakage predictions for cold and hot reactor heads are shown in Figure B-26 and Figure B-27; ejection predictions are shown in Figure B-28 and Figure B-29. For these results, volumetric and visual examinations were scheduled based on N-729-1 for unmitigated reactor vessel heads.

For reference, the hypothetical time of peening is shown on these plots. As discussed in the inputs section, this time of peening has been set to coincide with the next UT inspection scheduled after present day. Between the hypothetical time of peening and 60 calendar years (55.2 EFPY), the model predicts a cumulative probability of leakage of 16.8% for the cold reactor head and 20.8% for the hot reactor head; the model predicts a cumulative probability of ejection of 2.8E-05 for the cold reactor head and 7.5E-05 for the hot reactor head. Furthermore, during the same time span, the model predicts an average ejection frequency (AEF) of 8.5E-07 for the cold reactor head and 8.0E-06 for the hot reactor head[16]

These values will be important for assessing the performance of peening for leakage mitigation in the following section.

B.9.2 Results with peening mitigation

As discussed previously, a follow-up inspection is expected to be conducted either one, two, or three cycles after peening, and after the follow-up inspection, a new in-service inspection interval is expected to be utilized through the end of plant life. Various combinations of follow-up inspection time and in-service inspection frequency were used to make leakage and ejection risk predictions after peening. These results are summarized in Figure B-30 and Figure B-31 for the example cold reactor head and in Figure B-32 and Figure B-33 for the example hot reactor head. It is emphasized that a surface inspection is not modeled at the pre-peening inspection for these results (this is addressed as a sensitivity).

These results demonstrate a much larger trend with respect to the ISI frequency than the DM weld results. This is due in large part to the higher likelihood of cracks existing after the pre-peening inspection. It is predicted that one in approximately 800 cold heads and one in approximately 200 hot reactor heads would have unrepaired cracks after the pre-peening inspection.

For both the cold and hot reactor heads, the cumulative probability of leakage after peening is predicted to be reduced by a factor between 7 and 14 times, depending on the post-peening schedule. For example, using a ten-year (one interval) UT inspection frequency, the cumulative probability of leakage after peening is predicted to be reduced by a factor of approximately 11 and approximately 70% of leaks after peening are predicted to occur during one of the

[16] Average ejection frequency was calculated allowing for multiple ejections in a given Monte Carlo realization. Operating cycles for which no ejections were recorded across all Monte Carlo realizations were assumed to have 0.5 ejections.

first two cycles following peening. Figure B-34 demonstrates the decaying nature of leakage probability vs. time after peening, for both the cold and hot reactor head with relieved UT inspection intervals.

For the cold head reactor, the AEF after peening is predicted to improve compared to the unmitigated case when a post-peening ISI frequency of every ten years (one interval) is used. A post-peening ISI of two intervals results in similar ejection risks compared to the unmitigated case: 157%, 97%, and 90% of the unmitigated risk for follow-up inspections scheduled one, two, and three cycles after peening, respectively. This result suggests that it may be beneficial to delay the follow-up inspection to allow more significant cracks to grow such that they are more easily detected at the follow-up inspection, i.e., before entering the ISI schedule.

For the hot head reactor, the AEF after peening is predicted to improve compared to the unmitigated case when using a follow-up time of one or two cycles after peening and a post-peening ISI inspection interval of 3 two-year cycles. Using a post-peening ISI interval of ten years (1 interval) with a follow-up time of one or two cycles after peening results in similar ejection risks compared to the unmitigated case: 102% and 132% of the unmitigated reactor head risk, for follow-up inspections scheduled one and two cycles after peening, respectively.

It is important to consider the maximum incremental frequency of ejection (IEF) for any cycle, in addition to the AEF, in order to understand how concentrated the risk may be over particular spans of time and if there are particular cycles with considerably higher risk. For instance, for a peened cold reactor head (with a follow-up inspection two cycles after peening and an ISI interval of 10 cycles), the ratio of maximum IEF to AEF is 3.05. The same ratio for the unmitigated cold reactor head is 2.36. For a peened hot reactor head (with a follow-up inspection one cycle after peening and an ISI interval of 5 cycles), the ratio of maximum IEF to AEF is 2.56. The same ratio for the unmitigated hot reactor head is 1.38. The risk concentration is not substantially worse for the peened case than for the unmitigated case.

Comparing the leakage and ejection statistics recorded for the reactor head as a whole and the statistics recorded for individual nozzles, it is possible to draw conclusions regarding the number of incidences per reactor head assuming that the head has one of more of such incidences. For instance, hot reactor heads that are predicted to have one or more leaking penetrations between peening and the end of life are anticipated to have approximately 12 leaking penetrations; hot reactor heads that are predicted to have one or more ejected penetration nozzles between peening and the end of life are anticipated to have approximately 2 ejections (under the assumption that a unit would continue operating without head replacement after the first ejection).

Finally, some location-specific information is outputted by the RPVHPN program. This information indicates that leakage is approximately 4 times more likely at weld locations (under the previously stated assumption that initiation is as likely on the J-groove weld as on the penetration nozzle). This is due to the fact that partial cracks on weld locations are assumed to be undetected by UT

inspection and that they are predicted to grow faster (as demonstrated with deterministic calculations in Section 5.2).

B.9.3 Results for sensitivity cases

Various sensitivity studies were conducted with the RPVHPN probabilistic model in order to demonstrate the relative change in the predicted results given one or more changes to modeling or input assumptions. Each sensitivity has been classified as either a Model Sensitivity (in which an approximated input or model characteristic is varied) or an Inspection Sensitivity (in which a controllable inspection option is varied). Sections B.9.3.1 and B.9.3.2 present the sensitivity cases for cold and hot reactor heads, respectively.

B.9.3.1 Cold Reactor Head Sensitivity Cases

The cold reactor head sensitivity cases are described in Table B-14.

The relative changes in the predicted AEF after the hypothetical time of peening, for all sensitivity studies, are given in Figure B-35 (for cases in which peening was applied) and Figure B-36 (for cases in which peening was not applied).

Each of these cases are given a more detailed discussion below:

Cold Head Model Sensitivity Case 1 – Cold Reactor Heads with No Observed PWSCC to Date

Cold Head Model Sensitivity Case 1 explored the result of rejecting Monte Carlo realizations in which crack detection or nozzle ejection was predicted prior to present day. For the cold reactor head, present day was considered to occur 9 cycles, or approximately 18 years, into plant operation. This corresponds with the first inspection time (at 6 cycles) and the hypothetical time of peening (at 12 cycles).

This rejection logic results in probabilities that are conditioned on the premise that no detection or ejection has taken place to date; of the 19 active cold reactor heads with Alloy 600 nozzles, PWSCC has been reported for only two heads to date despite at least one volumetric examination having been performed of all the nozzles in each cold head [10].

Figure B-35 demonstrates that the AEF for a peened reactor head drops 51% when this rejection criterion is enforced. For this Monte Carlo run, approximately 7% of Monte Carlo realizations were rejected suggesting that if a small percentage of units with the most severe initiation and growth are removed from consideration, the average ejection frequency drops substantially. This result may be enlightening for cold reactor heads that have not experienced detected PWSCC and are considering peening.

Cold Head Model Sensitivity Case 2 – Correlation and Initiation Growth

Similar to DMW Model Sensitivity Case 6, this case explored the generally accepted tendency for cracks that initiate earlier to grow faster. It is interesting to note that large increases in ejection risk when such correlation is added for cold heads; the relative change in AEF was 378% and 610% compared to the base case for the peened and unmitigated reactor head, respectively.

This significant increase is due to the fact that any instance of PWSCC that initiates prior to the end of the unit lifetime are considered very early given the 550-570°F temperatures characteristic of a cold reactor head. The growth rates of these cracks could be biased upward of laboratory crack growth rate predictions (assuming that the conditions that led to early initiation also foster more rapid growth).

Cold Head Model Sensitivity Case 3 – Earlier Initiation of First PWSCC

Similar to DMW Model Sensitivity Case 9, this case explored the shifting of the initiation time model to earlier times, compensating for the fact that undetected cracks could not be included to fit the initiation time model. Again, t_1, the time at which 1% of all RPVHPNs are expected to initiate PWSCC, was reduced by a factor of 5.

This shift in the initiation model resulted in 7 to 8 times the risk of ejection. This large increase is partially due to the fact that the multiple initiation model is not temperature-dependent, i.e., once a single initiation occurs, the spread of PWSCC is not slowed by lower temperatures.

Cold Head Inspection Sensitivity Case 1 – Entering Post-Peening ISI without a Follow-Up Inspection & Cold Head Inspection Sensitivity Case 2 – No Pre-Peening Inspection

Cold Head Inspection Sensitivity Case 1 explored that result of skipping the follow-up UT inspection after peening and immediately entering a post-peening ISI with a UT inspection frequency of once every 10 cycles (2 intervals). Cold Head Inspection Sensitivity Case 2 explored that result of skipping the pre-peening UT inspection but conducting a follow-up UT inspection two cycles after peening before entering a post-peening ISI (with a UT inspection frequency of once every 10 cycles). In both cases, BMV inspection was performed according to N-729-1 schedule requirements.

Case 1 resulted in a relative change in the AEF of 432% compared to the base case in which both pre-inspection and the follow-up are conducted; Case 2 resulted in a relative change in the AEF of 234%. This result demonstrates the importance of both the pre-peening and follow-up examination and suggests that the follow-up examination may be the more important of the two in terms of removing significant cracks prior to entering the post-peening ISI schedule.

Cold Head Inspection Sensitivity Case 3 – Surface Inspection Performed During Pre-Peening Inspection

The base case did not include a surface (ET) inspection during the pre-peening examination. Even without surface inspection, peened RPVHPNs operating with select relieved inspection intervals were predicted to have lower or equivalent probabilities of leakage compared to unmitigated RPVHPNs operating with the currently stipulated inspection interval. Cold Head Inspection Sensitivity Case 3 explored what further risk improvement might be anticipated if a surface inspection were to be scheduled during the pre-peening inspection.

The AEF is predicted to be reduced by approximately 20-30% if an ET inspection is performed during the pre-peening inspection. This is far less of an improvement than that demonstrated for the analogous DM weld case. This is because ET inspection is only effective for detecting cracks open to the penetration nozzle ID (and in fact, ET was given no credit for detecting cracks that have grown through-wall from the penetration nozzle OD).

Cold Head Inspection Sensitivity Case 4 through 7 – Various Relief Options for Post-Peening Visual Examinations

As discussed previously, N-729-1 states that unmitigated reactor heads shall be visually examined once every 3 cycles (or 5 years, whatever comes first) until they reach an age of 8.0 EDY, and then shall be examined once every cycle. Cold Head Inspection Sensitivity Cases 4 through 7 explored the use of a different BMV schedule after peening:

- Case 4 performed a single unenforced BMV between the pre-peening and follow-up examination.
- Case 5 continued with two cycle BMV interval even after the plant age reached 8.0 EDY (during its 19th cycle).
- Case 6 used a three-cycle BMV interval after peening.
- Case 7 stopped BMV examinations altogether after peening.

Figure B-35 demonstrates the effect of each BMV scheduling change, relative to the N-729-1 case.

Among the conclusions that can be drawn from these results, the most important is that while inspection relief is justified, intermittent visual examination has a relatively large benefit after peening and is warranted.

The Case 4 result suggests that it may be useful to have multiple follow-up cycles with BMV of a cold reactor head after peening.

B.9.3.2 Hot Reactor Head Sensitivity Cases

The hot reactor head sensitivity cases are described in Table B-15 and Table B-16.

The relative changes in the predicted AEF after the hypothetical time of peening, for all sensitivity studies, are given in Figure B-37 (for cases in which peening was applied) and Figure B-38 (for cases in which peening was not applied).

A handful of intriguing cases have been selected for a more detailed discussion below:

Hot Head Model Sensitivity Case 1 – Hot Reactor Heads with No Observed PWSCC to Date

Hot Head Model Sensitivity Case 1 explored the result of rejecting Monte Carlo realizations in which crack detection or nozzle ejection was predicted prior to present day. For the hot reactor head, present day was considered to occur 16 cycles, or approximately 32 years, into plant operation. This corresponds with the first inspection time (at 12 cycles) and the hypothetical time of peening (at 17 cycles).

This rejection logic results in probabilities that are conditioned on the premise that no detection or ejection has taken place to date; of the five active hot reactor heads with Alloy 600 nozzles (excluding those scheduled for replacement by the end of 2014), PWSCC has been reported for only one head to date (affecting two nozzles) despite multiple volumetric examinations having been performed of all the nozzles in each non-cold head [10].

Figure B-37 and Figure B-38 demonstrate that the AEF for a peened and unmitigated hot reactor head drops 84% and 82%, respectively, when this rejection criteria is enforced. Approximately two of every three Monte Carlo realizations are rejected.

For interested readers, an ejection probability vs. time plot is provided in Figure B-39 for the example hot reactor head. The result has not fully converged in 1E06 Monte Carlo realizations but still demonstrates the general prediction trends (operating cycles with no predicted ejections after present day, across all realizations, are assumed to have 0.5 ejection realizations). This prediction warns that the probability of ejection may quickly ramp up after present day but the risk magnitudes stay very low through the unit lifetime.

Hot Head Model Sensitivity Case 4 – Earlier Initiation of First PWSCC

Similar to Cold Head Model Sensitivity Case 3, this case explored the shifting of the initiation time model to earlier times, compensating for the fact that undetected cracks could not be included to fit the initiation time model. Again, t_1, the time at which 1% of all RPVHPNs are expected to initiate PWSCC, was reduced by a factor of 5.

This shift in the initiation model resulted in 1.5 to 3 times the risk of ejection. However, it is noted that this initiation model results in a prediction of leakage before 20 EFPY in over 95% of hot reactor heads. This is not in line with the industry experience US PWRs.

Hot Head Model Sensitivity Cases 13 and 15 – Removal of Inspection Correlation

As discussed in the modeling and inputs section, the base case assumed correlation between successive inspections, i.e., a crack that goes undetected by a UT examination would be more likely to be missed in subsequent UT inspections (assuming it doesn't grow significantly); a leak that goes undetected by visual examination is more likely to be missed in subsequent visual examinations.

The inclusion of these correlations results in higher probabilities of leakage and ejection because it deters the detection of select cracks and leaks, allowing longer spans of time for growth. When UT inspection correlation is removed, the probability of ejection drops by a factor of approximately 2; when BMV inspection correlation is removed, the probability of ejection drops by a factor of approximately 4.

Hot Head Inspection Sensitivity Case 1 – Entering Post-Peening ISI without a Follow-Up Inspection & Hot Head Inspection Sensitivity Case 2 – No Pre-Peening Inspection

Hot Head Inspection Sensitivity Case 1 explored that result of skipping the follow-up UT inspection after peening and immediately entering a post-peening ISI with a UT inspection frequency of once every 5 cycles (1 interval). Hot Head Inspection Sensitivity Case 2 explored that result of skipping the pre-peening UT inspection but conducting a follow-up UT inspection two cycles after peening before entering a post-peening ISI (with a UT inspection frequency of once every 5 cycles). In both cases, BMV inspection was performed according to N-729-1 schedule requirements.

Case 1 resulted in a relative change in the AEF of 312% compared to the base case in which both pre-inspection and the follow-up are conducted; Case 2 resulted in a relative change in the AEF of 308%. This result demonstrates the importance of both the pre-peening and follow-up examination but does not suggest a preference for one over the other (contrary to findings from the cold reactor head inspection sensitivity cases).

Hot Head Inspection Sensitivity Case 4 through 6 – Various Relief Options for Post-Peening Visual Examinations

As discussed previously, N-729-1 states that unmitigated reactor heads with more than 8.0 EDY shall be visually examined every cycle. Hot Head Inspection Sensitivity Cases 4 through 6 explored the use of a different BMV schedule after peening:

- Case 5 used a two-cycle BMV interval after peening.
- Case 6 used a three-cycle BMV interval after peening.
- Case 7 stopped BMV examinations altogether after peening.

Figure B-37 demonstrates the effect of each BMV scheduling change, relative to the N-729-1 case.

As with the cold reactor head prediction, intermittent visual examination has a relatively large benefit after peening and is warranted.

The use of a relieved BMV after peening results in 139% and 185% increase in AEF for the 2 and 3 BMV interval cases, respectively.

These results may be misleading. The probability of new leakage decays sharply after peening as demonstrated in Figure B-34. As a corollary, the 2-3 fold increase in ejection risk is not due strictly to the BMV frequency relief after the follow-up examination through the remaining life of the plant, but is due predominantly to the schedule relief between peening and the UT follow-up inspection.

Table B-14
Description of Model Sensitivity Cases for RPVHPN Probabilistic Model with Cold Reactor Head Inputs

Category	Case No.	Sensitivity Case		
		Parameter	***Base Case***	***New Value(s)***
Base	0	Base Case: *See table of base case inputs*		
Model Sensitivity	1	Prior Plant Experience *Reject trials with detections/ejections before present day*	Did not apply rejection criterion	Rejected detections/ejections prior to 9 cycles of operation.
	2	Initiation-Growth Correlation *Include correlation*	$\rho_{weld} = 0.0$ $\rho_{heat} = 0.0$	$\rho_{weld} = -0.8$ $\rho_{heat} = -0.8$
	3	Initiation Reference Time *Decrease reference time by factor of 5*	t_1 =1.316 (nominal) 0.73 (lower bound) 2.38 (upper bound)	t_1 =0.2632 (nominal) 0.146 (lower bound) 0.476 (upper bound)
Inspection Sensitivity	1	Inspection Scheduling *Skip follow-up UT inspection and enter ISI immediately*	Performed follow-up UT inspection two cycles after peening before entering ISI with inspection every 10 intervals	Skipped follow-up UT inspection before entering ISI with inspection every 10 intervals
	2	Inspection Scheduling *Skip UT during pre-peening inspection*	Performed UT during pre-peening inspection	Skipped pre-peening UT inspection
	3	Inspection Scheduling *Perform ET during pre-peening inspection*	Did not perform ET during pre-peening inspection	Performed ET during pre-peening inspection
	4	BMV Inspection Schedule *Perform BMV for first two cycles after peening before returning to N-729 schedule*	Performed BMV according to N-729-1 schedule requirements	Performed BMV for first two cycles after peening before returning to N-729 schedule requirements
	5	BMV Inspection Schedule *Perform BMV every two cycles, after peening*	Performed BMV according to N-729-1 schedule requirements	Performed BMV inspection every two cycles, after peening
	6	BMV Inspection Schedule *Perform BMV every three cycles, after peening*	Performed BMV according to N-729-1 schedule requirements	Performed BMV inspection every three cycles, after peening
	7	BMV Inspection Schedule *Do not perform BMV after peening*	Performed BMV according to N-729-1 schedule requirements	Never performed BMV inspection after peening

Table B-15

Description of Model Sensitivity Studies for RPVHPN Probabilistic Model with Hot Reactor Head Inputs

Category	Case No.	Model Sensitivity Case		
		Parameter	***Base Case***	***New Value(s)***
Base	0	Base Case: *See table of base case inputs*		
Sensitivity	1	Prior Plant Experience *Reject trials with detections/ejections before present day*	Did not apply rejection criterion	Rejected detections/ejections prior to 16 cycles of operation.
	2	Penetration Nozzle Geometry *Decrease thickness and OD*	t=0.0158 m D_o=0.1016 m	t=0.00998 m Do=0.0888 m
	3	Peening Penetration Depth *Double standard deviation of peening penetration depths*	$\sigma(x_{1,PPRS,ID})$ =0.125 mm $\sigma(x_{1,PPRS,ext})$ =0.5 mm	$\sigma(x_{1,PPRS,ID})$ =0.25 mm $\sigma(x_{1,PPRS,ext})$ =1.0 mm
	4	Initiation Reference Time *Decrease reference time by factor of 5*	t_1=1.316 (nominal) 0.73 (lower bound) 2.38 (upper bound)	t_1=0.2632 (nominal) 0.146 (lower bound) 0.476 (upper bound)
	5	Multiple Flaw Initiation Model Slope *Increase to 3.0*	β_{flaw}=2.0	β_{flaw}=3.0
	6	Multiple Flaw Initiation Model *Sample slope a single time per head*	Sampled multiple flaw initiation model slope for each penetration	Sampled multiple flaw initiation model slope a single time per head
	7	Initiation-Growth Correlation *Include correlation*	ρ_{weld} = 0.0 ρ_{heat} = 0.0	ρ_{weld} = -0.8 ρ_{heat} = -0.8
	8	Initial Crack Depth *Decrease median by factor of 5and remove minimum*	a_0=0.8 mm (nominal) 0.5 mm (lower bound)	a_0=0.16 mm (nominal)
	9	Growth Integration Time Step *Halve*	1/12 yr	1/24 yr
	10	Initial Crack Depth and Minimum K Value *Decrease median initial crack depth by factor of 5 and remove minimum Impose minimum K value of 12.0*	*See case 8* Minimum allowable K value= 0.0	*See case 8* Minimum allowable K value= 12.0
	11	Crack Closure Methodology *Utilize*	Neglected effect of crack closure on stress intensity factor	Accounted for effect of crack closure on stress intensity factor
	12	Balloon Growth *Prevent*	Neglected peening stresses for crack length growth	Accounted for peening stresses for crack length growth
	13	UT Inspection Correlation *Remove correlation between inspections*	ρ_{insp} = 0.5	ρ_{insp} = 0.0
	14	Probability of Detection *Decrease maximum probability of detection to 90%*	$p_{max,UT}$ = 0.95	$p_{max,UT}$ = 0.90
	15	BMV Inspection Correlation *Removecorrelation between inspections*	$\rho_{insp,BMV}$=0.95	$\rho_{insp,BMV}$=0.0
	16	Ejection Criterion *Decrease critical flaw angle for nozzle ejection*	$\theta_{circ,crit}$=300 deg	$\theta_{circ,crit}$=250 deg
	17	Crack Environmental Factor *Remove*	Used triangular distribution with mode and min of 1.0, and max of 2.0	Used determinstic value of 1.0
	18	Initial Crack Depth *Increase median value*	a_0=0.8 mm (nominal)	a_0=3.5 mm (nominal)
	19	Laser Shock Peening Penetration Depth *Decrease median value*	$x_{1,PPRS,ext}$ = 3.0 mm (nominal)	$x_{1,PPRS,ext}$ =1.0 mm (nominal)

Table B-16

Description of Inspection Sensitivity Cases for RPVHPN Probabilistic Model with Hot Reactor Head Inputs

Category	Case No.	Inspection Sensitivity Case		
		Parameter	***Base Case***	***New Value(s)***
Base	0	Base Case: *See table of base case inputs*		
Sensitivity	1	Inspection Scheduling *Skip follow-up UT inspection and enter ISI immediately*	Performed follow-up UT inspection two cycles after peening before entering ISI with UT inspection every 5 intervals	Skipped follow-up UT inspection before entering ISI with inspection every 5 intervals
	2	Inspection Scheduling *Skip UT during pre-peening inspection*	Performed UT during pre-peening inspection	Skipped pre-peening UT inspection
	3	Inspection Scheduling *Perform ET during pre-peening inspection*	Did not perform ET during pre-peening inspection	Performed ET during pre-peening inspection
	4	Post-peening BMV Inspection Schedule *Perform BMV every two cycles*	Performed BMV inspection every cycle	Performed BMV inspection every two cycles, after peening
	5	Post-peening BMV Inspection Schedule *Perform BMV every three cycles*	Performed BMV inspection every cycle	Performed BMV inspection every three cycles, after peening
	6	Post-peening BMV Inspection Schedule *Do not perform BMV after peening*	Performed BMV inspection every cycle	Never performed BMV inspection after peening

Figure B-26
Prediction of Leakage vs. Time for Cold RPVHPNs

Figure B-27
Prediction of Leakage vs. Time for Hot RPVHPNs

Figure B-28
Prediction of Ejection vs. Time for Cold RPVHPNs

Figure B-29
Prediction of Ejection vs. Time for Hot RPVHPNs

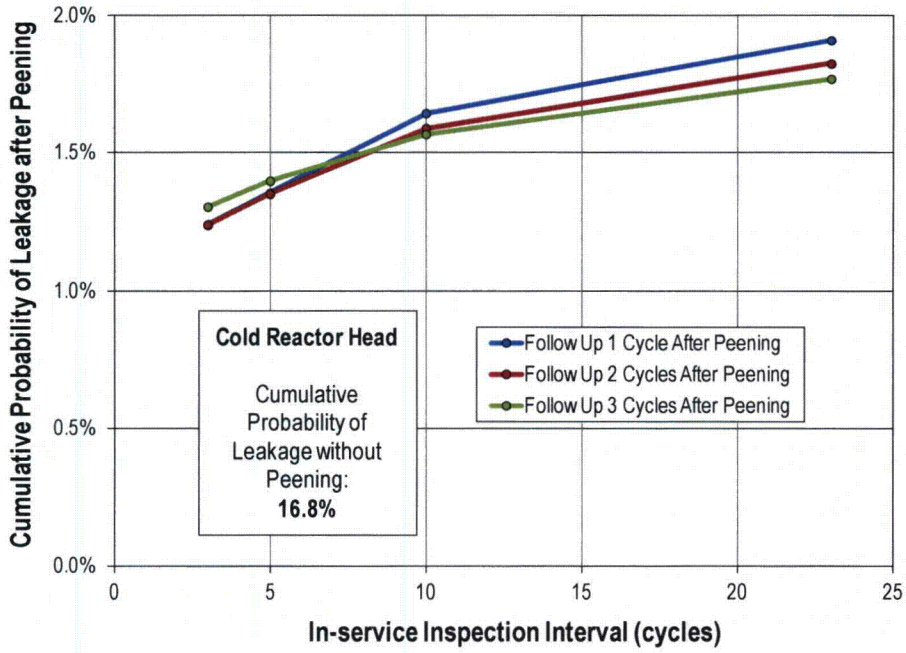

Figure B-30
Cumulative Probability of Leakage after Hypothetical Time of Peening vs. ISI Frequency for Cold Reactor Head

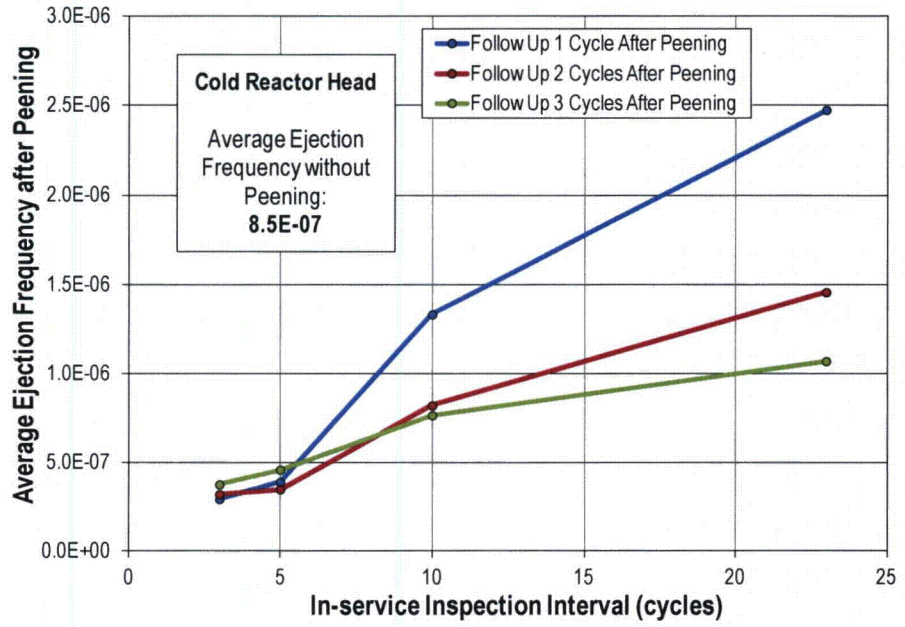

Figure B-31
Average Ejection Frequency after Hypothetical Time of Peening vs. ISI Frequency for Cold Reactor Head

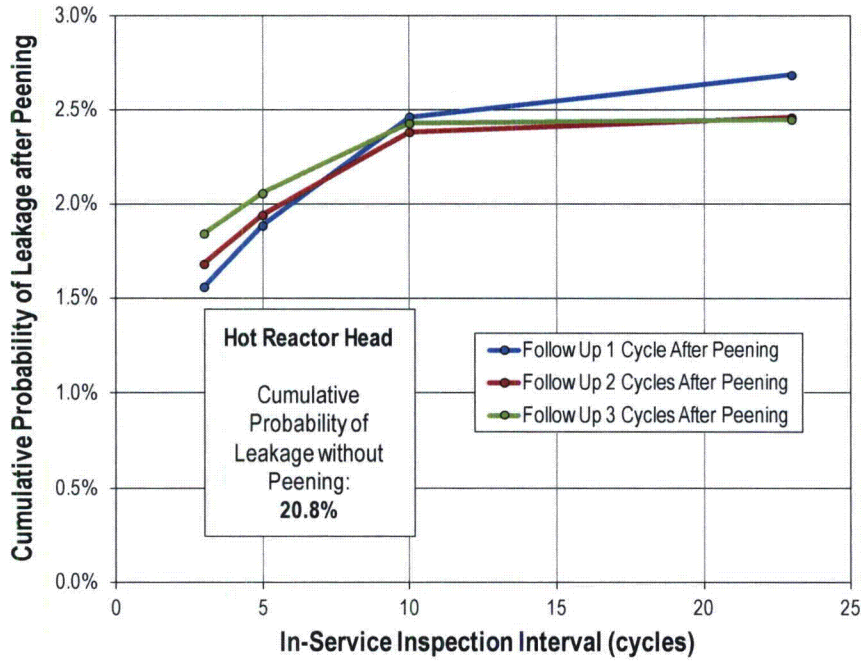

Figure B-32
Cumulative Probability of Leakage after Hypothetical Time of Peening vs. ISI Frequency for Hot Reactor Head

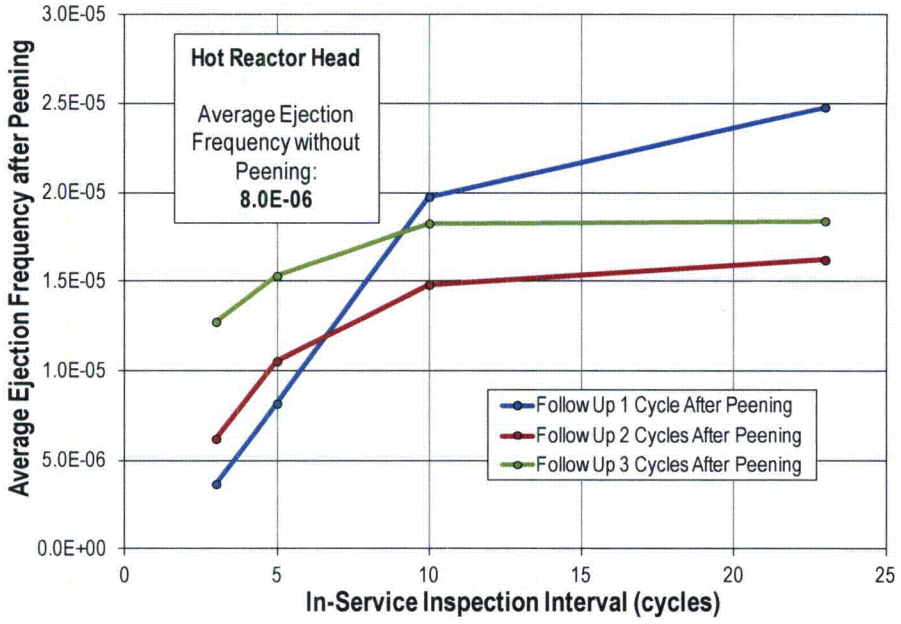

Figure B-33
Average Ejection Frequency after Hypothetical Time of Peening vs. ISI Frequency for Hot Reactor Head

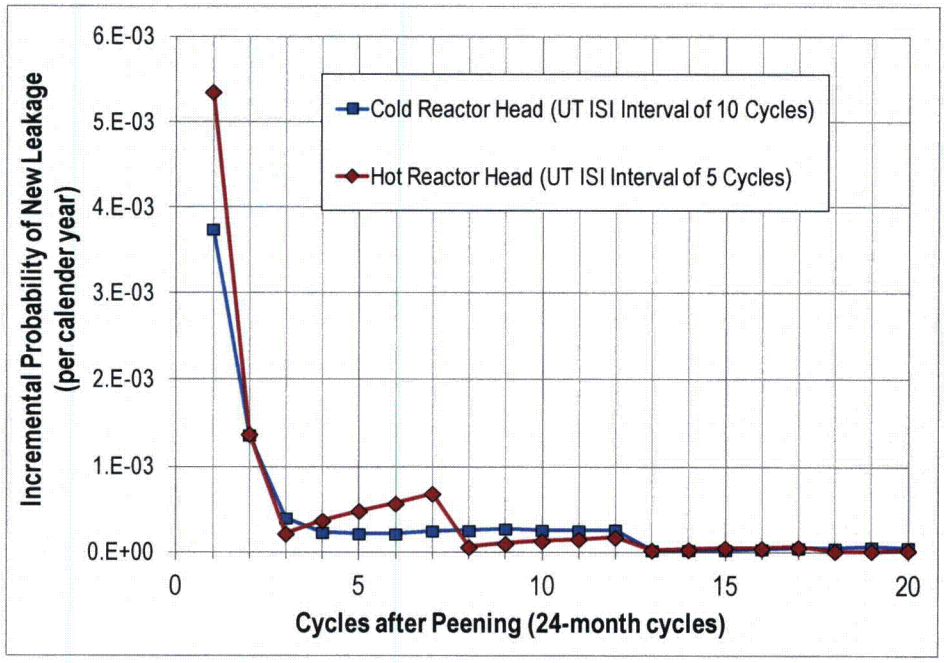

Figure B-34
Incremental Probability of Leakage after Peening with Relieved ISI Intervals (Follow-Up Inspection 2 Cycles After Peening)

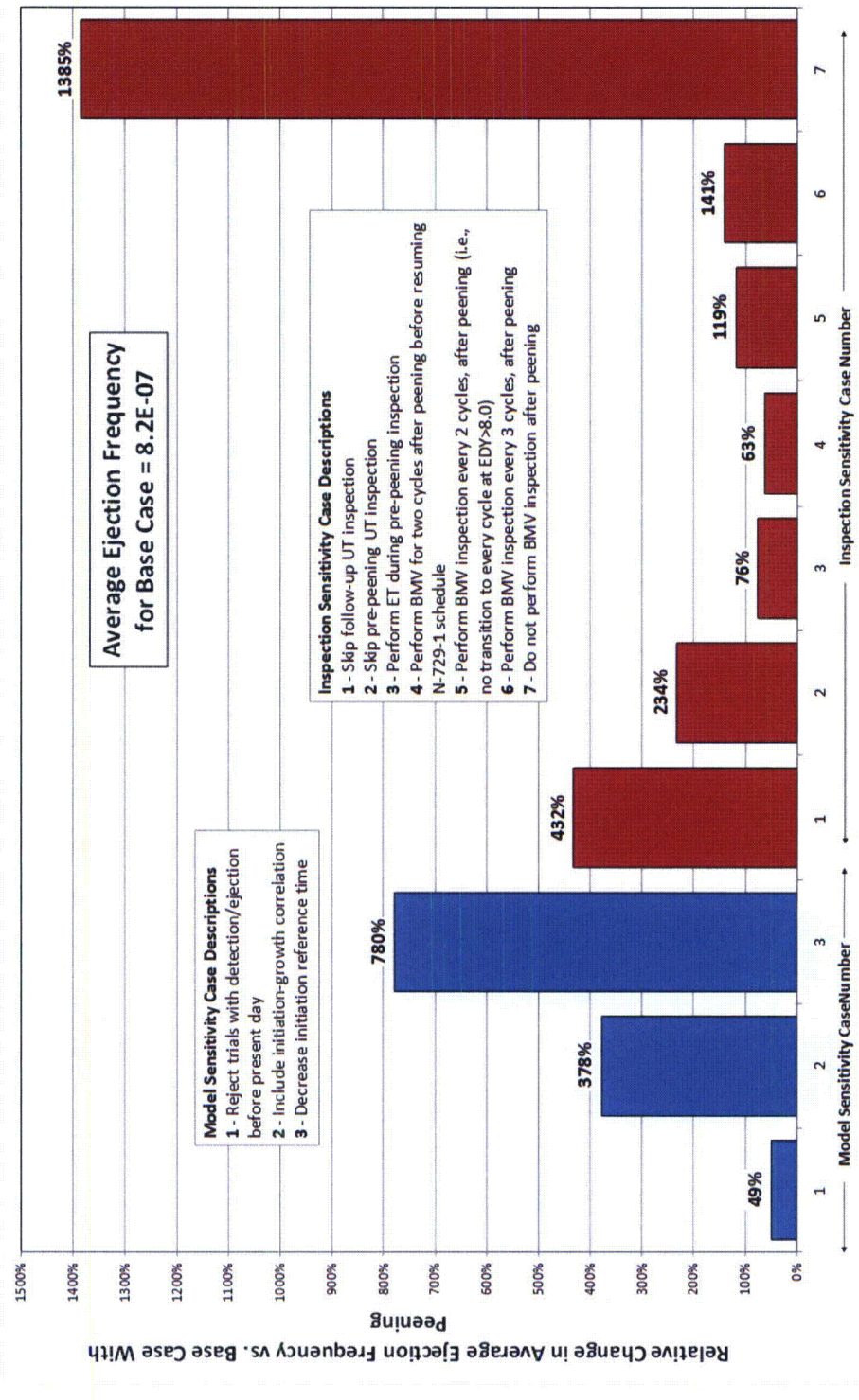

Figure B-35
Summary of Sensitivity Results for RPVHPN Probabilistic Model with Peening (Cold Reactor Head, Follow-Up Inspection 2 Cycles After Peening, ISI Interval of 10 Cycles; Two Intervals)

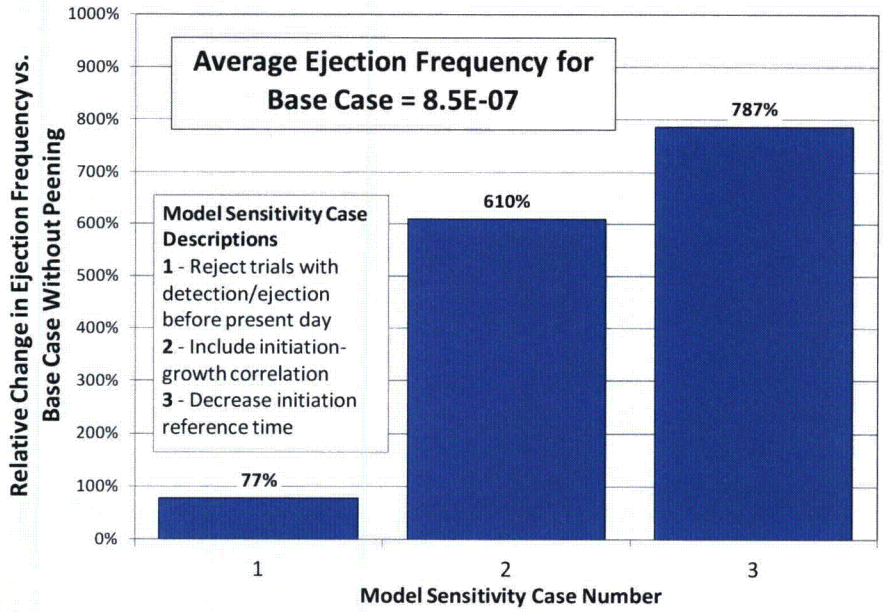

Figure B-36
Summary of Sensitivity Results for RPVHPN Probabilistic Model without Peening (Cold Reactor Head, Follow-Up Inspection 2 Cycles After Peening, ISI Interval of 10 Cycles; Two Intervals)

Figure B-37
Summary of Sensitivity Results for RPVHPN Probabilistic Model with Peening (Hot Reactor Head, Follow-Up Inspection 2 Cycles After Peening, ISI Interval of 5 Cycles; One Interval)

Figure B-38
Summary of Sensitivity Results for RPVHPN Probabilistic Model without Peening (Hot Reactor Head, Follow-Up Inspection 2 Cycles After Peening, ISI Interval of 5 Cycles; One Interval)

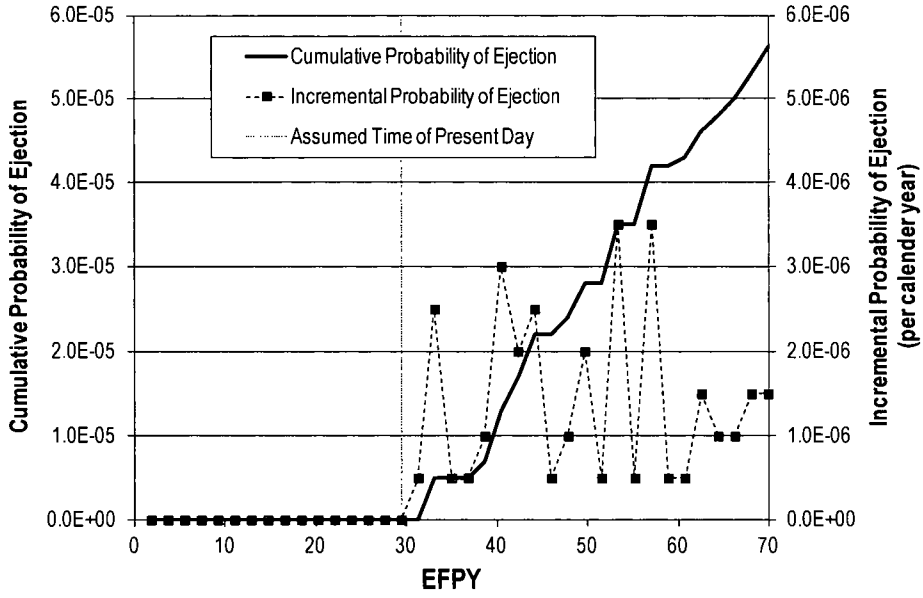

Figure B-39
Predicted Ejection Probabilities for Example Unmitigated Hot Reactor Head with No Crack Detections to Date

B.10 Conclusions regarding appropriate in-service examination requirements for RPVHPNs mitigated by peening

The results of the probabilistic analysis of PWSCC on a general cold reactor head support the relieved UT inspection schedules prescribed in Section 4 of this report. Specifically:

- The cumulative leakage probability after the hypothetical time of peening is predicted to be reduced by a factor of approximately 11 when the follow-up UT inspection is scheduled two or three cycles after peening and subsequent UT inspections are scheduled every 20 years (every two intervals).
- The average ejection frequency after the hypothetical time of peening is predicted to be remain approximately equivalent to the unmitigated case when the follow-up UT inspection is scheduled two or three cycles after peening and subsequent UT inspections are scheduled every 20 years (every two intervals).

The results of the probabilistic analysis of PWSCC on a general hot reactor head support the relieved UT inspection schedules prescribed in Section 4 of this report. Specifically:

- The cumulative leakage probability after the hypothetical time of peening is predicted to be reduced by a factor of approximately 11 when the follow-up UT inspection is scheduled one or two cycles after peening and subsequent UT inspections are scheduled every 10 years (every interval).

- The average ejection frequency after the hypothetical time of peening is predicted to be remain approximately equivalent to the unmitigated case when the follow-up UT inspection is scheduled one cycle after peening and subsequent UT inspections are scheduled every 10 years (every one interval).

For both hot and cold leg components, the probabilistic model predicts the rapid decay of incremental leakage probabilities after peening. However, sensitivity studies demonstrate that if visual examination is relieved immediately after peening, it could result in ejection probabilities substantially higher in comparison to the unmitigated case.

Many key input or modeling assumptions have been varied for Model Sensitivity Cases. The following cases resulted in increase in average ejection frequency for the peened component relative to the unmitigated component:

- Hot Model Sensitivity Case 4 – reducing the initiation reference time by a factor of five results in a 272% increase in predicted AEF for the peened component and a 191% increase for the unmitigated component (a 42% increase in peened AEF compared to unmitigated AEF).
- Hot Model Sensitivity Case 11 and 13 – reducing the initiation depth by a factor of five results in no significant reduction in predicted AEF for the peened component but a 10% decrease for the unmitigated component (a 13% increase in peened AEF compared to unmitigated AEF).
- Hot Model Sensitivity Case 14 – reducing the maximum POD for UT inspection results in a 182% increase in predicted AEF for the peened component and a 169% increase for the unmitigated component (a 8% increase in peened AEF compared to unmitigated AEF).
- Hot Model Sensitivity Case 17 – removing the environment factor for circumferential through-wall growth results in a 54% decrease in predicted AEF for the peened component and a 82% decrease for the unmitigated component (a 160% increase in peened AEF compared to unmitigated AEF).
- No Cold Model Sensitivity Cases resulted in an increase in AEF for the peened component relative to the unmitigated component.

Various Inspection Sensitivity Cases were carried out to predict the impact of optional alterations to the inspection schedule/scope. Several key observations are given below:

- Hot and Cold Head Inspection Sensitivity Cases 1 and 2 predict that skipping the pre-inspection or the follow-up inspection could result in significantly higher ejection frequencies for the unpeened component.
- Cold Head Inspection Sensitivity Cases 5 and 6 suggest that relaxing the BMV inspection frequencies after peening may be acceptable in the ejection probabilities are predicted to increase by only 19% and 41% respectively.
- Hot and Cold Head Inspection Sensitivity Cases 7 emphasize the considerable importance of intermittent BMV inspections. These predict

ejection frequencies to increase over tenfold if BMV is not conducted after peening.

B.11 References

1. D. Rudland, J. Broussard, et al., "Comparison of Welding Residual Stress Solutions for Control Rod Drive Mechanism Nozzles," *Proceedings of the ASME 2007 Pressure Vessels & Piping Division Conference: PVP2007*, San Antonio, Texas, July 2007.
2. *Materials Reliability Program Generic Evaluation of Examination Coverage Requirements for Reactor Pressure Vessel Head Penetration Nozzles, Revision 1 (MRP-95R1)*, EPRI, Palo Alto, CA: 2004. 1011225.
3. S. Marie, et al., "French RSE-M and RCC-MR code appendices for flaw analysis: Presentation of the fracture parameters calculation – Part III: Cracked Pipes," *International Journal of Pressure Vessels and Piping*, 84, pp. 614-658, 2007.
4. *Technical Basis for RPV Head CRDM Nozzle Inspection Interval H. B. Robinson Steam Electric Plant, Unit No. 2.* Dominion Engineering Inc.: Reston, VA: 2003. R-3515-00-1.
5. *Farley CRDM Through-Wall Circumferential Crack Fracture Mechanics.* Dominion Engineering Inc.: Reston, VA: 2003. C-7781-00-1.
6. *Materials Reliability Program: Technical Bases for the Chemical Mitigation of Primary Water Stress Corrosion Cracking in Pressurized Water Reactors (MRP-263)*, EPRI, Palo Alto, CA: 2009. 1019082.
7. *Materials Reliability Program (MRP) Crack Growth Rates for Evaluating Primary Water Stress Corrosion Cracking (PWSCC) of Thick-Wall Alloy 600 Materials (MRP-55) Revision 1*, EPRI, Palo Alto, CA: 2002. 1006695.
8. *Materials Reliability Program: Probabilistic Fracture Mechanics Analysis of PWR Reactor Vessel Top Head Nozzle Cracking (MRP-105)*, EPRI, Palo Alto, CA: 2004. 1007834.
9. ASME Code Case N–729-1, "Alternative Examination Requirements for PWR Reactor Vessel Upper Heads With Nozzles Having Pressure-Retaining Partial-Penetration Welds," Section XI, Division 1, American Society of Mechanical Engineers, New York, Approved March 28, 2006.
10. T_{cold} *RV Closure Head Nozzle Inspection Impact Assessment*, EPRI, Palo Alto, CA: 2011. MRP 2011-034.
11. *PWR Materials Reliability Program Response to NRC Bulletin 2001-01 (MRP-48)*, EPRI, Palo Alto, CA: 2001. 1006284.
12. *Materials Reliability Program: Reactor Vessel Closure Head Penetration Safety Assessment for U.S. PWR Plants (MRP-110): Evaluations Supporting the MRP Inspection Plant*, EPRI, Palo Alto, CA: 2004. 1009807.
13. D. Montgomery, G. Runger, and N. Hubele. *Engineering Statistics.* John Wiley & Sons, Inc., New York, NY 1994.
14. *PWSCC Prediction Guidelines*, EPRI, Palo Alto, CA: 1994. TR-104030.

15. *Materials Reliability Program: Technical Basis for Primary Water Stress Corrosion Cracking Mitigation by Surface Stress Improvement (MRP-267, Revision 1)*, EPRI, Palo Alto, CA: 2012. 1025839.

16. *Materials Reliability Program: Inspection Plan for Reactor Vessel Closure Head Penetrations in U.S. PWR Plants (MRP-117)*, EPRI, Palo Alto, CA: 2004. 1007830.

17. US NRC, Regulatory Guide 1.174, "An Approach for Using Probabilistic Risk Assessment in Risk-Informed Decisions on Plant-Specific Changes to the Licensing Basis," Revision 2, May 2011.

18. *PWR Materials Reliability Program, Interim Alloy 600 Safety Assessments for US PWR Plants (MRP-44): Part 2: Reactor Vessel Top Head Penetrations*, EPRI, Palo Alto, CA,: 2001. TP-1001491, Part 2.

The Electric Power Research Institute, Inc. (EPRI, www.epri.com) conducts research and development relating to the generation, delivery and use of electricity for the benefit of the public. An independent, nonprofit organization, EPRI brings together its scientists and engineers as well as experts from academia and industry to help address challenges in electricity, including reliability, efficiency, affordability, health, safety and the environment. EPRI also provides technology, policy and economic analyses to drive long-range research and development planning, and supports research in emerging technologies. EPRI's members represent approximately 90 percent of the electricity generated and delivered in the United States, and international participation extends to more than 30 countries. EPRI's principal offices and laboratories are located in Palo Alto, Calif.; Charlotte, N.C.; Knoxville, Tenn.; and Lenox, Mass.

Together...Shaping the Future of Electricity

Program:

Nuclear Power

3002000073

Electric Power Research Institute
3420 Hillview Avenue, Palo Alto, California 94304-1338 • PO Box 10412, Palo Alto, California 94303-0813 USA
800.313.3774 • 650.855.2121 • askepri@epri.com • www.epri.com